UNIVERSITY OF CALIFORNIA, SAN DIEGO

Intramolecular Dynamics and Domain Crosstalk in C-terminal Src Kinase (Csk)

A dissertation submitted in partial satisfaction of the requirements

for the degree Doctor of Philosophy

in

Chemistry

by

Sulyman Barkho

Committee in Charge:

Professor Patricia A. Jennings, Chair
Professor Joseph A. Adams
Professor Rommie E. Amaro
Professor Judy E. Kim
Professor José N. Onuchic
Professor Stanley J. Opella

2014

The dissertation of Sulyman Barkho is approved, and it is acceptable in quality and form for publication on microfilm and electronically.

_____

_____

_____

_____

_____

_____

_____
Chair

University of California, San Diego

2014

TABLE OF CONTENTS

LIST OF ABBREVIATIONS

ADP	adenosine diphosphate
aMD	accelerated molecular dynamics
ATP	adenosine triphosphate
cAMP	cyclic adenosine monophosphate
CBP	Csk binding protein
CD	circular dichroism
cMD	conventional molecular dynamics
CPM	counts per minute
Cryo-EM	cryo-electron microscopy
Csk	C-terminal Src kinase
Csk-GG	Csk variant with Gly-Gly loop insert
DTT	dithiothreitol
DXMS	Deuterium-Exchange Mass Spectrometry
E. coli	Escherichia Coli
EDTA	Ethylenediaminetetraacetic acid
Gdh-HCl	guanidinium hydrochloride
GST	glutathione S-transferase
HDX	hydrogen-deuterium exchange
HEPES	4-(2-hydroxyethyl)-1-piperazineethanesulfonic acid
HSQC	heteronuclear single quantum coherence
Lck	lymphocyte-specific protein tyrosine kinase
MD	molecular dynamics

MOPS	3-(N-morpholino)propanesulfonic acid
NMDAR	N-methyl-D-aspartate receptors
NMR	nuclear magnetic resonance
nrPTK	non-receptor protein tyrosine kinase
p-CBP	phosphorylated Csk binding protein
PAG1	phospho-protein associated with glycosphingolipid-enriched microdomains
PKA	protein kinase A
PTM	post-translational modification
pTyr	phosphorylated tyrosine
rPTK	receptor protein tyrosine kinase
SAXS	small angle x-ray scattering
SDS-PAGE	sodium dodecyl sulfate polyacrylamide gel electrophoresis
SFK	Src family kinase
SH1	Src homology 1
SH2	Src homology 2
SH2-GG	SH2 domain variant with Gly-Gly loop insert
SH3	Src homology 3
TCEP	tris (2-carboxyethyl) phosphine
TCR	T-cell receptor
Tris	tris(hydroxymethyl)aminomethane

LIST OF FIGURES

LIST OF TABLES

ACKNOWLEDGMENTS

The work presented in this dissertation was possible due to support from many people over the past 6 years. I'd firstly thank my adviser, Dr. Patricia Jennings, who supervised and helped me arrive to this point in my career. Over the years, Pat let me ask questions and pursue my interests and when I was stuck, she always found the resources and provided guidance to get me past hurdles. I consider myself very fortunate to know and work with an incredibly insightful and caring mentor. As a fellow New Jerseyan, I became Pat's *de facto* supporter in her attempts to get naive non-New Jerseyans to appreciate the fine scenery of the Garden State! I'd also like to thank my committee members: Drs. Stanley Opella, José Onuchic, Judy Kim, Rommie Amaro, and Hector Viadiu. Dr. Joseph Adams is considered a second mentor to me and was especially helpful with the enzymology work; his generosity and patience I'll always remember. My good friend and best collaborator Levi Pierce maintained incredible enthusiasm for this work from day one, I owe him and Dr. Andy McCammon many thanks for this fruitful collaboration. I thank Sheng Li for being informative and accommodating with last minute DXMS requests.

Present and past members of the Jennings, Adams, and Opella labs have been an incredible group of people to be around in scientific and social settings. Dr. Melinda Roy helped me with initial NMR training and I always enjoyed talking with (and occasionally joking with her) about science and other topics. Kendra Hailey provided some of the most valuable contributions to experiments and helped with countless tools and techniques; her challenging thoughts and excitement about big questions resulted in endless conversations, arguments, pranks, puns and (usually) bad jokes. She truly enjoys helping others and I'd often find encouragement in her enthusiasm and good-heartedness. Dominique Capraro was both resourceful and made the lab a cheery fun place to be; despite her Juve connection, we'd usually be on the same soccer page especially during the world cup (at least until Maradona and/or Messi

start sobbing or when Balotelli gets his foreseen red card). “DNA mommy” Maria McGlone’s skills in molecular biology helped me move forward with the project at a crucial point. His questionable taste in beer notwithstanding, Christian Cole provided both good company over tacos and “deep” conversations that often deviated significantly from the starting premises. My good friends Gabe Cook and Lindsay Dawson were always down the hall when I needed to complain, seek advice, or simply lighten up; but oftentimes for more practical things like a DC burrito run or an RB pool challenge. Brandon Aubol and Ryan Plocinik assisted me in getting proper initial training in kinetics in the Adams lab. Brandon’s colorful conversations (and candles, soaps, “bath bombs” etc.) added quality fun to my time there; he made me appreciate the “qualitatively quantitative” nature of things -usually after few Rasputins. I also thank Andrea Conlan, Michael Jamros, Ellinor Haglund, Liz Baxter, John Zuris, Kaitlin Fisher, DJ Burban, Colin Lipper, Nick (cat) Tiee, Jason Stofleth and Josh Chan.

My family’s endless support and encouragement were invaluable throughout my graduate school experience. Almost every time I spoke to them, my parents Chukri and Georgette Barkho would ask what exactly is it that I do, yet kept showing excitement and understanding of my choices in good and tough times. I’m grateful to my loving sisters: Nancy, Patricia, Gabriela and Angelina who -despite the long distances- provided an incredible feeling of familial warmth and support in many ways throughout the years. Last *and* least, I “thank” my two nieces: Julie and Chloé for providing endless entertainment!

Chapter 2, in part, is a reprint of the material as it appears in the PLoS Computational Biology by Barkho, Sulyman, Levi CT Pierce, Maria L. McGlone, Sheng Li, Virgil L. Woods Jr, Ross C. Walker, Joseph A. Adams, and Patricia A. Jennings. (2013). The dissertation author was the primary investigator and author of this paper.

VITA

Education:

2014	Ph.D. Chemistry, University of California, San Diego
2010	M.S. Chemistry, University of California, San Diego
2007	B.A. (*Honors*) Chemistry, Rutgers University, Newark, New Jersey

Publications:

Barkho, S., Pierce, L. C., Li, S., Adams, J. A. & Jennings, P. A. (2014). Newton's Cradle and the Effects of the SH3 and SH2 Domains on Csk Activity. *under review*.

Barkho, S., Pierce, L. C., McGlone, M. L., Li, S., Woods Jr, V. L., Walker, R. C., Adams, J. A. & Jennings, P. A. (2013). Distal Loop Flexibility of a Regulatory Domain Modulates Dynamics and Activity of C-Terminal Src Kinase (Csk). *PLoS computational biology, 9*(9), e1003188.

Hailey, K. L., Capraro, D. T., Barkho, S., & Jennings, P. A. (2013). Allosteric switching of agonist/antagonist activity by a single point mutation in the interleukin-1 receptor antagonist, IL-1Ra. *Journal of molecular biology*, *425*(13), 2382-2392.

ABSTRACT OF THE DISSERTATION

Intramolecular Dynamics and Domain Crosstalk in C-terminal Src Kinase (Csk)

by

Sulyman Barkho

Doctor of Philosophy in Chemistry

University of California, San Diego, 2014

Professor Patricia A. Jennings, Chair

Organisms rely on complex forms of chemical, physical and structural sensors that wire their communication networks at the cellular and molecular levels. These signal transduction pathways were classically treated as binary switches that relay information along specific routes from origins to destinations; however, this view is insufficient to describe the scale and diversity of responses offered by a limited number of molecular actors and pathways. Therefore, a more nuanced examination of structural components is needed for deeper understanding of high specificity and diversity of generated signals in the cellular context.

The studies presented herein aim to explore the special molecular features of a major signaling component, the C-terminal Src kinase (Csk). It is a master regulator of the Src family of

tyrosine kinases (SFKs) whose members participate in almost all aspects of cellular regulation and functions. We first studied the importance of a site-specific divergence within Csk's regulatory Src Homology 2 (SH2) domain and examined its effects on kinase behavior and functions using extended biophysical and activity techniques coupled to molecular dynamics simulations. Induced flexibility in the distal loop position was sensed throughout the protein as it modulated kinase functional motions and activity; revealing intramolecular routes of long-range communications in Csk. Along with insights on intrinsic functions, the results may provide a general framework for identifying potential effector sites for specific targeting by design. And since the distal motif is within a common adaptor domain, we characterized the changes in Csk's interaction with its physiological, membrane-recruiting activator, the Csk Binding Protein (CBP). Our enzymatic activation assays and Nuclear Magnetic Resonance binding analysis indicate that while the magnitude of maximal p-CBP activation of the kinase is largely unaffected, the overall catalytic efficiency is hampered by the non-contacting loop and allows for simultaneous, tunable control of localization and intrinsic activity. Lastly, unlike many modular scaffolds that could routinely be captured in multiple functional states, Csk's intrinsically dynamic character precludes extensive analysis through traditional structural techniques. Therefore, we used computational tools to study full-length Csk aiming to predict molecular transitions and large-scale coupled motions. The theoretical results were corroborated experimentally using our established kinetic, mutational, and structural-dynamic techniques; and construct a clearer model of dynamic intramolecular regulation. The data suggest that previously undetected, directional-global motions of the modular domains about the kinase core are inherently linked to Csk's enzymatic tasks of binding its substrates and catalyzing the phosphotransferase reaction.

Chapter I

General Introduction

Biological Signal Transduction

Cellular communications are foundational aspects in the biology of all organisms. Biological systems evolved efficient gauges to sense inputs (stimuli) in order to adapt to environmental changes, formulate an internal response, or propagate their own signals to other proximal or distal sensors [1,2]. This collective process is termed signal transduction.

In eukaryotes, many signaling events are cascades of chemical reactions among numerous membrane receptors and signaling molecules that relay information by structural or chemical changes along the pathway. Classically, such cascades were viewed as linear, directional, and composed of molecular switches possessing "on/off" duality. However, it is now understood that signaling pathways are more complex networks that are managed spatiotemporally to efficiently orchestrate information relays to cellular destinations [3,4]. Moreover, an intermediate signaling molecules oftentimes receives multiple inputs from upstream regulators to trigger their own signaling output downstream (Figure 1-1).

In light of such complexity, detailed study of signaling networks and their molecular underpinnings is of extreme value for understanding healthy and aberrant behaviors that lead to various diseased states due to misregulation in signal transduction pathways; thus, it should be of no surprise that major branches of therapeutic research are directed towards this goal [5].

Protein post-translational modifications

The "genomic revolution" confirmed that organisms have more protein variants than there are genes and revealed previously unknown mechanisms of control at the DNA level [6]. Although alternative splicing of coding transcripts can be one way to increase molecular diversity, one of evolution's elegant solutions to overcome the finite number of unique gene

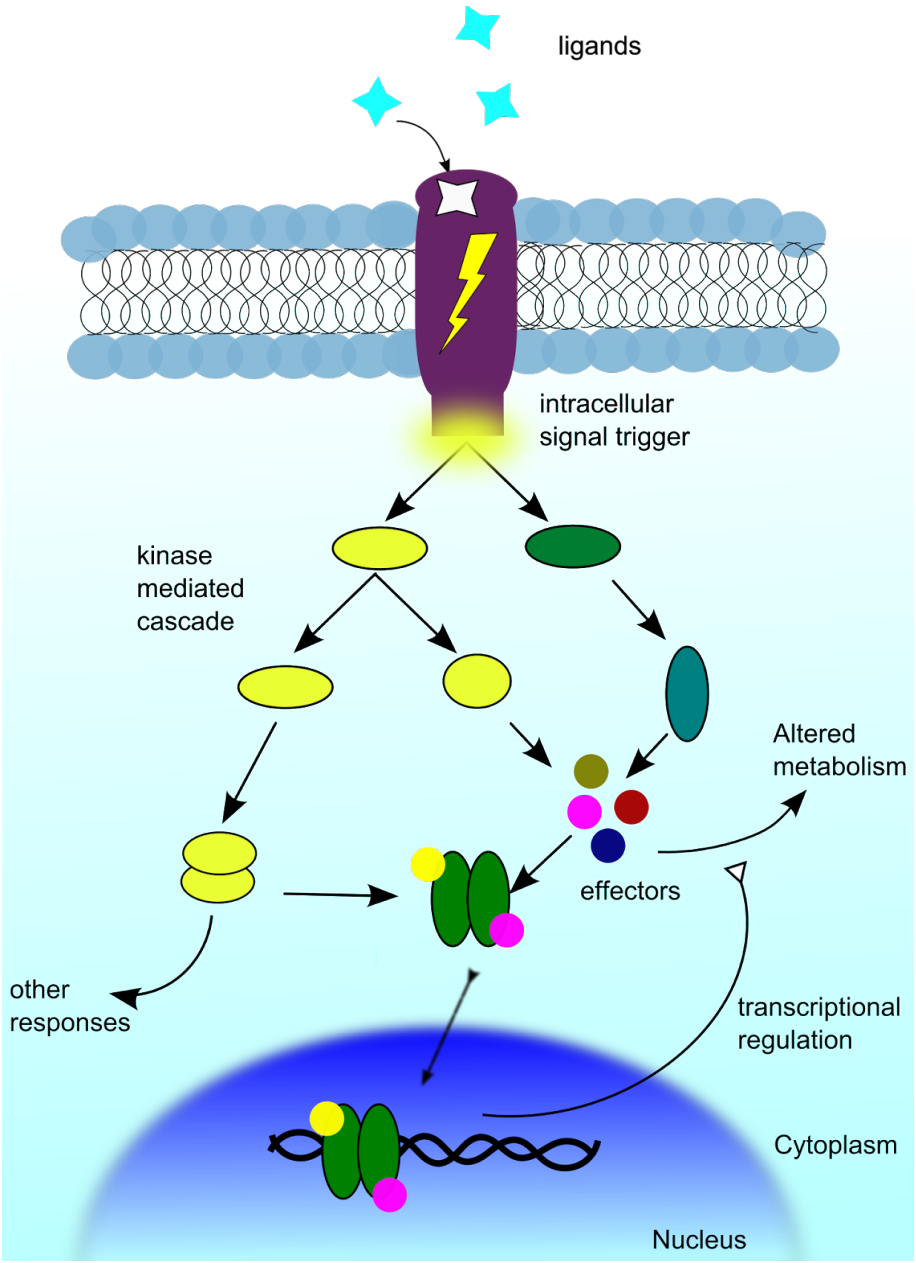

Figure 1-1. Cellular Communications

In biology, cells communicate via complex networks of molecular and structural elements. Information from the outside is relayed to various targets inside the cell.

outputs was introducing additional diversity to the proteome (the final products). The process of modifying a protein after it has been biosynthesized is termed Post-translational modification (PTM) and is the cellular mechanism for introducing the needed diversity in the proteome to carry out many different biological functions [7]. PTMs include site-specific attachment of different functional biochemical groups (or whole proteins/domains) to amino acids of nascent or mature polypeptides.

Kinases, phosphatases, and reversible protein phosphorylation

Protein phosphorylation is the process of transferring a phosphate group from a donor molecule (usually a nucleoside triphosphate) to an acceptor molecule (a protein sidechain) and is a ubiquitous cellular regulatory mechanism. Research articles about phospho-proteins has grown to include hundreds of thousands of reports since phosphate was first detected in proteins over a century ago and the subsequent identification of enzyme-catalyzed protein phosphorylation [8,9]. The name given for the early enzymes was "protein(phospho) kinase" to indicate their ability of "moving" a phosphate group from donor to acceptor [10]. Today, the accepted definition of a kinase is a protein that binds substrate proteins and ATP and transfer a phosphate group from ATP to amino acids with free hydroxyl (-OH) groups (serine, threonine or tyrosine). The products are the phospho-protein and ADP [11].

It is estimated that the human genome encodes over 500 unique protein kinases constituting about 2% of all human genes [12]. Eukaryotic protein kinases are organized into seven major groups and subdivided into families -and sometimes subfamilies- based on sequence and structure (Figure 1-2). Aside from response to extracellular stimuli, the diverse biological

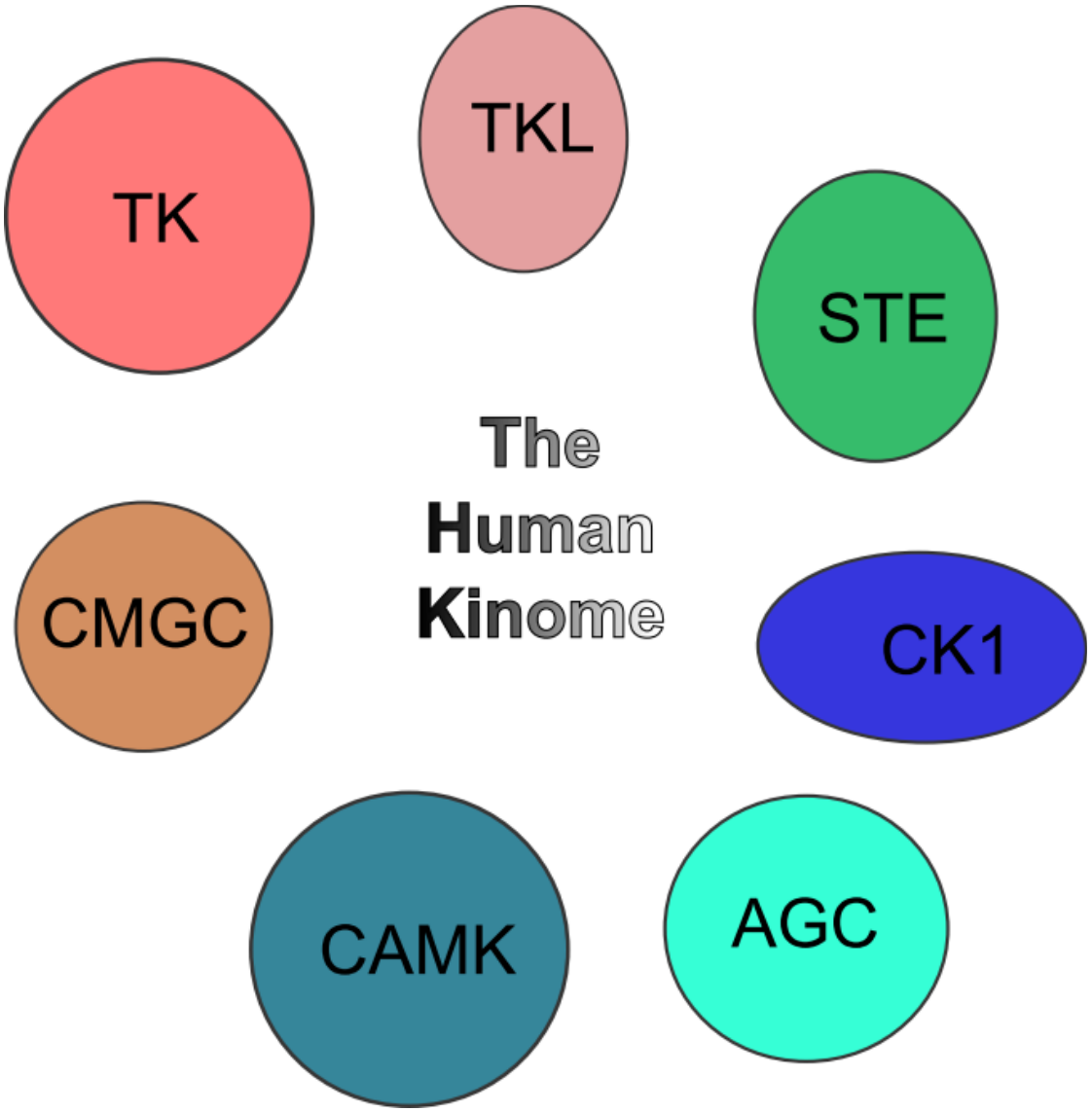

Figure 1-2. Schematic of The Human Kinome

Categories of all identified human kinases in indicating relative size of each group. **AGC** Named after the Protein Kinase A, G, and C families (PKA, PKC, PKG), this group contains many core intracellular signaling kinases which are modulated by cyclic nucleotides, phospholipids and calcium. **CMGC** Named after another set of families (CDK, MAPK, GSK3 and CLK), this group has a diversity of functions in cell cycle control, MAPK signaling, splicing and other unknown functions. **CAMK** Best known for the Calmodulin/Calcium regulated kinases (CAMK) in CAMK1 and CAMK2 families, this also has several families of non-calcium regulated kinases. **CK1** A small but ancient family. Originally known as Casein Kinase 1 (from a biochemically assay with a non-physiological substrate), and now renamed to Cell Kinase 1. **STE** Homologs of the yeast STE7, STE11 and STE20 genes, which form the MAPK cascade, transducing signals from the surface of the cell to the nucleus. Tyrosine Kinase **(TK)** This group phosphorylates almost exclusively on tyrosine residues, as opposed to most other kinases that are selective for serine or threonine Tyrosine Kinase-Like **(TKL)** The group most similar to tyrosine kinases, but whose activities are generally on serine/threonine substrates. Based on Poster in *Manning et. al 2002.*

functions of kinases range from metabolic control and DNA damage response to cell cycle regulation. Since kinases and their substrates make up the backbone of signaling networks in eukaryotes, it is not surprising that about 30% of human kinases are mutated or misregulated in various diseases. Kinase activity is counterbalanced by that of protein phosphatases that catalyze the removal of the phosphate group. Both actors are regulated in signaling pathways by dynamic switching of activity, binding, and localization [4] with the overall outcome controlling output through a delicate balance of reversible phosphorylation.

Physiological functions of Src Family of Tyrosine Kinases (SFKs)

In one of the most important medical discoveries of the 20th century, Francis Rous proved that infections agents can induce uncontrolled cellular proliferation (tumors) in the host organism [13]. He noticed that chicken sarcoma can be induced by a tumor extract from another animal that did not contain chicken cells or bacteria; he termed the infection agent the Rous Sarcoma "Virus" [14,15]. It took more than 70 years to identify the molecular basis of this retroviral phenomena when the gene product responsible for tumorigenesis was discovered [16]. The *v-src* gene produces an active protein that cannot be "turned off" because of deletions in the sequence; it became representative of what is known today as oncogenes. *c-src* is the functional version of *v-src* in normal cells and is a "proto-oncogene" since it has the potential to transform into the "viral" oncogenic state due to mutations or altered expression.

The Src family of protein kinases (SFKs) are the protein products of normal Src genes that are integral in regulating many cellular functions [17,18]. In healthy cells, SFKs are under tight regulatory control at the plasma membrane where they phosphorylate numerous protein substrates associated with cell growth, angiogenesis, differentiation, adhesion and invasion [18–20]. SFKs are also involved in pathways controlling the turnover of cell surface receptors (including GPCRs), modulating actin cytoskeleton rearrangements, promoting cell motility and survival [21]. The prototypical SFK Src is often overexpressed or unregulated in many cancers

[22,23] and aberrant activity of SFKs is correlates with the development of various cancers and autoimmune diseases and induce cell transformations through interactions and cross-activation of receptor tyrosine kinases (rPTK), growth factor receptors, and participation in pathways required for DNA synthesis [24].

Src protein function in the central nervous system has been implicated in synaptic transmission and plasticity. SFKs relay output from multiple signaling pathways regulating *N*-methyl-d-aspartate receptors (NMDAR) and SFK molecules, such as Src and Fyn, closely associate with their NMDA receptors, via indirect and direct binding mechanisms [25]. Perhaps one of the most studied function of SFK signaling is in B-cell and T-cell antigen receptor activation where they initiate adaptive immune responses by recruitment to phosphorylate TCR at specific sequences and initiate a signaling cascade that leads to activation. SFKs themselves are governed by specific positive and negative regulators within these cells [19].

Structure, domain organization, and regulation of SFKs

As a non-receptor protein tyrosine kinases (nrPTK), SFKs have conserved domain content that include a kinase domain (also known as an SH1 domain for "Src homology") that consists of a small and large lobes and is responsible for binding substrates and catalytic phosphotransferase function. SFKs also contain myristic or sometimes palmitic acid moiety for membrane tethering attached to a unique SH4 domain, conserved SH3 and SH2 domains, and a C-terminal regulatory segment [23,26]. Intrinsic regulation of SFKs primarily occurs in a form of activation loop autophosphorylation and tertiary structure rearrangement in response to different phosphorylation states as a result of kinase/phosphatase actions [26]. Most importantly, the C-terminal regulatory tail contains a highly conserved tyrosine. Phosphorylation at this site leads to intramolecular binding of the SH2 domain to the tyrosine-phosphorylated (pTyr) tail (Y527), inactivating the kinase. Concurrently, the SH3 domain is positioned to bind the SH2-kinase linker containing a conserved poly-proline binding -motif sequence. Extrinsic regulation of Src is also

mediated by the regulatory SH2/3 domains (Figure 1-3) through interactions with other kinases, phosphatases, and binding various adaptor proteins [19,27].

Csk-mediated regulation of SFKs and eEF2

Almost thirty years ago, it was recognized that the main event in c-Src activation was tyrosine dephosphorylation at Y527 in the C-terminal tail [28,29]. The exact molecular mechanism of Src regulation later became apparent when the crystal structures of the active and inactive molecules were solved [30–32] in which an extended active form is converted to a compact form with the SH2 domain binding the phosphorylated tail tyrosine. A few years later, a co-purified kinase named Csk (C-terminal Src kinase) was determined to be the main negative regulator of SFKs and responsible for the specific inhibitory phosphorylation of the tail tyrosine [33]. *In vitro* and *in vivo* studies of this kinase revealed that it is essential for maintaining proper SFK functions and its misregulation causes many of the diseases associated with SFK-dependent pathways [34].

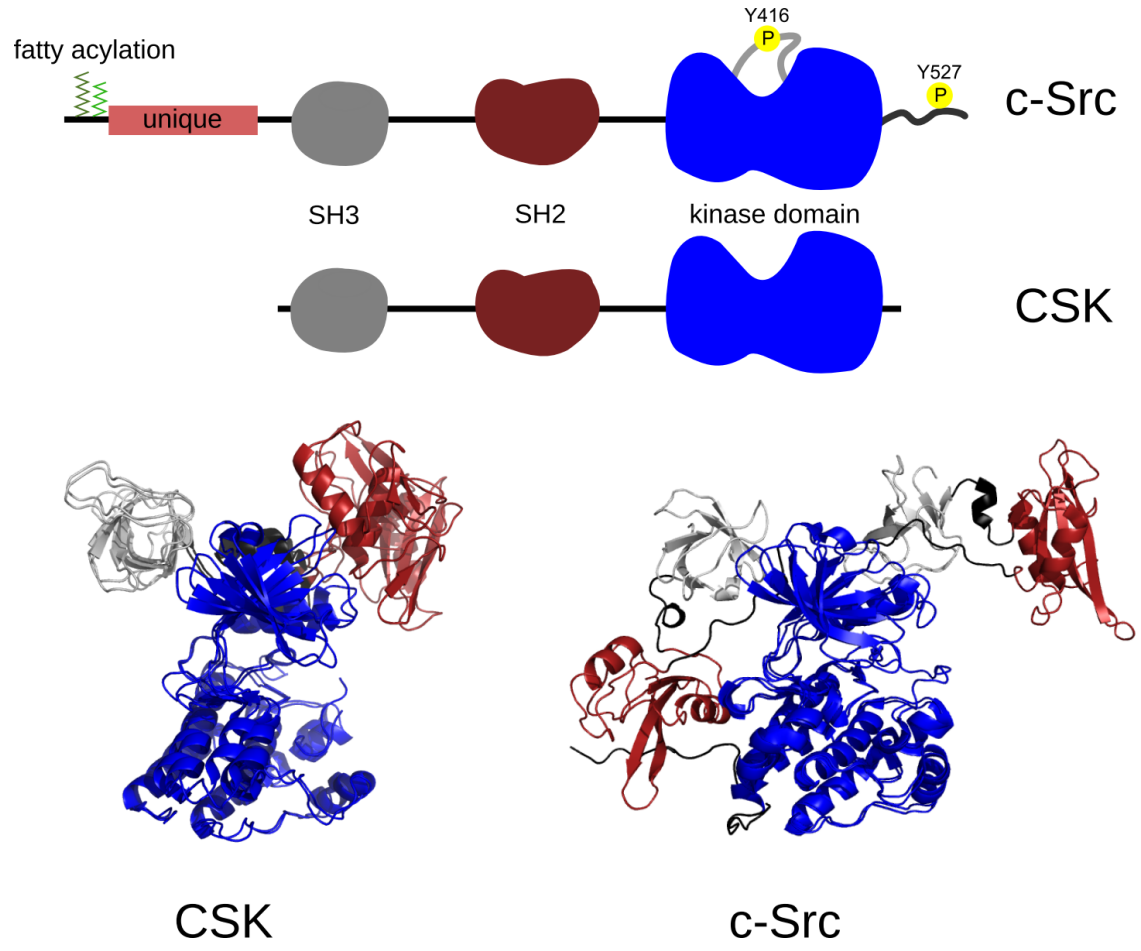

Figure 1-3. Domain content and organization in Csk and c-Src

The two kinases share the three main domain modules. c-Src possesses more regulatory motifs for localization, activation, and inhibition. Structures with PDB IDs: 1K9A (Csk), 1FMK and 1Y57 (c-Src) were used to generate the bottom figure. Superposition of active and inactive forms were aligned with respect to the kinase domains for each protein. The tertiary domain arrangement about the kinase core shows drastic differences between the two enzymes.

Also a nrPTK, the 50 kDa, 450 residue Csk contains three domains found in all SFKs: the kinase domain (SH1), SH2 and SH3 domains arranged in the same primary order but lacks other conserved elements in SFKs like the N-terminal fatty acylation sites, activation loop phosphorylation site, and regulatory phosphorylation site at the C-terminus (Figure 1-3). All the data hinted to a different mode of function and regulation for Csk than that of Src's family. Further biochemical and structural analysis showed the structural basis for the high substrate specificity exhibited by Csk towards Src family members [35,36]. These studies showed that the 3D docking surface on Csk is specialized to bind the kinase domains of SFKs to subsequently position the C-terminal tail close to the active site cleft for efficient phosphorylation of Y527.

A recent report implicated Csk in physiological regulation of a non-SFK substrate [37]. Eukaryotic elongation factor 2 (eEF2) is phosphorylated in a Csk-mediated manner, SUMOylated, and subsequently cleaved into a large and small fragments. A cleavage product of eEF2 is then translocated from the cytoplasm to the nucleus and induces nuclear morphological changes and aneuploidy similar to those found in cancer cells. The significance of this finding is that Csk's activity can be a crucial tier of signaling induction for two very different pathways where one is tumor suppressing and the other is tumor promoting through control of substrate localization. Thus, the balance of Csk's activity and perhaps its own localization maybe a primary signaling determinant to maintain healthy functions and responses via two different routes.

Signalosome assembly at the membrane

Given such a broad-acting kinase, Csk's localization and substrate specificity can link its activity to a certain pathway and the diseased states that arise from misregulation within that signaling cascade. However, a full understanding of the exact mechanisms by which Csk switches between two pathways requiring inherent adjustments of kinase activity remain elusive. Further, phosphoprotein associated with glycosphingolipid-enriched microdomains PAG1 -also known as Csk-binding protein (referred to hereafter as CBP)- is the main platform where the canonical

SFK-Csk signalosome assembles at the lipid rafts to which CBP is attached [38–40] but is also involved in other signaling pathways. Like other adaptor proteins, CBP contains many cytosolic interaction sites that allow for the assembly of a variety of cytoplasmic and membrane-tethered components by various mechanisms including phosphorylation (SH2 associations), proline-rich sequences (SH3 associations), a PDZ domain-binding motif, and a palmitoylation motif for a strong raft association [41]. With regards to SFK signaling, a running hypothesis is that kinase/phosphatase action on CBP determines cooperative association of upregulated SFKs with the adaptor and signal for Csk recruitment to the membrane to turn SFK signaling off.

Probing Protein Dynamics in signaling Networks

The principle of "structure-function" relationship in biochemistry is as old as the field itself. The human body is composed of billions of biomolecules whose flexible nature was realised by researchers since the early days in what we today call "structural biology". For modular systems like SFKs and Csk, cross-domain communications are what makes these nanomachines work as they relay their signals within and across networks. Early inquiries about the 3D atomic structures of protein kinases employed powerful tools like X-Ray crystallography and Cryo-Electron Microscopy to obtain frozen snapshots of enzymes in action or report on molecular assemblies. Indeed, the structure of c-AMP dependent Protein Kinase A (PKA), the first kinase structure to be solved, provided the basic molecular hypothesis on how these classes of proteins are regulated [42].

The classic enzymatic approach to probe kinase structure and function received a huge boost with the development of Nuclear Magnetic Resonance (NMR) spectroscopy and Mass Spectrometry methods for biomolecular research [43–45]. Monitoring kinase conformational changes, solution equilibria shifts, response to substrates and allosteric effectors became possible with abundant information generated from inherent observables in these techniques at peptide and site-specific resolutions under native solution states. In the last decade, our group and others have

used these experimental techniques to address Csk's unique mode of regulation, catalytic efficiency, and molecular recognition [46,47].

Here, we expanded these experimental biophysical and enzymatic approaches to answer specific questions about allosterically coupled regions in Csk, focusing on peripheral sites ranging from the exposed CD loop in the SH2 domain to its short N-terminal tail. Additionally, and for the first time using the full-length protein, we coupled our experimental approaches to advanced Molecular Dynamics (MD) studies that access a broad range of relevant timescales of fluctuations at atomic resolution. We believe this hybrid approach is useful as a general template to study big, dynamic systems like Csk as it provides complementary and bi-directional validation of experimental and theoretical results. The results in the following chapters highlight important new insights on Csk's molecular actions, malleable framework, dynamic landscape, its coupled internal motions and intramolecular interactions. Further, our results can be important for studies aimed at therapeutics developments and protein engineering of modular signaling components.

Chapter II

Distal loop flexibility of a regulatory domain modulates dynamics and activity of C-terminal Src kinase (Csk)

ABSTRACT

Csk and SFKs share a modular design with the kinase domain downstream of the N-terminal SH2 and SH3 domains that regulate catalytic function and membrane localization. While the function of interfacial segments in these multidomain kinases are well-investigated, little is known about how surface sites and long-range, allosteric coupling control protein dynamics and catalytic function. The SH2 domain of Csk is an essential component for the down-regulation of all SFKs. A unique feature of the SH2 domain of Csk is the tight turn in place of the canonical CD loop in a surface site far removed from kinase domain interactions. We used a combination of experimental and computational methods to probe the importance of this difference by constructing a Csk variant with a longer SH2 CD loop to mimic the flexibility found in homologous kinase SH2 domains. Our results indicate that while the fold and function of the isolated domain and the full-length kinase are not affected by loop elongation, native protein dynamics that are essential for efficient catalysis are perturbed. We also identify key motifs and routes through which the distal SH2 site might influence catalysis at the active site. The results here underscore the sensitivity of intramolecular signaling and catalysis to native protein dynamics that arise from modest changes in allosteric regions while providing a potential strategy to alter intrinsic activity and signaling modulation.

INTRODUCTION

Like its substrates, Csk possesses N-terminal SH2 and SH3 domains (Figure 2-1) [48]. A notable difference between SFKs and Csk is the tertiary arrangement of the SH domains [49] and the absence of activation loop phosphorylation in Csk. The kinase domain of Csk requires activation by the peripheral motifs and SH2 and SH3 domains, whereas these domains are important for localization and activity repression in SFKs via binding the phosphorylated tail [49]. Biochemical and structural characterization of SH2 and SH3 modules of many proteins is

abundant in the literature as these domains have been utilized extensively to investigate protein folding and stability [50–52], thus providing a rich database that enables further nuanced exploration. Recently, discoveries of unique and non-canonical modes of intramolecular dynamic regulation by these domains [53] may be taken as evidence that our understanding of how modular kinase domains collectively function within a macromolecular assembly remains in its infancy.

As Csk orchestrates the activity of all SFKs, the quest to understand how the non-catalytic domains in Csk enhance its catalytic efficiency is of paramount importance. The classical approach taken in previous studies is based on modifying predicted or known interdomain contacts between the SH modules on one hand and the kinase domain on the other [54–58]. These studies successfully identified several key residues and motifs essential for relaying signals from peripheral regions to the active site. The SH2 domain is central to Csk's function whether it is direct activation via the small kinase lobe interactions on the interface [56,58] or the binding of phosphotyrosine ligands like Csk Binding Protein (PAG/CBP) that was shown to transmit its activating signal via the SH2-Kinase linker [59]. In addition, mammalian Pragmin and bacterial peptide effectors possessing the EPIYA sequence competitively interact with Csk via the SH2 domain and binding of the bacterial motifs may lead to Csk's recruitment to the membrane and down-regulating SFKs to facilitate infections [60].

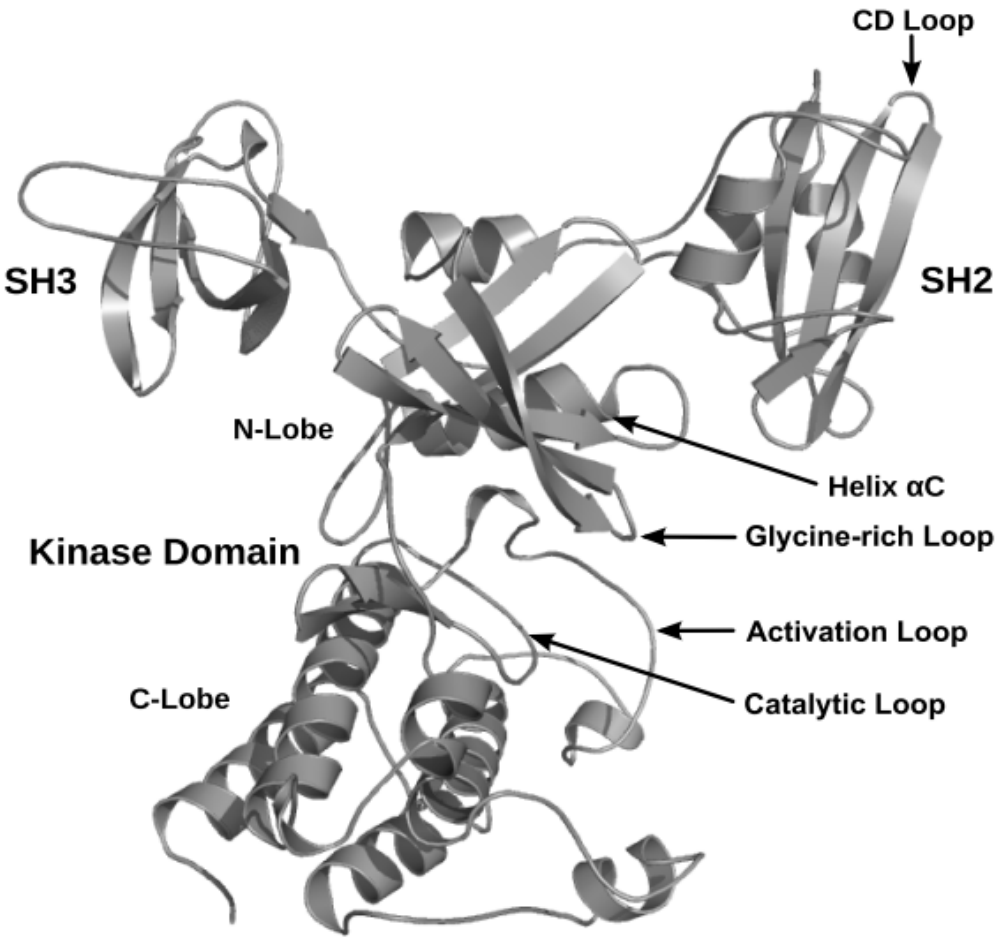

Figure 2-1. Csk's structural and functional motifs

Structure and domain arrangement in full-length Csk (PDB ID 1K9A). Functional elements important for catalytic function are annotated.

An important allosteric site within the SH2 domain is its unique disulfide bridge whose redox state can provide further intramolecular activity modulation [47]. Perturbations to these sites within the SH2 domain or its flanking linker regions, which are removed from the active site, produce effects in local and global flexibility and in turn influence enzymatic efficiency. A close inspection of homologous kinases shows subtle yet notable differences between the SH2 domains of tyrosine kinases. Examples of such variations are shown for Csk, Src and Itk in Figure 2-2. While the global fold and structural elements in the domain are conserved, distinct differences are apparent in loops/turns connecting the central antiparallel beta strands. All-atom MD suggested communication between the CD/DE loops and that tethering the Csk SH2 domain is important in regulating activity [47], our approach involved emulating a more flexible CD loop as observed in Src and Itk in the SH2 domain of Csk and monitor the effects on kinase activity and structure. For Itk, proline-mediated switching of loop conformation was shown to be responsible for conformer-specific ligand recognition [61]. Importantly, our approach does not interrupt native contacts between the SH2 and kinase domain and preserves the overall fold and domain arrangement of Csk. Using glycine insertion has the added advantage of introducing loop flexibility while minimizing the impact on secondary structure formation. Using a combination of theoretical and experimental techniques on the isolated domains and the intact protein, we found that our loop variant did not alter the global fold of the isolated SH2 domain or full length Csk. However, the double glycine insertion in the SH2 domain loop at a site greater than 45Å from the active site reduces the catalytic activity. Given that PAG/CBP's interaction with wild type Csk via the SH2 domain does not affect the catalytic rate but the apparent affinity of Csk towards Src is increased [59], the SH2 domain can potentially serve both as a hub for *activating* and *deactivating* the kinase. Taken together, we show experimentally that a

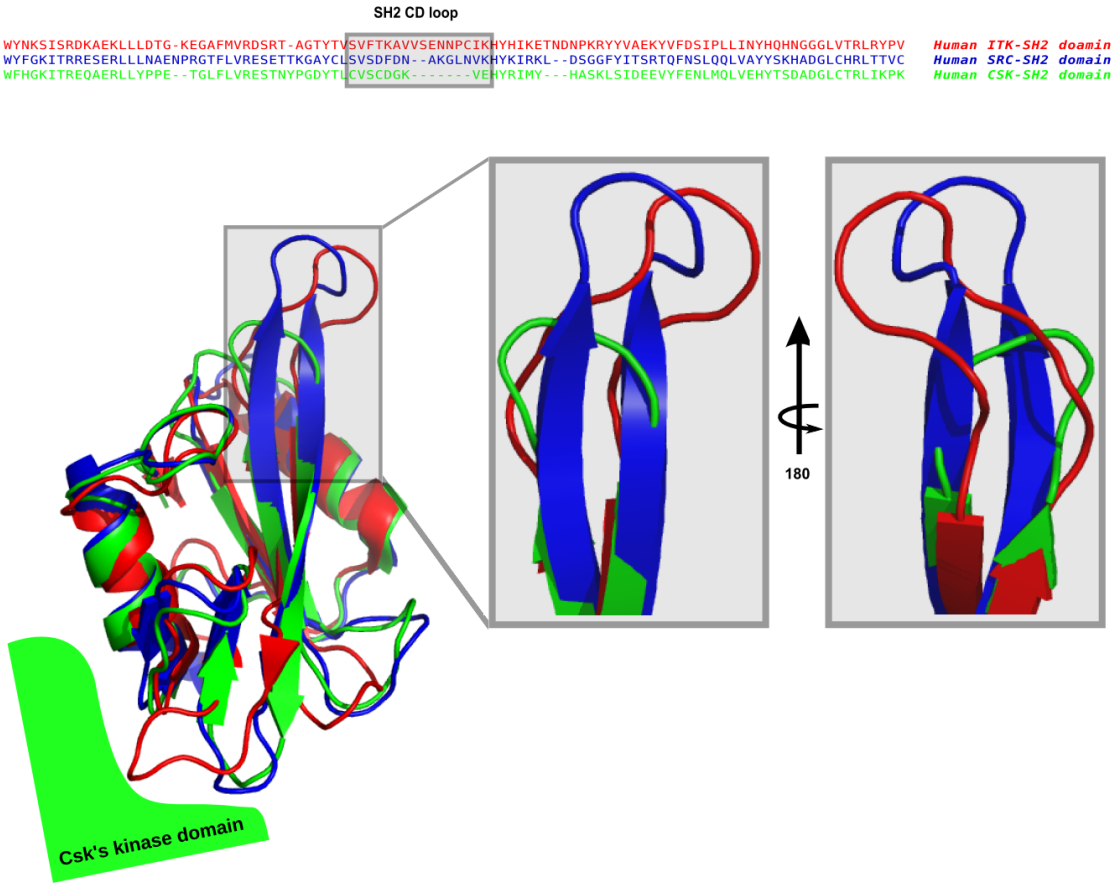

Figure 2-2. Sequence and structural alignment of SH2 domains of homologous kinases

Itk (red), Src (blue), Csk (green) illustrating the stark differential loop lengths among these domains. Most notably, Csk possesses the shortest CD loop (turn) of the three modular domains. Sequence alignment was performed using Clustal Omega through UniProt web server. Structural alignment was performed in PyMol using PDB entries 2ETZ, 2SRC, and 3EAC for Itk, Src, and Csk, respectively.

seemingly subtle distal perturbation to the framework of the enzyme can lead to reduction in catalytic activity while our computational methods outline the network paths that may facilitate such long-range communication between remote regions in the enzyme.

RESULTS

Characterizing the Stability and Folding of the Csk SH2 Domain and its loop variant

Equilibrium Unfolding

The folding and stability of the WT and variant SH2 (SH2-GG) domains of Csk were investigated by performing a chemical unfolding titration using Guanidine Hydrochloride. The unfolding titration curves shown in Figure 2-3 indicate that the variant domain is slightly less stable than the wt protein. fitting the data to a two-state model [62] yields a difference in ΔΔG of ~2kcal/mol.

The variant SH2 domain was generated by inserting two glycines between residues Gly124 and Lys125 using site-directed mutagenesis protocols. Chemical denaturant-induced equilibrium unfolding studies on the expressed variant indicate that elongating the CD loop in Csk's SH2 domain does not interfere with the ability of the isolated domain to fold. A comparison plot of the fraction of folded protein (F_{app}) as a function of final denaturant concentration for the wild type and variant SH2 domains is given in Figure 2-3. A cooperative unfolding transition is observed for both the wild type and the variant SH2 domains. The variant shows destabilization with respect to the wild type domain, with transition midpoints of 2.9M and 3.6M Guanidine-HCl, respectively, and a calculated destabilization free energy of ~1.5 kcal/mol. This small apparent change in stability does not suggest a change in the folding of the domain.

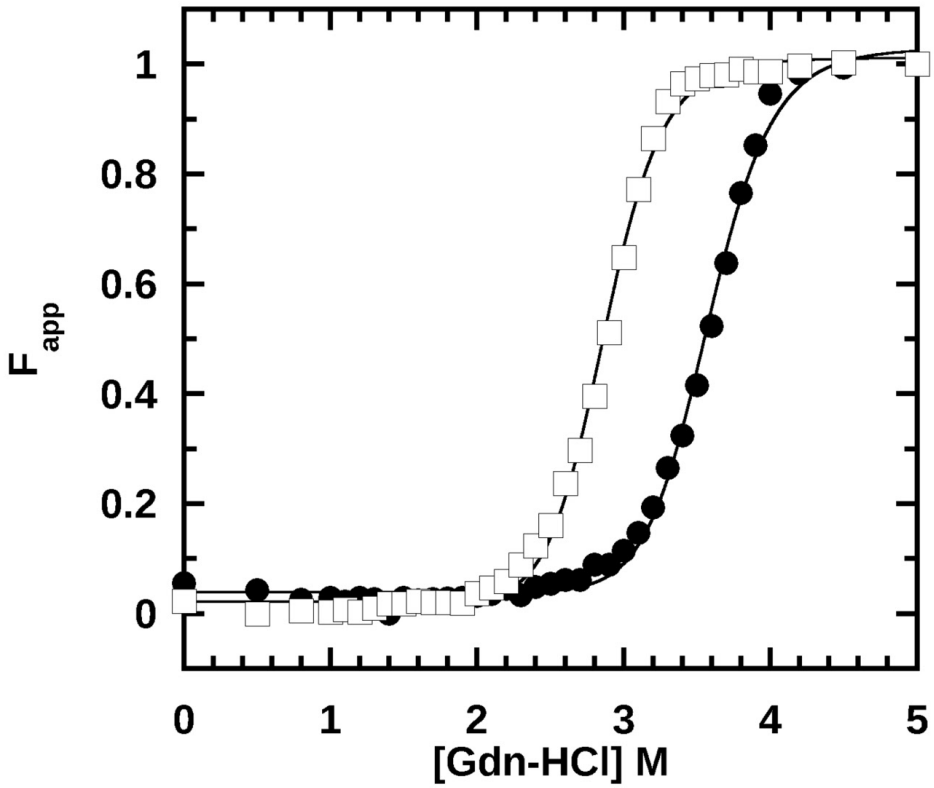

Figure 2-3. Equilibrium Unfolding Titration of wild type and variant Csk SH2 domains

The stability of the SH2 domains is measured as a function of chemical denaturant concentration. Csk's variant SH2 domain (□) is slightly less stable than the wild type (●) by a ΔΔG of ~1.5 kcal/mol. The calculated value was determined as described in methods.

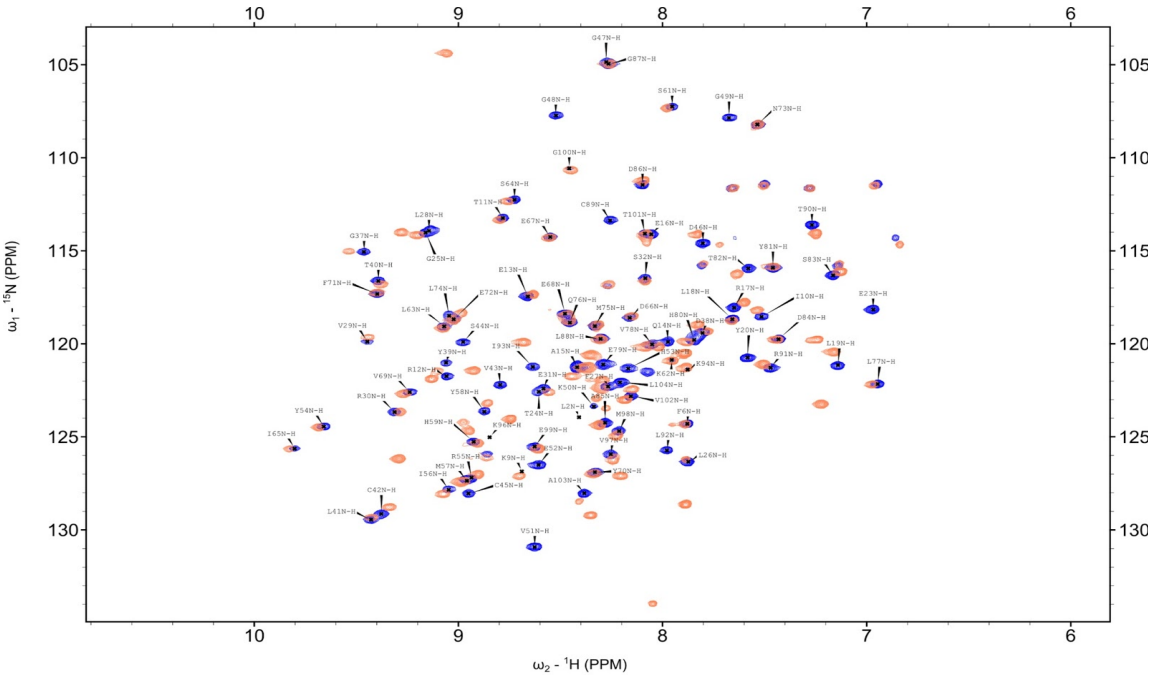

Figure 2-4. Comparison of the global fold of SH2 domains

Overlays of the ^{1}H-^{15}N Heteronuclear Single Quantum Correlation (HSQC) spectra of wild type (pink) and variant (blue) SH2 domains. The observed chemical shift dispersion indicates retention in globular domain fold. Differences in backbone amide resonances indicate that regions around the insertion site are affected by the CD loop elongation. For clarity, backbone amide assignments are shown for the variant (SH2-GG) domain only.

NMR spectroscopy

Resonance Assignments

To verify that the global fold of the SH2 domain remains intact, we employed ^{1}H-^{15}N Heteronuclear Single Quantum Correlation (HSQC) NMR spectroscopy. An overlay view of HSQC spectra of the two domains is given in Figure 2-4. The overall chemical shift pattern observed for the SH2 domain variant is similar to that observed for the wild type domain and is indicative of a well-folded protein. The largest chemical shift changes observed in the variant map to the site of insertion and nearby motifs. The integrity of the unique disulfide bridge between C122 and C164 remained intact as judged by chemical modification and by the unique cysteine beta carbon chemical shifts [63].

Subsequently, resonance assignments were completed using standard NMR techniques for further solution characterization of SH2 domain dynamics. Preservation of secondary structure elements of the SH2 domain are confirmed by chemical shift information when compared to random coil shifts. A chemical shift index plot is shown in Figure 2-5 and confirms that a canonical SH2 fold (central beta strands flanked by two helices) is retained.

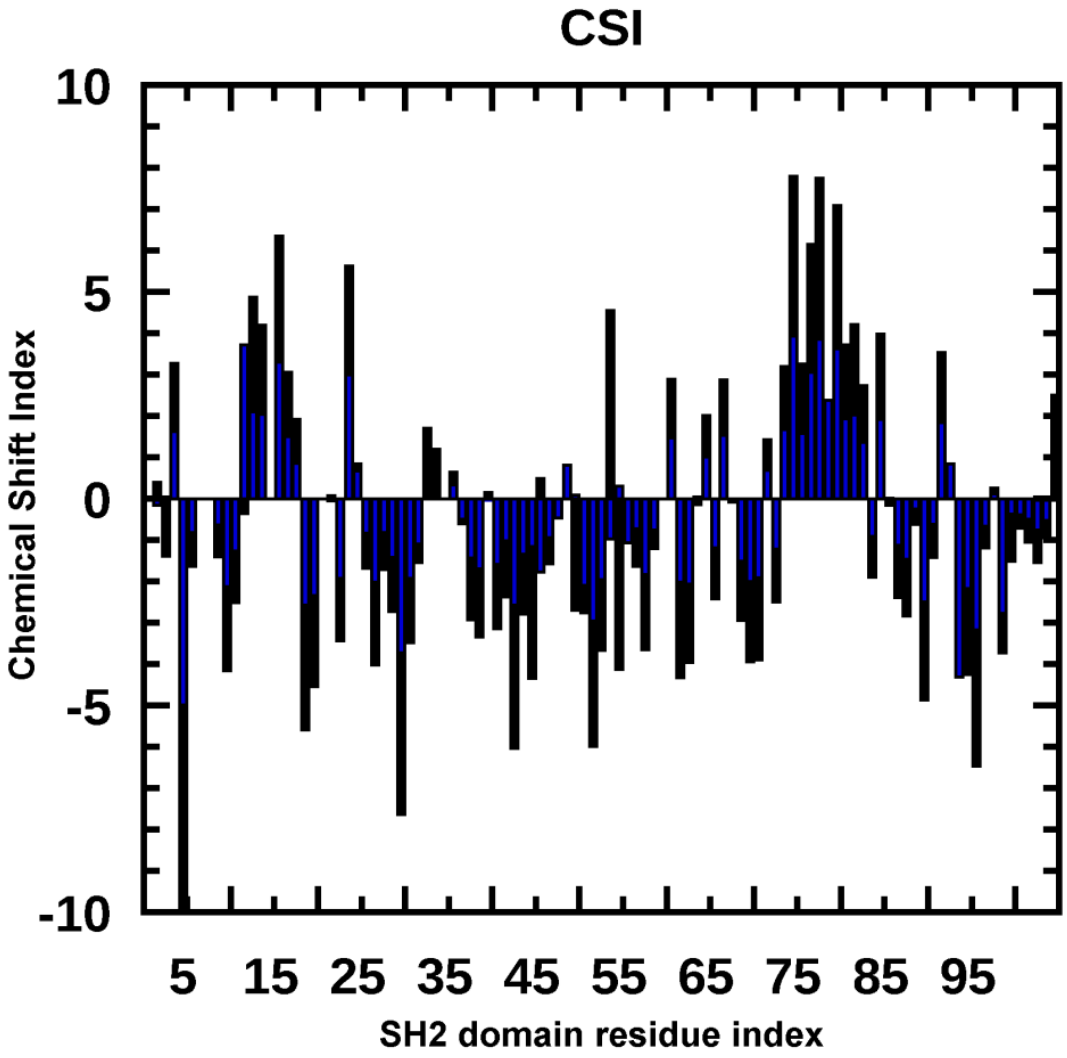

Figure 2-5. Chemical Shift index for WT Csk-SH2 (black) and Csk-SH2-GG (blue)

CSI is plotted as a function of residue number of the SH2 domain. positive values are indicative of alpha helical secondary structure while negative values indicate beta strand propensities.

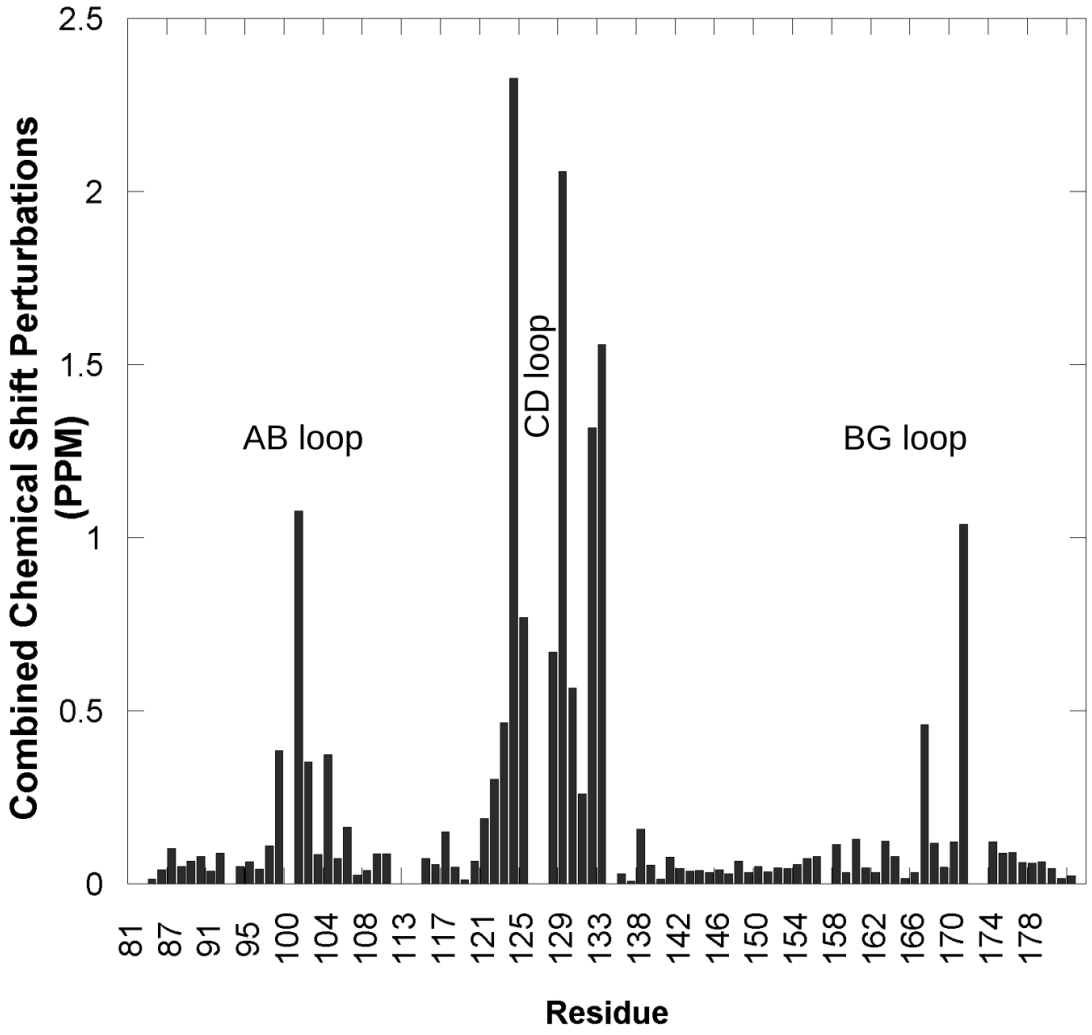

Figure 2-6. Chemical shift perturbations observed upon CD loop elongation

The Gly-Gly insertion caused chemical shift changes to amide resonances of residues that are spatially proximate to the CD loop.

Chemical Shift perturbations (CSP) and domain structure prediction

Chemical shift perturbations due to the GG insertion are observed in the overlaid spectra in Figure 2-4. The CSP plot (Figure 2-6) shows that the largest differences are localized in and around the CD loop region and the spatially proximal regions. Additionally, ^{13}C, ^{15}N and ^{1}H chemical shifts and sequential homology chemical shifts were used to predict the structure of the WT and variant domains using SHIFTOR [64].

Figure 2-7 shows the local structure around the CD loop with marked difference in loop orientation. Overall, the chemical shift differences (Figures 2-7; 2-8) and the destabilization seen in the unfolding titrations indicate that the native folds of WT SH2 and the GG variant are not affected; however, variances in dynamics between the two are strongly implied.

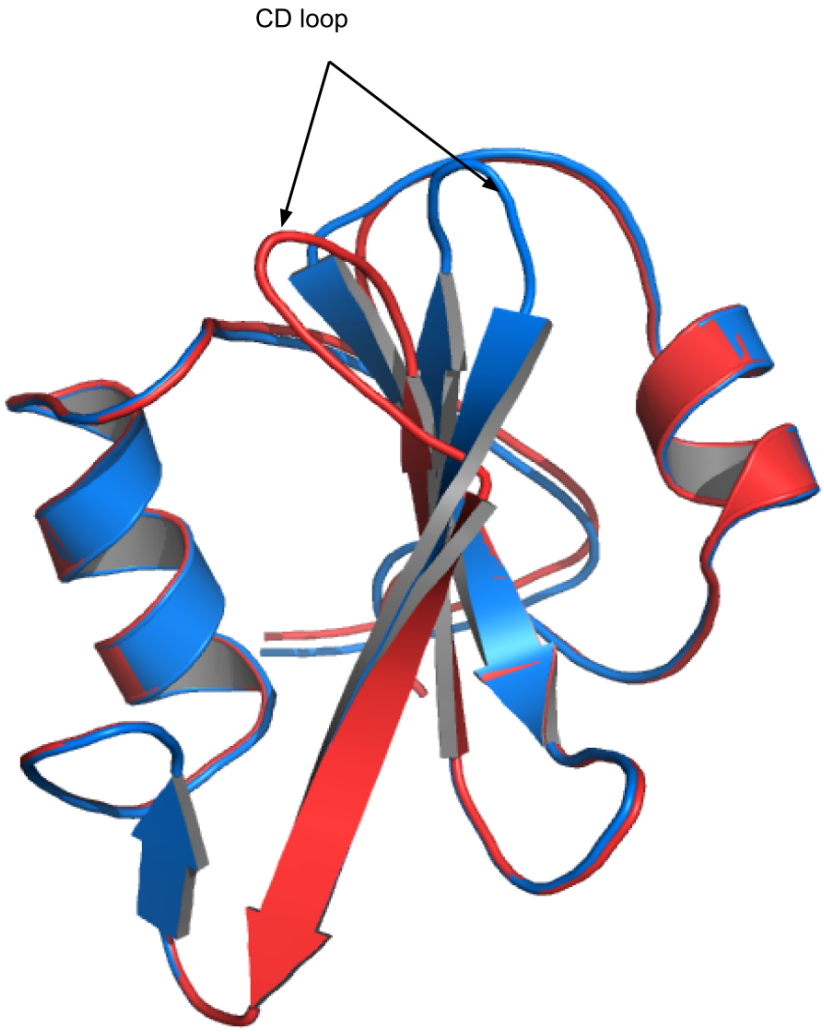

Figure 2-7. Predicted loop structures based on chemical shifts

Chemical shift and sequence homology were used as input to predict the structural variations between WT-SH2 (blue) and SH2-GG (red) using SHIFTOR.

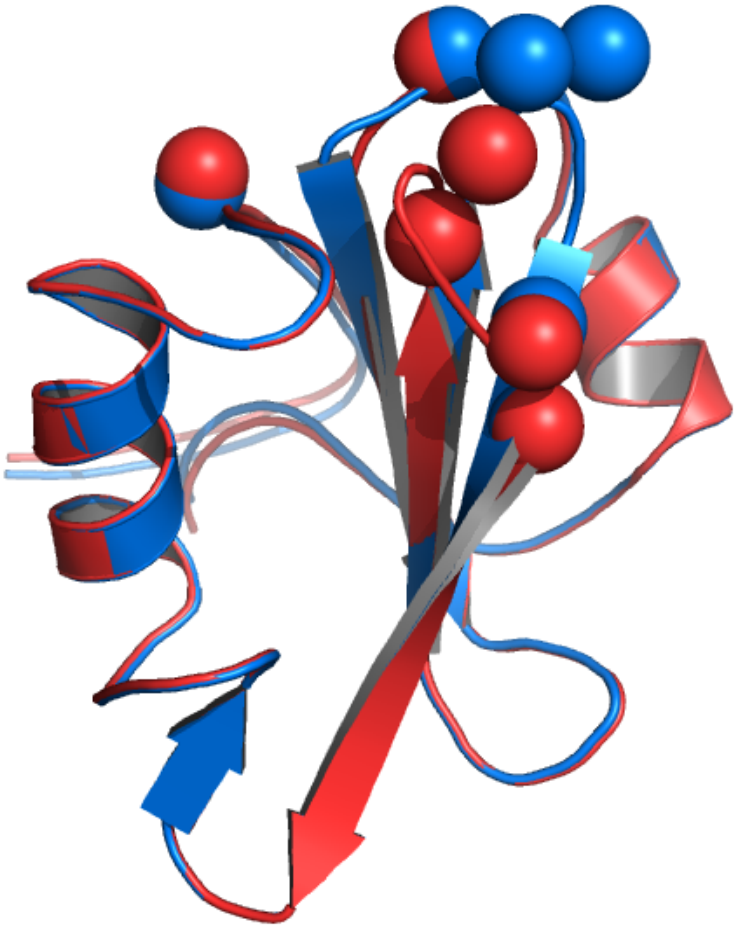

Figure 2-8. Structure-modeled CSP between WT and Varinat SH2

The most significant chemical shift perturbations due to loop elongation are plotted onto the predicted structures of WT and variant SH2 domains. Cα atoms are shown as spheres for the same residue in both domains.

HDX-NMR

While the SH2 domain structural fold was maintained upon insertion, this modification alters the global stability of the intact domain. The structural determinants of this destabilization were further explored by monitoring site-specific Hydrogen-Deuterium Exchange (HDX) rates for individual amide protons within the two domains by NMR. This experiment involves initiating an HDX time course by placing the purified protein in ~99% deuterated buffer and monitoring the change in intensities of backbone amide resonances over time by recording a series of sequential ^{1}H-^{15}N HSQC spectra. Plots of resonance intensity over time are indicative of the stability of individual sites (see [43] and references therein for full review) and can be compared between wild type and the variant domain. The results of these studies are shown in Figures 2-9; 2-10. Areas colored in red indicate destabilization, blue indicates stabilization, and yellow is for no change in protection against exchange. Changes in exchange rates are observed not only around the CD loop region (insertion site) as expected but also distal to this site with deprotection observed for probes that map to the αB and SH2-Kinase interface (surrounding the DE loop) whose hydrophobic minicore is known to be important for cross-domain communications [56,58] and is a good candidate for potential allosteric regulation of kinase activity.

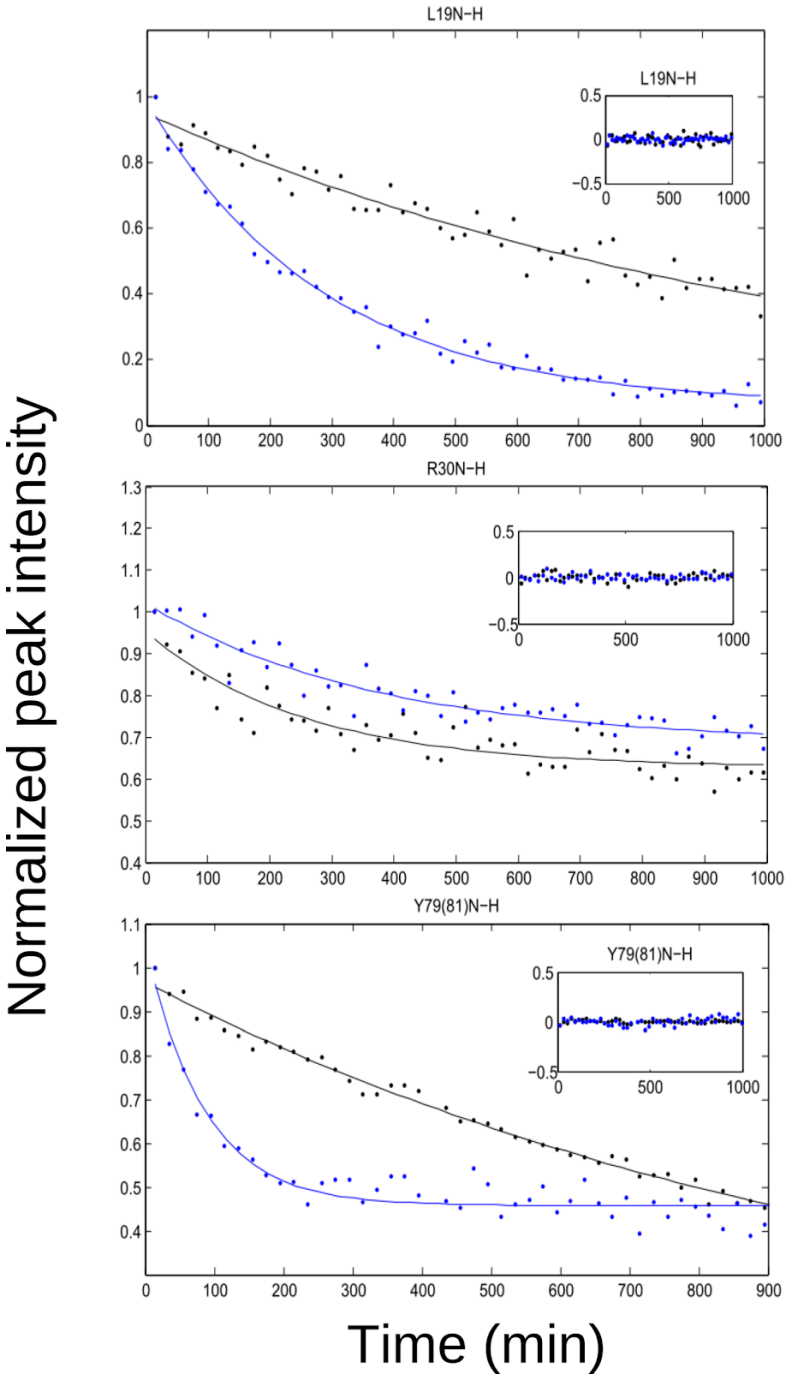

Figure 2-9. HDX decay plots for select sites in SH2 domains

Exchange profiles for select residues in WT SH2 (black trace) and SH2-GG (blue traces) Normalized peak intensities from HSQC spectra are plotted as a function of detection time post deuteration. The data is fitted to a single exponential function to obtain apparent exchange rates.

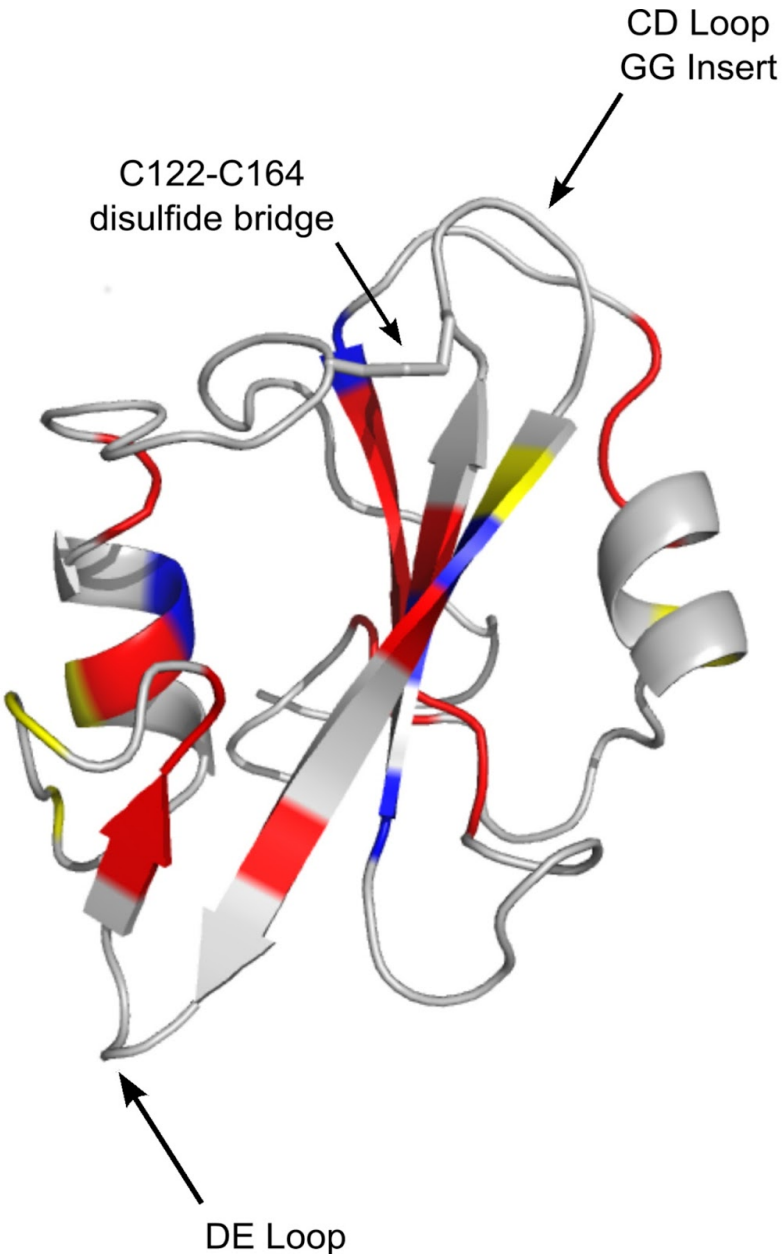

Figure 2-10. NMR detected Hydrogen-Deuterium exchange in SH2 and domain dynamics

Residue-specific Hydrogen-Deuterium exchange (HDX) effects mapped on the structure of Csk's SH2 domain. Red indicates faster exchange with solvent deuterons in the variant domain with respect to wild type while blue indicates slower exchange. Yellow indicates backbone amides that exhibit the same degree of protection while residues in gray indicate absence of probes whose exchange is too fast to measure. The unique disulfide bridge in Csk's SH2 domain and the CD loop are shown.

CD Loop Elongation Preserves Fold but Affects SH2 Dynamics and Stability

In general, global domain destabilization observed in the unfolding titration (Figure 2-3) is not manifested by global faster exchange as might be expected but revealed as a more complex mix of faster exchange together with unaffected as well as stabilized sites within the central beta sheet and interacting α-helices. This behavior was also observed previously in another context, and may be a reflection of the unique role of Csk's SH2 domain in relaying information from the periphery to the central active site within the intact kinase [47,65]. In an effort to determine whether incorporation of the Gly-Gly insertion into the SH2 domain in the *full length protein* altered the conformation of the kinase, circular dichroism (where the signal is dominated by the large lobe of the kinase domain) and further native state HDX studies (see below) were conducted. The data indicate the full length kinase's helical content is maintained by the double glycine insertion as both the wild type and variant Csk proteins show equal molar ellipticities with overlapping double minima Figure 2-11.

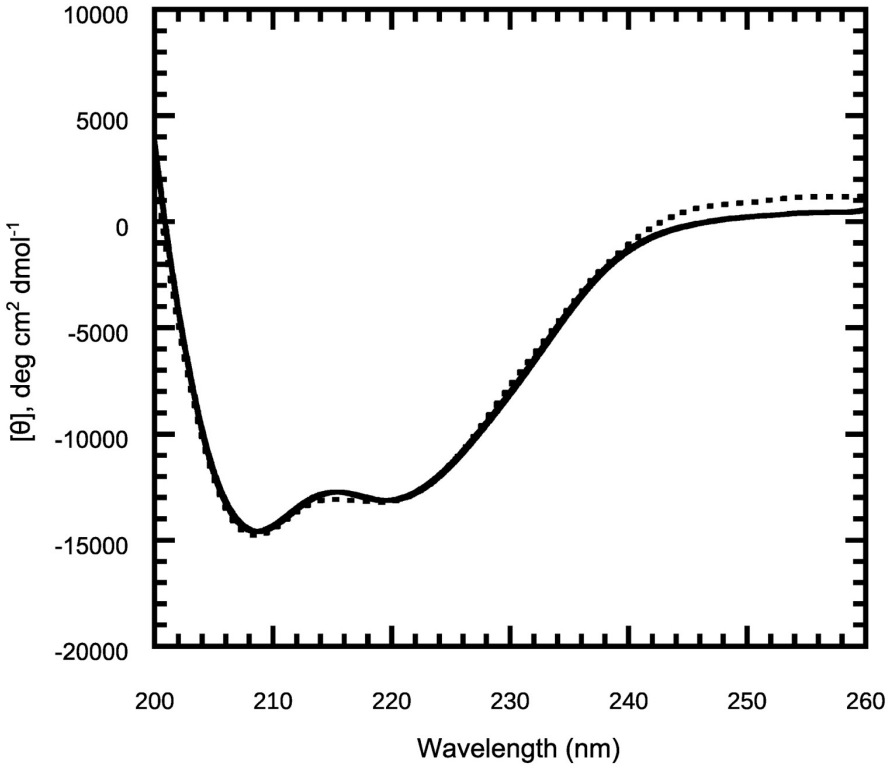

Figure 2-11. Circular Dichroism spectra show the full-length variant is folded

Wild type Csk (solid) and the variant (dashed) have similar CD signature spectra. The two minima at equal molar ellipticity value is indicative of a folded enzyme with dominant alpha-helical secondary structure.

Steering the Kinase Activity by Distal Loop Elongation

Proximal regions to the active site have significant influence on the catalytic activity of protein tyrosine kinases [66]. For example, the activation loop in Csk, which lacks a phosphorylation site, maintains functional importance as an inhibitory structure within Csk's catalytic machinery [36,67]. In addition, an interesting observation from the crystal structure [68] of Csk is the presence of two distinct conformations for the SH2 domain. The "down" conformation indicates extensive SH2 domain contacts with the small lobe of the kinase domain and was proposed to influence the ordering of the functionally important αC motif. Further exploration of proximal regions via site-directed mutagenesis and alanine scanning studies has identified contacts that are deemed essential for kinase activation via the SH2 domain.

As a modular enzyme, Csk's domain linkers also play key roles in domain packing and arrangement of the active kinase conformation [49]. A specific site in the SH2-kinase linker (residue 183), which packs against the small lobe of the kinase domain, is very sensitive to the size of its side chain (Phe in wild type Csk) and is essential for functional flexibility and Csk activation via the SH2 domain [59]. These studies formed the framework for understanding how docking interactions between regulatory sites coordinate to control catalysis in Csk.

In a departure from the investigation of directly coupled functional motifs in regulating activity, we identified that the redox state of the unique disulfide bridge in the SH2 domain of Csk that links the CD loop to the SH2 kinase linker modulates kinase activity [47]. This important allosteric site is 45Å removed from the active site. Here, we focused on the properties of solely the CD loop region in the SH2 domain as this motif shows significant variance among homologous kinases (Figure 2-2). Interestingly, in Itk this loop is an important motif for recognition gating [61]. Rather than adaptor recognition, we hypothesized that this loop would be an important regulator of the active site in Csk based on earlier theoretical and experimental studies [47]. To determine the effects of loop elongation on substrate and scaffold binding as well

as kinase activity we employed a variety of kinetic and thermodynamic techniques. Csk's time-dependent phosphorylation of its physiological substrate, Src, was monitored in a [γ-^{32}P]-ATP radioactive assay. In all assays, a kinase defective Src (kdSrc) is used to eliminate the possibility of substrate autophosphorylation and interference [69]. A plot of the γ-^{32}P incorporation into Src as a function of time for both Csk proteins is given in Figure 2-12

Incorporation of γ-^{32}P into kdSrc for the variant was reduced by approximately 3-fold compared to wild type Csk. Consistent with the observation that Csk utilizes substrate-assisted catalysis [70], phosphorylation of the generic poly(Glu_4Tyr) kinase substrate is also reduced, though to a lesser extent (Figure 2-13).

The slower observed rate of phosphorylation by the variant Csk could be a function of reduced substrate binding and/or catalysis. To determine what limits catalysis in the variant, we performed comparative studies for substrate binding. Initial velocity plots of the observed rate as a function of both substrates (kdSrc and ATP) binding for the wild type and variant are given in Figure 2-14. The affinities for either phosphoryl accepting or donating substrates seem unaffected (within error) for the variant. Therefore, enzyme-substrate complex formation is not responsible for the observed phosphorylation rate reduction.

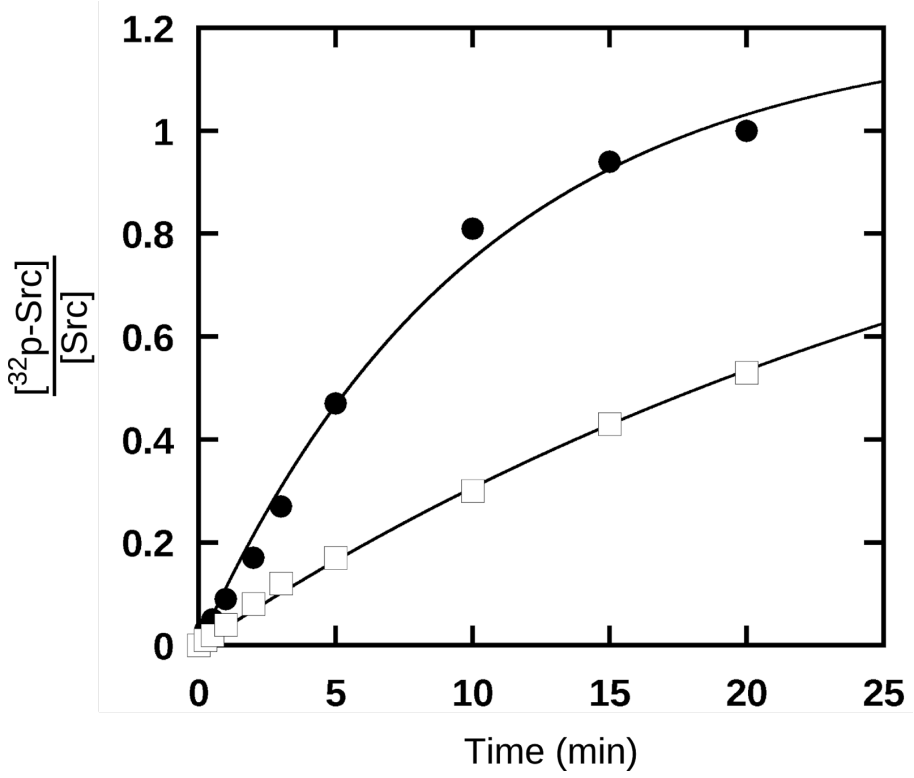

Figure 2-12. CD loop elongation in the SH2 domain reduces Csk towards Src

WT Csk's (circle) and the variant's (square) kinase activity was monitored in a [γ-^{32}P]ATP coupled radioactive assay in which a kinase dead substrate (kdSrc) is phosphorylated as a function of time.

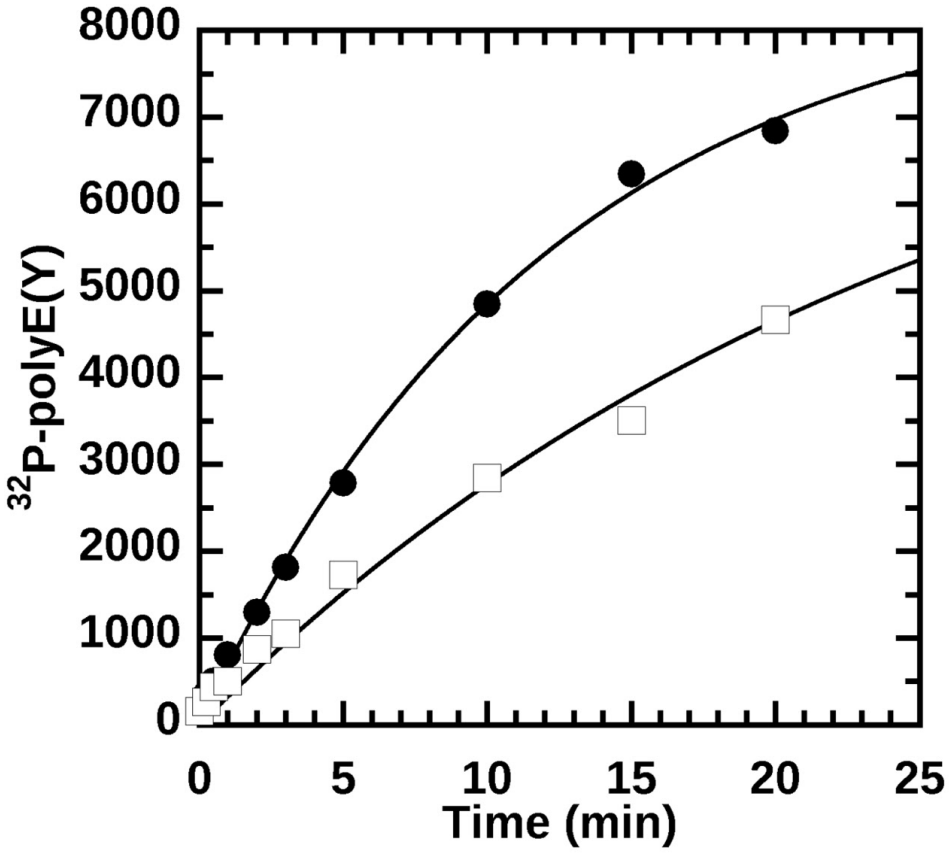

Figure 2-13. Reduced kinase activity of full length Csk towards a generic substrate

WT Csk's (circle) and the variant's (square) kinase activity was monitored in a [γ-^{32}P]ATP coupled radioactive assay in which a generic kinase substrate (polyEY) is phosphorylated as a function of time. The reactions typically included 200 nM Csk, 2 mg/mL polyEY, and 50 μM ATP at 23°C.

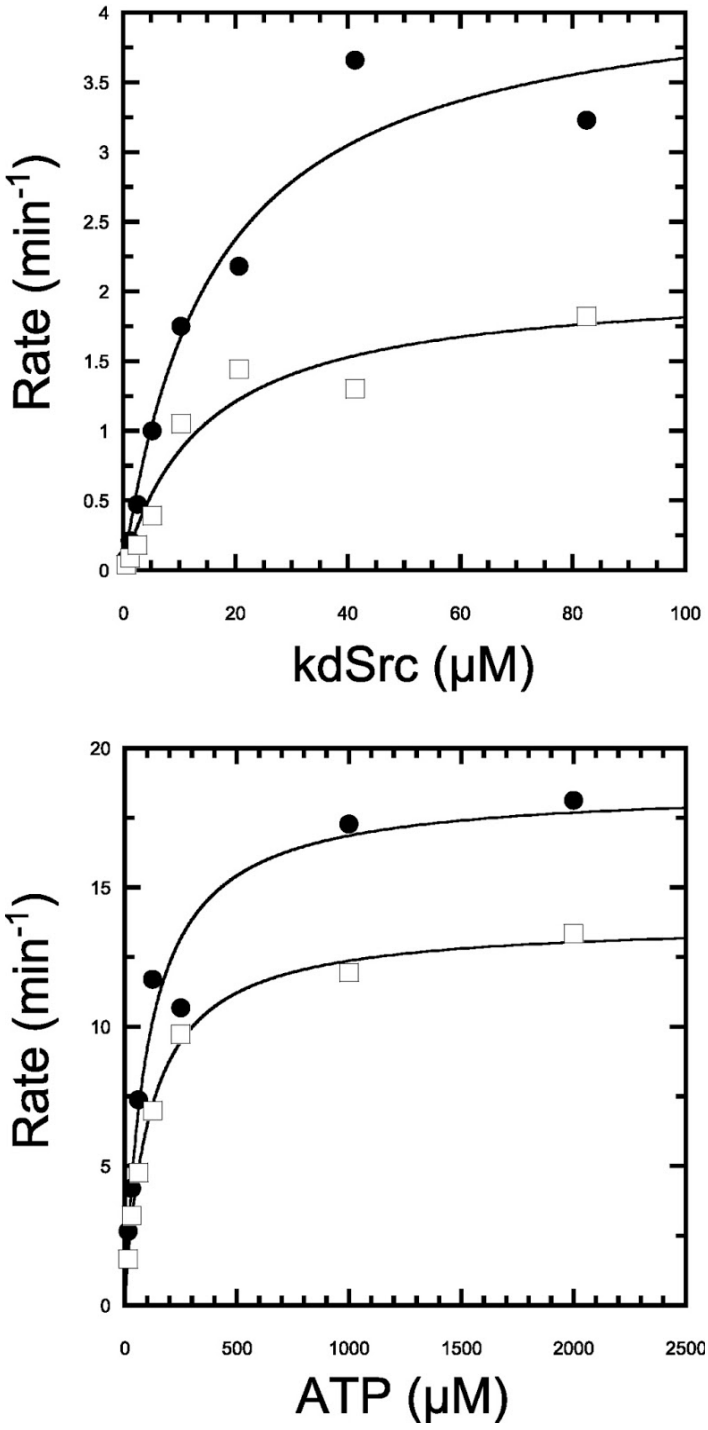

Figure 2-14. Km(s) of substrates

Rate of substrate phosphorylation is measured as a function of substrate concentration for Csk's physiological substrate Src (top) and ATP (bottom). Initial velocities were determined after incubating Csk or the variant (100 nM) with kdSrc or ATP for 6 minutes before quenching.

In addition, a peptide derived from the membrane-anchored Csk binding protein (CBP), which up regulates Csk by binding to its SH2 domain, activates both the wild type and variant enzymes to the same extent. Thus, the loop elongation does not appear to have a significant effect on how CBP activates Csk via the phosphotyrosine-SH2 interaction. Since maximum turnover is limited by a conformational change in Csk [70], we suspect that the decreased rate for the variant is the result of changes in overall protein dynamics.

Deuterium Exchange Mass Spectrometry (DXMS) of Native State Dynamics

Previous studies have shown that reduced flexibility in Csk can result in dramatic decreases in kinase activity (Phe183Gly). In addition, alterations in stability can perturb the interconversion between active and inactive forms of Csk within the native ensemble [71]. To determine if the overall conformational ensemble is altered in Csk we utilized DXMS methods to explore the native state dynamics of the enzyme and its variant. In this experiment a fragmentation map is established for the protein as described [72]. The non-deuterated protein is exposed to deuterated buffer for varying amounts of time, and the mass of each peptide-probe is measured as a function of incubation time to determine the number of in-exchanged deuterons incorporated with respect to a fully protonated and deuterated probe (see Materials and Methods). Csk and the variant were first treated with a protease for digestion and the resulting peptide fragments were identified by sequence matching ([44], Materials and Methods); both proteins produced nearly identical fragmentation patterns, which allowed for optimal analysis by DXMS. Incubation of the proteins in deuterated buffer led to increases in mass envelopes of identifiable peptides due to deuterium incorporation as shown for a representative probe from the variant and the wild type protein in (Figure 2-15). These time-dependent analyses were performed on fragments that cover most of the protein's sequence.

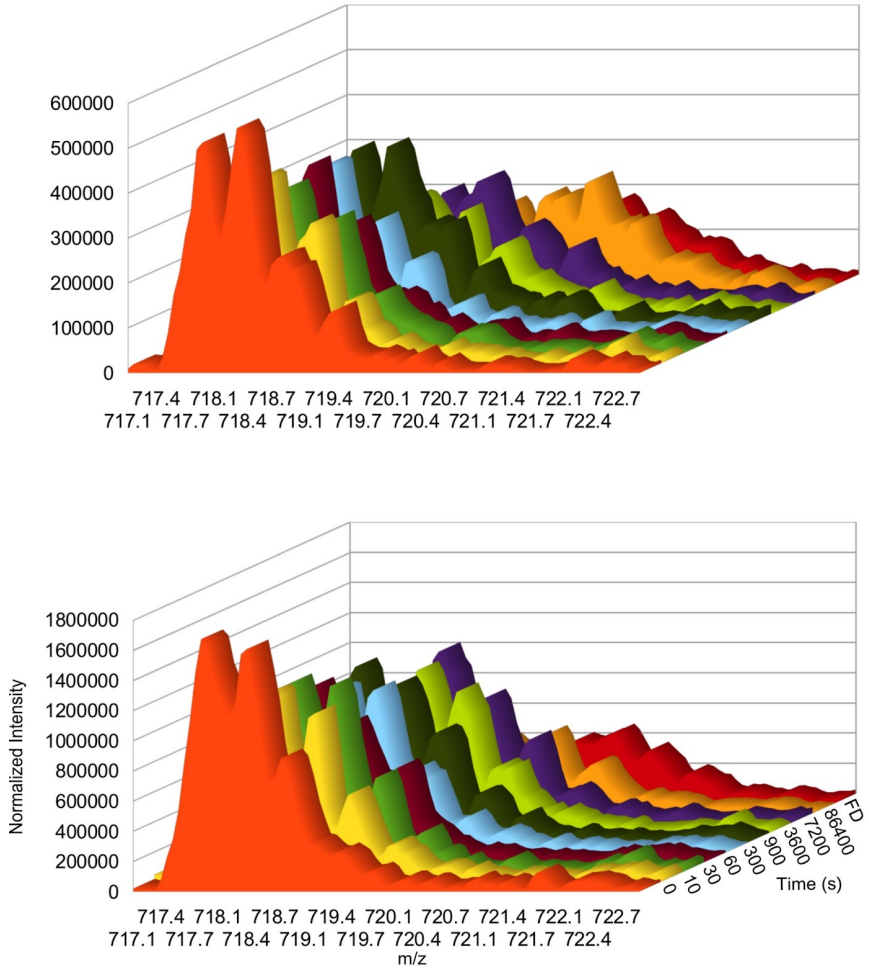

Figure 2-15. Representative time-dependent solvent deuterium incorporation

Mass envelope shift of a representative peptide probe in wild type (WT-Csk, bottom) and variant (Csk-GG, top) is indicative of the differences observed for time-dependent incorporation of solvent deuterons into the probe E93-F104. The key on the right shows color-coded time-points corresponding to mass spectra in each graph that show deuteration mass envelope of the same peptide in both the wild type and the variant Csk.

Comparative color-coded heat maps for the variant and wild type are given in Figure 2-16 and illustrate the relative deuteration levels for the detected probes in both wild type and variant Csk. Several significant regions of the protein are influenced by the insertion and clearly show differences in the rates of deuterium incorporation as a function of time. The blue and red arrows in indicate some of these notable segments. An expected difference is noted for the regions flanking the insertion site in the CD loop and show faster exchange relative to the wild type protein. The sequence in this region corresponds to the C, D, and E β-strands of the SH2 domain, which agrees with the residue-specific HDX profiles from the NMR-detected exchange on the isolated domains. Slower exchange (consistent with stabilization) is noted for peptides that are part of the kinase domain of Csk.

Plots of the number of deuterons as a function of time for specific motifs that are important for localization, regulation and kinase activity are given in Figure 2-17. Regions in which dynamics are affected by the CD loop elongation include *deprotection* in the flanking strands around the insertion site (βC and βD) and in the alpha helix of the SH2 domain in contact with kinase linker. *Protection* is observed in the SH2-kinase linker, the beta structure of the nucleotide-binding lobe of the kinase domain, specifically, the phosphate binding motif (glycine-rich loop), the hinge linking the two kinase lobes, and the activation loop all show slower solvent deuterium incorporation in the variant. The absence of the activation loop from the crystal structure is indicative of its high mobility in the wild type protein and this is also observed in our DXMS studies as probes from the loop are readily deuterated to >50% within the first deuteration time point (10s) and computational studies agree with this interpretation (see below). Although experimental data we provide here indicate that Csk's catalytic efficiency in kdSrc phosphorylation is likely reduced due to disruption of coordinated motions in the native ensemble that are part of the catalytic

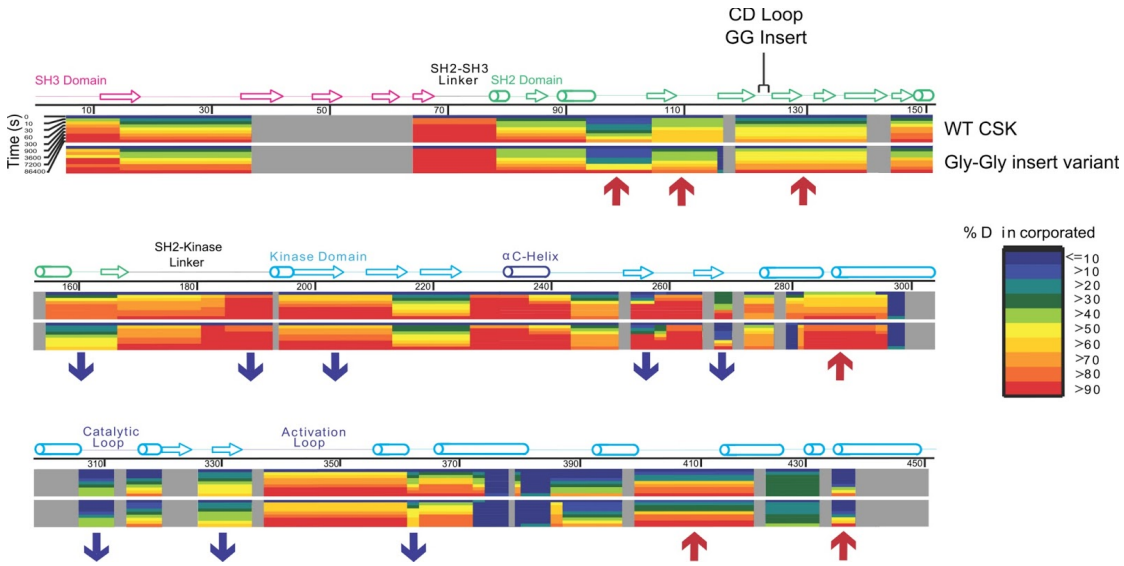

Figure 2-16. Heatmap schematic of % Hydrogen-Deuterium exchange showing relative amide proton protection from D_2O solvent in full length variant and wild type Csk

Color-coded blocks show levels of deuteration for peptide probes in wild type Csk (top row) and the variant (bottom row) as indicated on the right. Regions of secondary structure motifs and domains identified from the crystal structure are shown above the sequence. The figure was generated by mapping all reliably-identified peptides onto Csk's wild type sequence then overlaying the resulting blocks with exactly matching peptides that have the same mass, charge and retention times in LC-MS analysis for both proteins. The level of protection is indicated by coloring each peptide at any given time-point based on the maximum percentage of deuterons incorporated according to the key on the right. Observed differences are indicated with red upward arrows for segments that show relative deprotection while blue downward arrows indicate relative protection in the variant with respect to wild type. A difference greater or equal to 10% in protection is considered significant if observed in at least two time points. Gray blocks indicate absence of reliable probes for that part of the sequence. Peptide identification and analysis were performed after combining two independent pools of generated peptides for each of the wild type and variant Csk for verification.

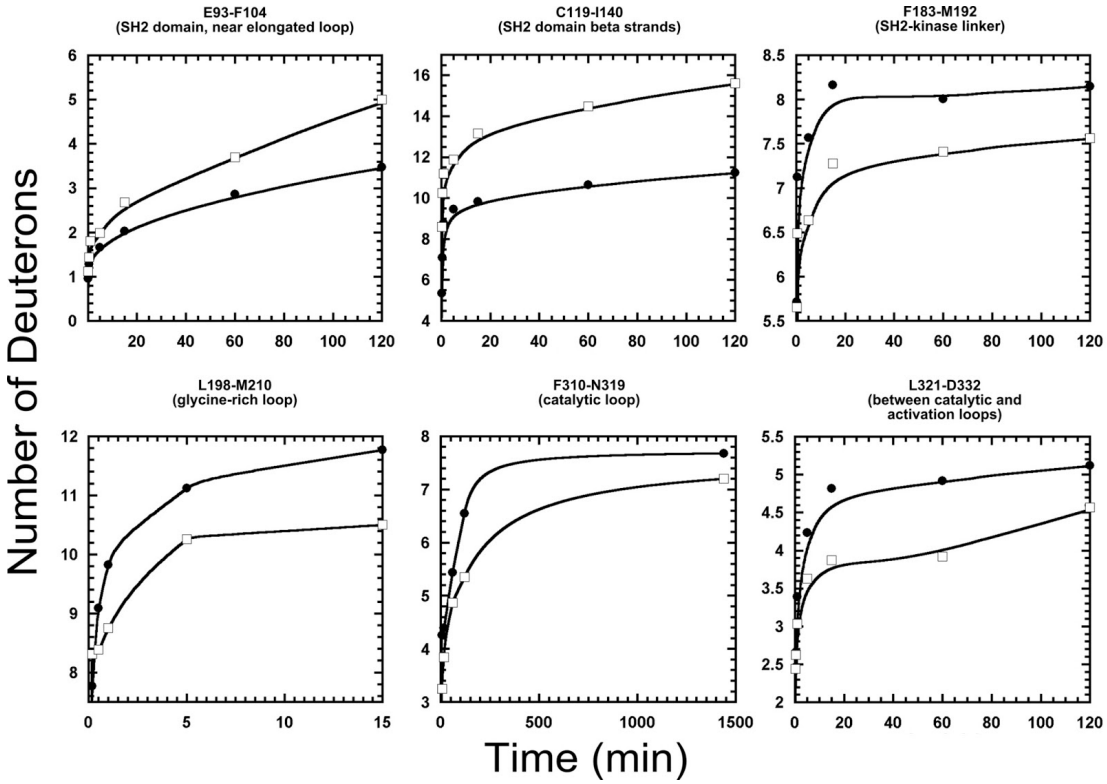

Figure 2-17. Effects of CD loop elongation on Time-dependent solvent Deuterium incorporation into Csk peptide probes

Deuterium incorporation into several probes in wild type (circle) and variant (square) Csk is plotted as a function of time. Data were obtained over time courses of 1440 minutes in deuterated buffer. Only relevant time frames are displayed for comparison and clarity. In general, a probe mass difference of 1 deuteron is considered significant between wild type and the variant if observed in at least two time points. Peptide identification and analysis were performed after combining two independent pools of generated peptides for each of the wild type and variant Csk for verification. Residue name and numbering are based on the wild type sequence.

machinery, the routes for such long range effects need to be elucidated. Therefore, we turned to recent advances in computational methodology and analysis [73] with additional tools to address that question with atomic details.

Experimental and Computational Studies Reveal Trans-domain Crosstalk Important for Catalysis

For an inherently complex system like Csk, where cross-domain communications are essential for function, computationally robust and statistically relevant tools are essential. Thus, to understand the coupling of distal residues to catalytic hubs in Csk, we employed Molecular Dynamics (MD) studies [74–76] by running four independent simulations for more than 100 ns each for the two proteins.

The eight simulations were first aligned to the crystallographic structure [68] used to build the system (PDB entry 1K9A; chain A). The root mean square fluctuations (RMSF) were computed for each individual simulation and then averaged for all trajectories. In Figure 2-18, we combine results of MD runs and DXMS experiments into a hybrid representation of the fluctuations observed in the full length protein. The relative difference we report here is the absolute divergence between the averaged magnitudes of fluctuations between the variant and wild type simulations. Thus, the thickness of the tube represents statistically significant divergence in fluctuations (backbone heavy atom RMSF values) observed in the MD simulations for the two proteins whereas the color gradient represents the observed protection differences between wild type and variant Csk in DXMS.

Interestingly, while the SH3 domain shows no significant differences in DXMS, simulations reveal a likely concerted motion of the SH3 domain as a whole unit giving rise to observed fluctuations as most of the residues exhibit high RMSF values and a form of periodicity (Fig. 2-18, boxed). MD fluctuations within the SH2 domain correlated well with hydrogen-

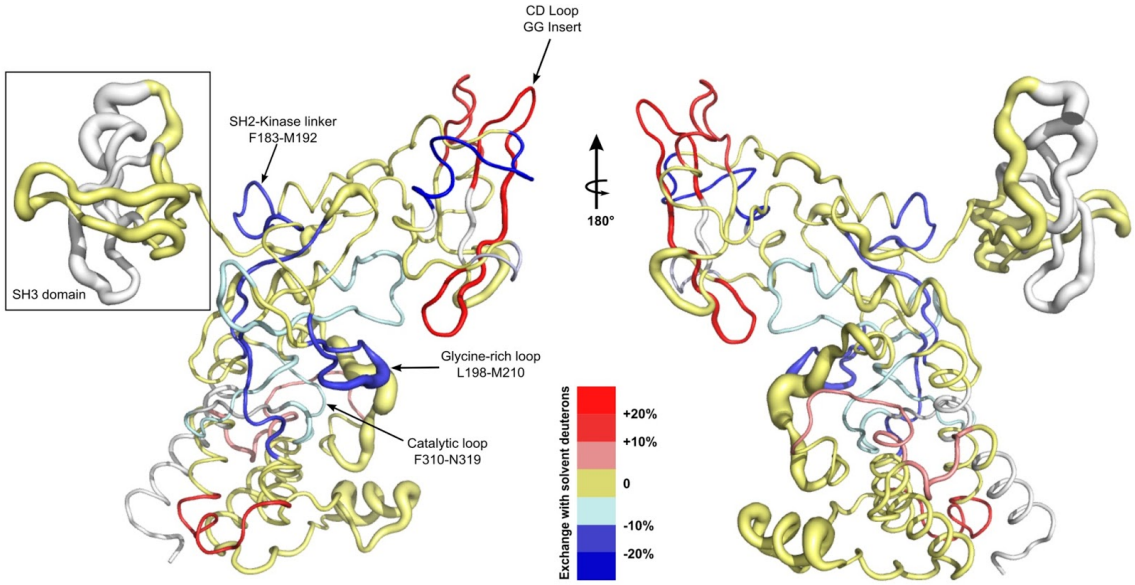

Figure 2-18. A combined representation of Molecular Dynamics simulations MD and DXMS data

Effects of SH2 domain's CD loop elongation mapped on a worm representation of the crystal structure of full length Csk. DXMS data are shown according to the key at the bottom. Protected regions are represented by the blue gradient for the variant with respect to wild type while deprotected regions are represented by the red gradient. Regions in gold represent probes that show no significant difference in protection between the wild type and variant and gray represents absence of reliable DXMS probes. Protection criteria and classification are determined as described in figures 3 and 4 and the methods section. MD data are represented by the most statistically relevant divergence in root mean square fluctuation (RMSF) for the backbone heavy atoms represented by the thickness of the worm at any given position. Important motifs and domains are annotated based on the crystal structure of Csk.

deuterium exchange results in several regions. Around the elongated CD loop, DXMS shows faster exchange in the variant relative to the wild type. Inspection of the MD trajectories shows that the reduced Cys122 is stabilized in the variant where this local stabilization is achieved by the formation of two hydrogen bonds: 1) between the backbone carbonyl of the cysteine residue and the backbone N-H group of the inserted Gly125′, and 2) between the backbone N-H group of Cys122 and the carbonyl backbone of Lys125. These bonds formed only transiently during the wild type simulations likely because of the shorter CD turn. While the short loop length in wild type may contribute to strain leading to higher RMSF values in the wild type, the formation of local backbone loop contacts may explain the corresponding loss of protection upon Gly-Gly insertion, which would allow for longer exposure of *surrounding* amide protons to solvent. Stabilizing effects are seen in other regions that correspond to distal motifs and are part of the catalytic machinery. Such long-range coupled effects underlie the intrinsic cross-domain communications that are integral to Csk's function as a multidomain enzyme [49]. Notably, the conserved Arg313 of the catalytic loop (*i*-1 to the catalytic base) is overall more stable in the variant trajectories than in the wild type. This is consistent with an *activation* loop that displays larger ranges of motion in the wild type that may sterically influence the apparent stability of the proximal Arg313 of the catalytic motif. Moreover, Phe183 is an important allosteric modulatory site in Csk [65]. While our simulations do not reveal significant divergence for this residue between the wild type and the variant, DXMS data indicate protection in the region (Figure 2-18, SH2-Kinase linker). Regions that do not show overlap or significant correlation between MD and DXMS most likely undergo motions on time scales that were not accessible in our 100 ns simulations, or are regions that lacked sufficient reliable probes in our DXMS experiments. Thus, the computational and experimental techniques are complementary. It is worth noting that residues 341-346 of the activation loop were modeled using *Prime* from the Schrodinger suite [77] since they are missing from the starting crystal structure. DXMS studies of wild type Csk

indicate high mobility of this loop and MD studies reveal that the identically modeled loop has an overall larger range of motion in the wild type simulations than in the variant, as did a small helix in the kinase domain (residues 393 to 403). Like the SH3 domain, this helix was observed moving as a unit and is proximal to the identified [35] substrate-docking site. On the whole, our experimental and computational studies highlight the importance of distal sites communications and sensitivity of Csk's activity to allosteric motif modifications; they also emphasize the usefulness of utilizing such complementary approaches in detecting intramolecular signaling networks.

DISCUSSION

Csk's kinase activity is dependent on its kinase domain interactions with the modular SH2 and SH3 domains. Previous mutagenesis and HDX experiments revealed the presence of communication networks across the protein framework by identifying important (and often conserved) residues in the linkers and domain interfaces that are akin to signaling hubs [46,56,58,65]. We utilized experimental and computational techniques to investigate the importance of an allosteric site in Csk's SH2 domain. It's interesting to note that in a recent study of a longer CBP peptide scaffold mimic, the BC loop is shown to be a novel, non-canonical binding motif that is important for tumor suppression [78]. Our MD studies show increased fluctuations in that region upon CD loop elongation highlighting the fact that conventional models do not fully explain SH2 domain regulation of Csk's activity. Indeed our data show that the enzyme's native dynamics are sensitive to changes in a region that is even farther removed from the active site (45Å) and respond to modifications to a variable segment in homologous SH2 domains. In addition to the SH2-kinase linker, the αC and β3 in the kinase small lobe are thought to be important anchors for residues that are essential for activation of Csk by its SH2 domain [58]. The reduced flexibility in the kinase small lobe is likely to have arisen from changes routed

to the active site via these motifs. We propose that the reduced flexibility observed in the small lobe of the kinase domain is responsible for the observed reduction in catalytic activity affecting k_{cat} but not substrate recognition. A conformational change in Csk was previously proposed to be a rate limiting step in the catalytic cycle [70], the observed changes in native motions are likely involved in that same rate limiting step for the variant. Moreover, the induced dichotomy in dynamics between the SH2 and kinase domains is in agreement with previous observations where mechanical stress in Csk was shown to be balanced along the framework of the protein [47]. Relieving loop strain and introducing new contacts in the SH2 domain could lead to disruption in balanced native stress within the SH2 domain which induces compensatory effects in the highly coupled framework of Csk. Thus, stresses seem to be tuned in Csk where increases in some regions are balanced by decreases in strain at other regions. Studies on dihydrofolate reductase have uncovered similar behavior in that enzyme where a network of coupled motions work cohesively to facilitate substrate binding and catalysis [79].

CONCLUSIONS

The scaffolding of Csk-CBP-SFKs system is thought to be essential for SFK inactivation. In modular proteins like Csk and Src, the SH2 domain is an essential molecular component for activation (Csk) or inactivation (SFKs) [80]. While the manipulation of scaffolding signaling pathways by domain swapping was proposed as a way to reshape cellular behavior [81], the approach requires switching whole components to achieve new signaling routes or alternative pathways. Coupling this strategy to conservative motif modifications (functional loop length engineering) that alter intrinsic activity may produce a more efficient signaling modulation and selectivity in more than one pathway.

MATERIALS AND METHODS

Protein Expression and Purification

The Csk SH2 domain and its variant (SH2-GG) constructs were expressed in *E. coli* strain BL21(DE3) in LB media. Cells were grown at 30°C, induced with 0.5 mM isopropyl-1-thiol-β-D-galactopyranoside (IPTG), and harvested after 18 hrs of incubation at 25°C. After cell lysis, WT-SH2 cleared lysate was loaded on a charged Ni^{2+} affinity column equilibrated with binding buffer (20 mM Tris, 500 mM NaCl, pH 7.9) and placed on a rocking platform at 4°C for 1 hr. The column was then washed with 5 resin volumes using wash buffer (20 mM Tris, 500 mM NaCl, 40 mM Imidazole, pH 7.9) and 2 resin bed volumes of elution buffer (20 mM Tris, 500 mM NaCl, 400 mM Imidazole, pH 7.9) was used to elute the proteins. The SH2-GG variant was purified under denaturing conditions where the cell pellets were solubilized in Buffer B (QIAGEN The QIAexpressionist, 5th edition) by stirring at room temperature for 45-60 min. The cleared lysate was loaded on a charged Ni^{2+} affinity column equilibrated with Buffer B and rocking at 4°C for 1 hr. Refolding was done by flowing 5 resin bed volumes of native binding buffer over the column. Subsequent purification steps were identical to that of WT-SH2 above.

C-terminus $(His)_6$ tagged full length Csk enzymes were expressed in *E. coli* strain BL21(DE3) (Novagen) expression vector were grown at 30°C, induced with 0.5 mM isopropyl-1-thiol-β-D-galactopyranoside, and harvested after 18 hrs of incubation at 25°C. The wild type and variant Csk enzymes were purified by affinity chromatography as follows: Harvested cell pellets was resuspended in binding buffer (50 mM Tris, 20 mM Imidazole, pH 8.0) and lysed by sonication. The cell lysate was then cleared by centrifugation at 20000 × *g* for 20 min. The cleared supernatant was applied to a Ni^{2+} affinity column packed with Ni-NTA resin pre-charged with 100 mM $NiSO_4$ solution and equilibrated with the binding buffer. The sample was placed on a rocking platform in the cold room for 1hr. The column was washed with 5 resin volumes of wash buffer (50 mM Tris, 60 mM Imidazole, pH 8.0). 2 resin bed volumes of elution buffer (50

mM Tris, 300 mM Imidazole, pH 8.0) was used to elute the proteins. The purified full-length enzymes were dialyzed against 50 mM Tris (pH 8.0), 150 mM NaCl, 10% (v/v) glycerol, 2 mM DTT and then concentrated and stored at –80°C. Purity was assessed by SDS-PAGE analysis and concentrations determined via UV absorption at 280 nm using an extinction coefficient of 74425 M^{-1} cm^{-1}.

Catalytically defective Src (kdSrc) was expressed and purified as described previously [35] with the following changes: 1) A Ni^{2+} affinity column was used in binding the $(His)_6$ tagged kdSrc 2) An extensive washing step with the detergent-containing binding buffer was performed to remove all the non-specific binding of the co-expressed chaperone complex.

Stability Measurements

Equilibrium unfolding titrations were measured by monitoring the average fluorescence wavelength of the single tryptophan in the SH2 domain. Fluorescence emission spectra were collected from 300 to 450 nm using a spectrofluorimeter. Samples were prepared at constant protein concentration in a buffered solution (Tris) containing varying concentrations of denaturant ranging from 0 to 5.0 M (Gdn-HCl).

NMR Experiments

NMR samples were prepared by growing in modified M9 medium containing [^{15}N] Ammonium Sulfate (2 g/L) and/or [^{13}C] glucose (2 g/L) for uniformly ^{15}N-labeled and ^{13}C,^{15}N-labeled protein, respectively. NMR experiments were run on a DMX 500 spectrometer (Varian) using standard pulse sequences in the Varian BioPack. Assignments of the SH2 domains were done using standard assignment methods [53] through a series of 2D and 3D experiments on ^{13}C and ^{15}N enriched samples: ^{1}H-^{15}N HSQC, HNCA, HNCACB, CBCACONH. 85-90% of backbone atom resonances were assigned for the WT and variant domains. NMR data were processed using the NMRPipe package [82] and analyzed using Sparky [83] and CARA software [84]. Chemical shift perturbation values were obtained from the following equation:

$$CSP\,(\delta PPM) = \sqrt{(^{1}H\ ppm)^2 + (\frac{^{15}N\ ppm}{5})^2}$$

The purified Csk SH2 constructs were dialyzed against 10 mM phosphate buffer (pH 7.0), 50 mM NaCl, ±2 mM DTT then concentrated to approximately 0.7 mM for NMR experiments. All non-deuterated protein samples contained 10% (v/v) D_2O for NMR experiments. Purity was assessed by SDS-PAGE analysis and concentrations determined via UV absorption at 280 nm using an extinction coefficient of 16055 M^{-1} cm^{-1} (ExPasy-Protparam). NMR-detected Hydrogen-Deuterium exchange in SH2 constructs was monitored by measuring intensities of assigned ^{1}H-^{15}N cross peaks by recording a series of ^{1}H-^{15}N HSQC NMR spectra (50 total, 21 min each) immediately after protein deuteration. Typically, a 0.8 mM protein sample (in 10 mM Na_2HPO_4, 50 mM NaCl, ±2 mM DTT, pH 7.5) is split into a non-deuterated (ND) and fully-deuterated (FD) samples. The total volume in ND samples is brought up to 0.6 mL with buffer and 10% (v/v) D_2O for spectrometer referencing. The FD samples are prepared by applying 300 µL of the protein sample to a Quick Spin Protein Column (Roche) pre-equilibrated with the deuterated (99.9% D_2O) buffer (10 mM Na_2HPO_4, 50 mM NaCl, ±2 mM d_{10}-DTT, pD 7.9) then centrifuging the column for 3 min at 750 × *g*. The collected deuterated eluate is brought up to volume by adding deuterated buffer and 10% (v/v) D_2O to maintain buffer composition as the ND samples.

Kinase Activity Assay for Src Phosphorylation by Csk and Its Variants

Time-dependent phosphorylation of kinase dead Src (kdSrc) by wild type or variant Csk enzymes was typically carried out in assay buffer: 100 mM MOPS (pH 7.0), 100 mM KCl, 10 mM $MgCl_2$, 100 µM [γ-^{32}P]ATP (4000-6000 cpm $pmol^{-1}$) and 10 mM DTT at lab temperature (23°C). Reactions were initiated by adding ATP to the master mix containing all enzymes and reagents. 10 µL from the master mix reactions was quenched directly into 10 µL of 2x SDS

loading buffer at several time points. The quenched samples were analyzed by SDS-PAGE and bands corresponding to the phosphorylated kdSrc were excised from the dried gels and quantified on the ^{32}P channel in liquid scintillator. The specific activity of [γ-^{32}P]ATP was determined by measuring the total counts of the reaction mixture. The time-dependent concentration of ^{32}P-Src was then determined by considering the total counts per minute (CPM), the specific activity of the reaction mixture, and the background phosphorylation. Initial velocity reactions were typically performed in 10 μL volumes at 23˚C and initiated by adding Csk enzymes to substrates and allowing the reaction to proceed for 6 minutes before quenching with 2x SDS loading buffer. The quenched samples were analyzed as described above.

Deuterium Exchange-Mass Spectrometry (DXMS)

DXMS Operation and fragmentation Conditions

The instrument setup and operation was previously described [72]. All frozen samples were thawed and run using the conditions determined during fragmentation optimization. The initial conditions for the sample composition and instrument parameters were determined before starting the exchange time course experiments. 1.4 mg/ml stocks of wild type or variant Csk were diluted with storage buffer (50 mM Tris, 150 mM NaCl, 10% glycerol, 2 mM DTT, pH 7.0) at room temperature and quenched with 0.5% formic acid, 16.6% glycerol, and 3.2 M Guanidine-HCl (quench buffer) at 0°C then immediately frozen on dry ice and stored at -80°C until analysis.

Deuterium On-exchange Experiments

The exchange time course experiments for wild type and variant Csk were all performed simultaneously at lab temperature (23°C) with the following procedure. A full time course experiment was initiated by adding 77 μL of protein in H_2O buffer (50 mM Tris, 150 mM NaCl, 10% glycerol, 2 mM DTT, pH 7.0) to 187 μL of the equivalent deuterated exchange buffer for a final D_2O of 71%. The deuterated exchange buffer (50 mM d-Tris, 150 mM NaCl, 10% glycerol, 2 mM deuterated DTT) was prepared using 99.9 % D_2O and adjusted to pD 7.4 with DCl. The

exchange was monitored over the course of 24 hours at intervals of 0.1, 0.5, 1, 5, 15, 60, 120 and 1440 min. Aliquots of 24 μL from the master reaction were removed and quenched in pre-chilled high pressure liquid chromatography vials containing 6 μL of quench buffer. The vials were sealed and frozen over dry ice, then stored at -80°C. The in-exchange control consisted of the protein added directly to the pre-chilled deuterated and quench buffers, then immediately followed by the normal sample preparation procedure. The back exchange control was determined by incubating the samples in 0.5% formic acid in D_2O for 24 hours All samples were injected and run on the instrument with the same conditions listed in the fragmentation optimization screening. Data for the time course exchanges were acquired in the MS1 mode.

Sequence Identification of Peptide Fragments

The most likely identity of the parent peptide ions was determined using the SEQUEST software program (Thermo Finnigan, Inc.) and MS1 and MS2 data. The quality of each peptide was monitored by individually examining each measured isotopic envelope spectrum for the entire time course exchange. The deuterium content was calculated for each time point by using specialized software as previously described [85].

Computational Methods

The structure was selected from the first active conformation (chain A) of the crystal refined structure with PDB ID 1K9A [68]. Missing loops were modeled with the PRIME module in the Schrodinger suite and residues were changed to match the human Csk sequence [77]. The H++ web-server (http://biophysics.cs.vt.edu/H++) was used to predict the protonation state of the residues in the structure at a pH of 7.0. The Csk system was solvated in a cubic box and additional Na^+ and Cl^- ions were added to achieve 150 mM physiological conditions. The variant structure was generated by inserting two glycine residues between Gly124 and Lys125. The reduced conditions were modeled by defining residues 122 and 164 as Cys residues. The water was modeled with the 4-particle TIP4P-Ew force field [86], which was previously shown to better

describe the rotational motion of proteins [87] than the related 3-particle water model, TIP3P [88]. SHAKE was applied to all bonds involving hydrogen atoms [89]. Minimization was applied to the resulting structure to remove any clashes. Harmonic positional restraints of strength 10 kcal/mol/Å^2 were applied to the protein backbone atoms, keeping the pressure at 1 atm and increasing the temperature from 10 K to 300 K as a linear function of time over the course of 1.2 ns, using Berendsen temperature and pressure control algorithms with relaxation times of 0.5 picoseconds for both the barostat and the thermostat [90]. Restraints were removed and a 6 ns simulation was performed at constant isotropic pressure of 1 atm and a temperature of 300 K. We used a 10 Å cutoff radius for range-limited interactions, with Particle Mesh Ewald electrostatics for long-range interactions [91].

The production simulations of Csk were carried out using NVT conditions. A Langevin thermostat was used to maintain the temperature at 300 K with a collision frequency of 2 ps. The simulation time step was 2 fs and snap shots were saved every 2 ps. For all simulations performed the first 5 ns of the NVT production runs were excluded allowing the systems to fully equilibrate for further analysis. All simulations were performed using the PMEMD module within the Amber11 simulation package. Production NVT runs were performed on GTX580 GPUs using the Amber11 pmemd.CUDA engine [76,92]. Four independent 100 ns simulations were run for each the wild type and the Gly-Gly insert Csk variant.

Chapter 2, in part, is a reprint of the material as it appears in the PLoS Computational Biology by Barkho, Sulyman, Levi CT Pierce, Maria L. McGlone, Sheng Li, Virgil L. Woods Jr, Ross C. Walker, Joseph A. Adams, and Patricia A. Jennings. (2013). This dissertation's author was the primary investigator and author of the paper.

Chapter III

Analysis of interaction between Csk's modified SH2 and its physiological activator

ABSTRACT

Csk's recruitment from the cytoplasm to the plasma membrane is an essential step in its role as a master SFK repressor. The adaptor molecule CBP/PAG1 is a primary platform for Csk-SFK co-localization where multiple tyrosine sequences are temporally phosphorylated for dynamic, SH2-domain mediated recruitment of signaling assemblies. We have previously shown that flexibility in specific motif (CD loop) in Csk's SH2 domain can affect the catalytic efficiency despite lack of direct coupling to the kinase core. Here, we address whether the CD loop also controls the rate of membrane attachment and subsequent SFK inactivation. Enzymatic, binding, and structural analyses hint to a dual role of the CD loop whereby localization and catalytic efficiency are controlled simultaneously. The results suggest that "rheostatic" control in multi-functional molecules may be a common feature to introduce with minimal structural perturbations to junction point motifs in signaling assemblies.

INTRODUCTION

The human kinome employs shared, non-catalytic modules to assemble larger scaffolds that are functionalized for specific cellular signaling events or pathways. The needed diversity for such functions is manifested on the sequence, domain, and tertiary arrangements levels of these proteins. Canonical ligands of Src Homology 2 (SH2) domains constitute peptides and sequences containing phosphorylated tyrosine residues. For cytoplasmic signaling molecules, the SH2 domain is usually located at the N-terminal to the kinase catalytic core and is responsible for substrate recruitment and localization to cellular compartments (e.g. lipid rafts/membrane) and also serves as a direct activator of the kinase [51]. Thus, SH2 domains are central nodes for inter- and intramolecular communications in signaling scaffolds.

In Csk, dynamic localization and shuttling of this master regulator is primarily done by reversible tethering to the adaptor protein PAG1/CBP via a phosphotyrosine-SH2 domain

interaction. This bimolecular interaction has been studied in vivo [93] and characterized in vitro [78] and the available data hints to unique mode of interaction between the intrinsically disordered binding platform CBP and Csk's SH2 domain. Y314 is the canonical interaction site of phosphorylation by SFKs upon activation which facilitates recruitment of Csk via a specific CBP-SH2 interaction. Undesirable interference with this feedback mechanism by non-native pTyr containing motifs -such as the bacterial peptide effectors possessing the EPIYA sequence that competitively interact with Csk via the SH2 domain- may lead to Csk's recruitment to the membrane and down-regulating SFKs to facilitate infections [60].

For the Csk CD loop variant (Csk-GG) which had a longer, more flexible CD loop in the SH2 domain (chapter 2), it was evident that the intrinsic level of kinase activity was perturbed due to apparent attenuation of functional motions within the native state ensemble in the kinase core. Since the CD loop occupies a focal site in this multimolecular assembly, the influence of its intrinsic flexibility on SH2 binding properties warrants further examining. Therefore, we sought to characterize how the variant domain responds to its natural ligands and identify possible implications on net signaling output.

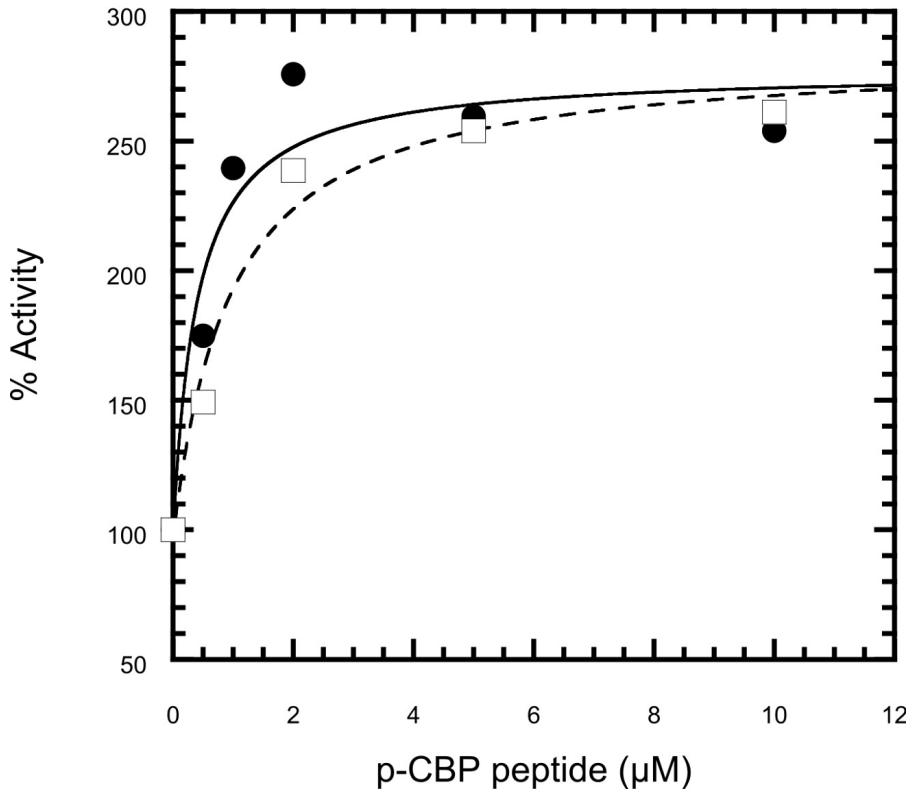

Figure 3-1. Activation of Csk by CBP phosphopeptide

Percent activation of wild type Csk (circle) and the variant (square) by CBP phosphopeptide was monitored using kdSrc as a substrate. Equal amounts of wild type Csk and the variant (60 nM) were mixed with 100 μM [γ-^{32}P]ATP, 20 μM kdSrc, and various amounts of CBP phosphopeptide (0-10 μM) at 23°C. The activities were measured as a function of phosphopeptide concentration and the rates were normalized to the zero point values for each enzyme (100%).

RESULTS

Csk Kinase Activation Measurements by p-CBP

Phospho-CBP peptide activates WT Csk and Csk-GG to the same level

The CD loop with Csk's SH2 domain does not harbor any of the sub-domain motifs or residues that are canonically responsible for binding phosphotyrosine sequences. However, our biophysical data (stability, NMR, HDX) studies on the isolated SH2 domain (chapter 2) indicated that differential effects are transmitted farther than the immediate locale of the perturbed loop. We performed kinetic binding analysis with a synthetic phosphorylated (p-Y314) CBP peptide with full length WT and variant (Csk-GG) enzymes and monitored the rates of Src phosphorylation by Csk as a function of activator (Figure 3-1). The data shows similar activation levels with respect to basal rates for both kinases. This result is consistent with previously reported values of similar magnitude [59]. Differences in the apparent binding affinities (K_d) for the peptide-SH2 complexes were not significant either, indicating that the variant SH2 retained its functional ability to bind tyrosine phosphorylated peptides, specifically the CBP derived peptide.

Activation of WT and variant Csk by a Src-phosphorylated cytoplasmic domain of CBP

The activity changes that are associated with p-CBP peptide are also present when the fully phosphorylated, cytoplasmic domain of CBP is used as an activator. A striking observation, however, is the apparent difference in binding kinetics of CBP to the variant SH2 with respect to the WT protein (Figure 3-2). A summary of the kinetic parameters obtained for WT and variant Csk using Src as a substrate and p-CBP or the CBP peptide as activators is given in Table 3-1. The data show that although both WT and variant Csk proteins are activated to approximately the same extent, there's a significant difference in binding affinities (22 nM vs. 240 nM for WT and the Gly-Gly variant, respectively.

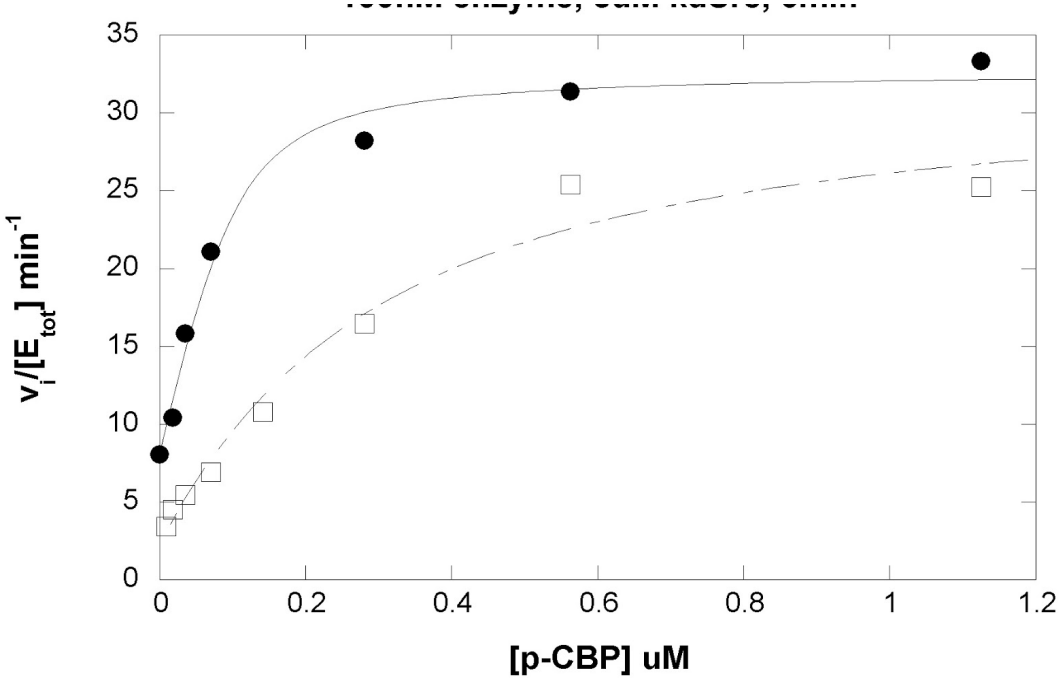

Figure 3-2. Activity changes associated with full CBP binding to Csk

Initial velocities of Csk (WT: black circles; GG: white squares) phosphorylation of kdSrc (5uM) are plotted as a function of p-CBP concentration. Data are fit to a standard quadratic function (see methods).

Moreover, the binding kinetics between the two proteins seem to differ in the apparent measure for catalytic efficiency, that is, the ratio of the maximal turnover number to the apparent binding affinity (k_{cat}/K_d).

Overall, the data indicate that modification of the CD loop by introducing non-native flexibility not only reduced the intrinsic rate for catalysis but also reduced the efficiency of activation by Csk's physiological activator that is also responsible for membrane recruitment.

Table 3-1. Steady-state kinetic parameters for Csk activation by phospho-CBP and phospho-CBP peptide

Activator	CSK	K_d (uM)	Basal activity (% of WT)	Maximal activity (%)	k_{cat}/K_d ($uM^{-1}min^{-1}$)
Full pCBP	WT	0.09 (±0.03)	100	746 (±5)	204
	GG	0.62 (±0.21)	30	699 (±11)	28
pCBP peptide	WT	0.39 (±0.25)	100	186 (±32)	7
	GG	0.74 (±0.27)	8	15 (±1)	0.3

SH2-CBP interaction studies by solution-state NMR spectroscopy

Since CBP activates Csk by an SH2-domain bimolecular interaction, we sought to study the binding between the cytosolic domain of CBP (or a peptide thereof) and the WT and variant isolated Csk SH2 domains using solution-state NMR spectroscopy (Figure 3-3). The method has the advantage of providing site-specific information on this bimolecular interaction through changes in the three main detectable parameters (chemical shift, δ, intensity, I and linewidth, λ). Binding processes that are monitored by NMR fall in a range of chemical exchange regimes that are dependent on the rates of association (k_{on}) and dissociation (k_{off}), which in turn dictate the behavior of the primary NMR observables along the titration coordinates. The dissociation constant of any complex is described by the ratio of these two rates ($K_d = k_{off}/ k_{on}$), and thus, tight-binding complexes typically fall in the "slow exchange" NMR timescale (Figure 3-4).

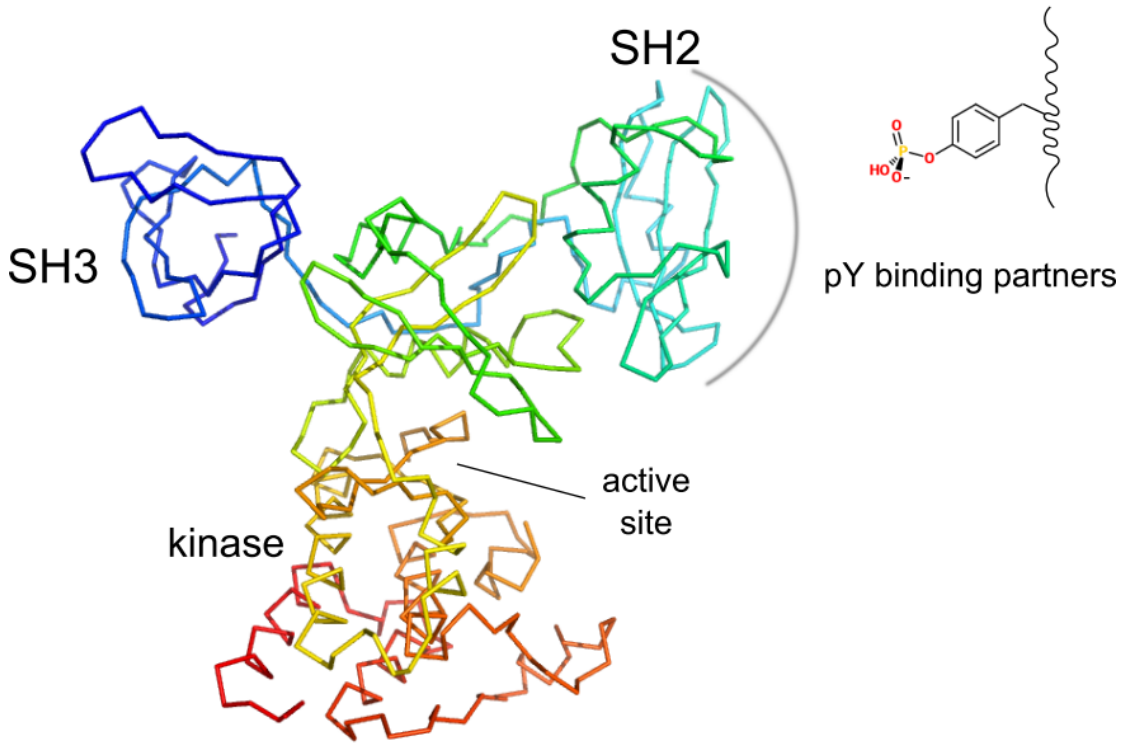

Figure 3-3. Csk's SH2 domain mediates interaction with motifs possessing phosphorylated tyrosine residues

The SH2 is a common module that mediates localization and kinase activation in signaling molecules. Titration of Csk with its physiological pY ligands can be monitored using amide backbone resonances of the isolated ^{15}N-SH2 domain.

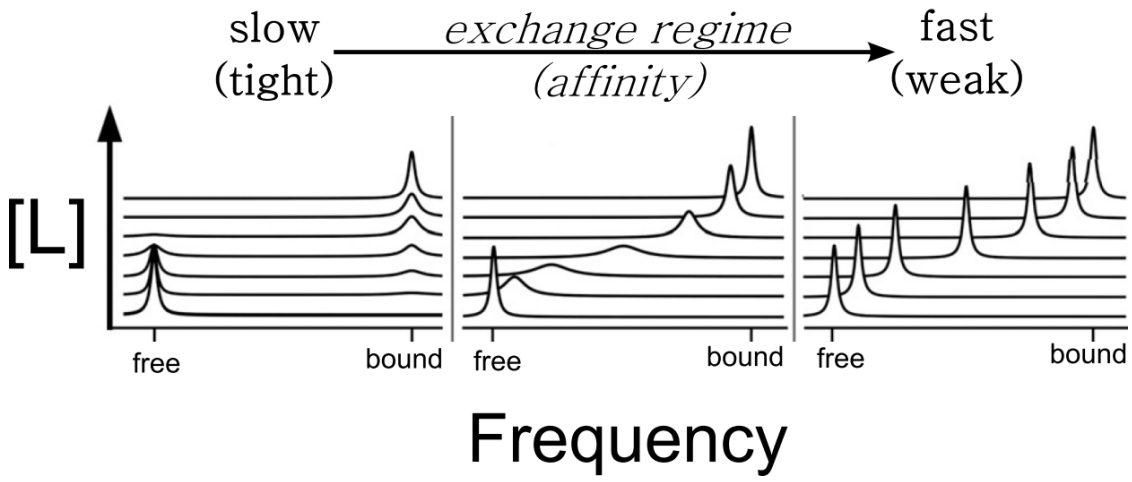

Figure 3-4. Lineshape analysis in protein-ligand interactions and the effects on exchange regimes

Theoretical behavior of NMR observables along a ligand titration coordinates**.** adapted from: Kleckner, Ian R., and Mark P. Foster. "An introduction to NMR-based approaches for measuring protein dynamics."*Biochimica et Biophysica Acta (BBA)-Proteins and Proteomics* 1814.8 (2011): 942-968.

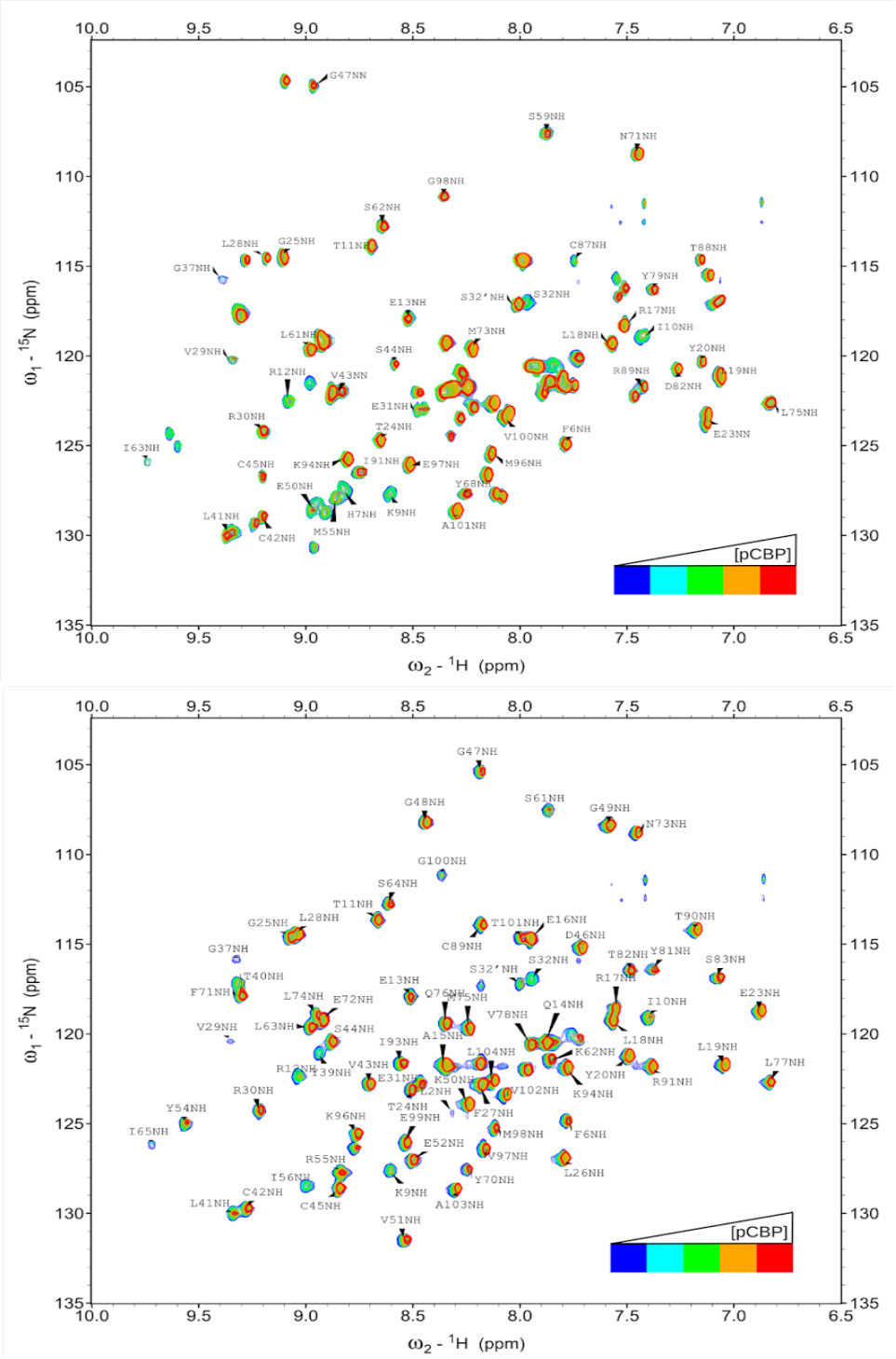

Figure 3-5. NMR-detected SH2 domain binding to phosphorylated CBP

NMR titration experiment for the WT (top) and variant (bottom) Csk SH2 domains as a function of [p-CBP]. Color-coded 2D ^{1}H-^{15}N HSQC spectra are overlaid and shown for each domain along with resonance assignments.

Full-length CBP:SH2 interaction

Although the full, phosphorylated cytoplasmic domain of CBP activates Csk and the variant more robustly than the short peptide, the larger size of the activator (MW ~43 kDa) with respect to the SH2 domain renders characterization of this interaction thru NMR more challenging. As amide resonances arising from the SH2 domain backbone are used to probe site-specific information on this bimolecular interaction, we performed a titration experiment of the activator (CBP) into 1H-15N-labeled SH2 domain and the variant (Figure 3-5). The tight, sub-micromolar apparent binding affinity of CBP to the SH2 domain is corroborated by the observation of minimal chemical shift changes and significant line broadening (indicative of slow exchange regime) for all resonances due to the the increase in molecular weight and correlation time upon complexation (~12 kDa to ~55 kDa). Nonetheless, this effect can be used to extract information about binding sites on the SH2 domain. Differential line-broadening is a measure for the sites most affected by the interaction (most immediate binding residues). Therefore, intensity change plots as a function of residue number (Figure 3-6) indicate regions with extreme line broadening with respect to the global intensity loss seen for all resonances.

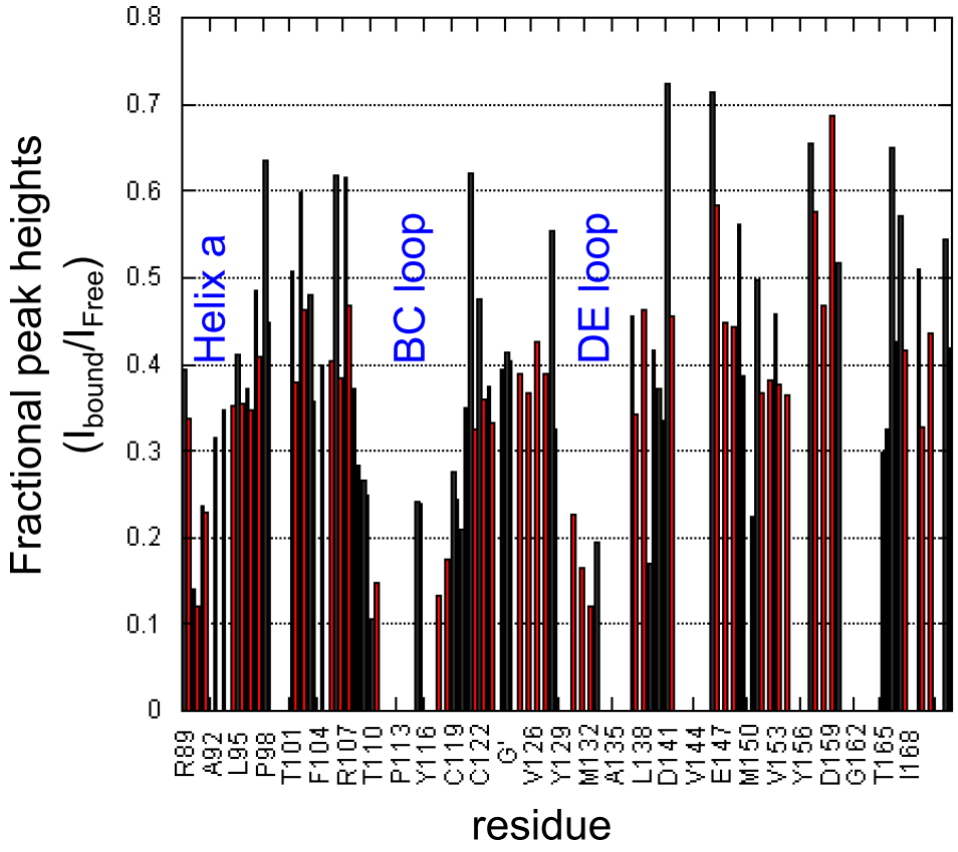

Figure 3-6. Plot of resonance intensity changes for WT (black) and GG (red) SH2 domains upon binding p-CBP

For both domains, differential line broadening is seen for the BC loop (pTyr binding) and DE loop (kinase domain interaction) indicating that the canonical interaction mode is preserved in both domains.

Phospho-CBP peptide: SH2 interaction

The shorter phospho-peptide derived from CBP is used hereafter to further characterize the effects of SH2 CD loop length on the interaction with the activator. Advantages of using the shorter peptides that it drives the exchange regime to the fast-intermediate limits where chemical shift perturbations, linewidths, and intensities are more readily available to measure. The SH2-peptide titration was performed with an experimentally feasible maximum of 1.5 molar excess of ligand (p-CBP peptide). Inspection of the overlaid titration spectra shown in (Figure 3-7) confirms that this protein-ligand interaction fall in the fast-intermediate exchange time regime for most residues.

Chemical Shift Perturbations

Changes in chemical shifts of backbone amides indicate that the binding of the phospho-CBP peptide to the SH2 induces chemical shift changes throughout the domain. The most significant of these changes are for residues involved in direct binding/coordination of phosphorylated CBP (Figure 3-8). As seen for full length CBP, the bound domains showed large CSPs for the residues involved in canonical binding of the phospho-peptide which localized to three primary regions: the p-Tyr binding BC loop, the DE loop at the kinase small lobe interface, and the BG loop that binds the C-terminal end of the peptide. Interestingly, this similarity in structural perturbations in the fully bound states suggests that both the WT and the CD loop variant domains respond the activator and transmit the binding information in identical fashions, and therefore, any differences in activation efficiency between the two proteins must arise from changes in the kinetics of binding the phospho-ligand rather than the sites of the interactions on the receptor domain.

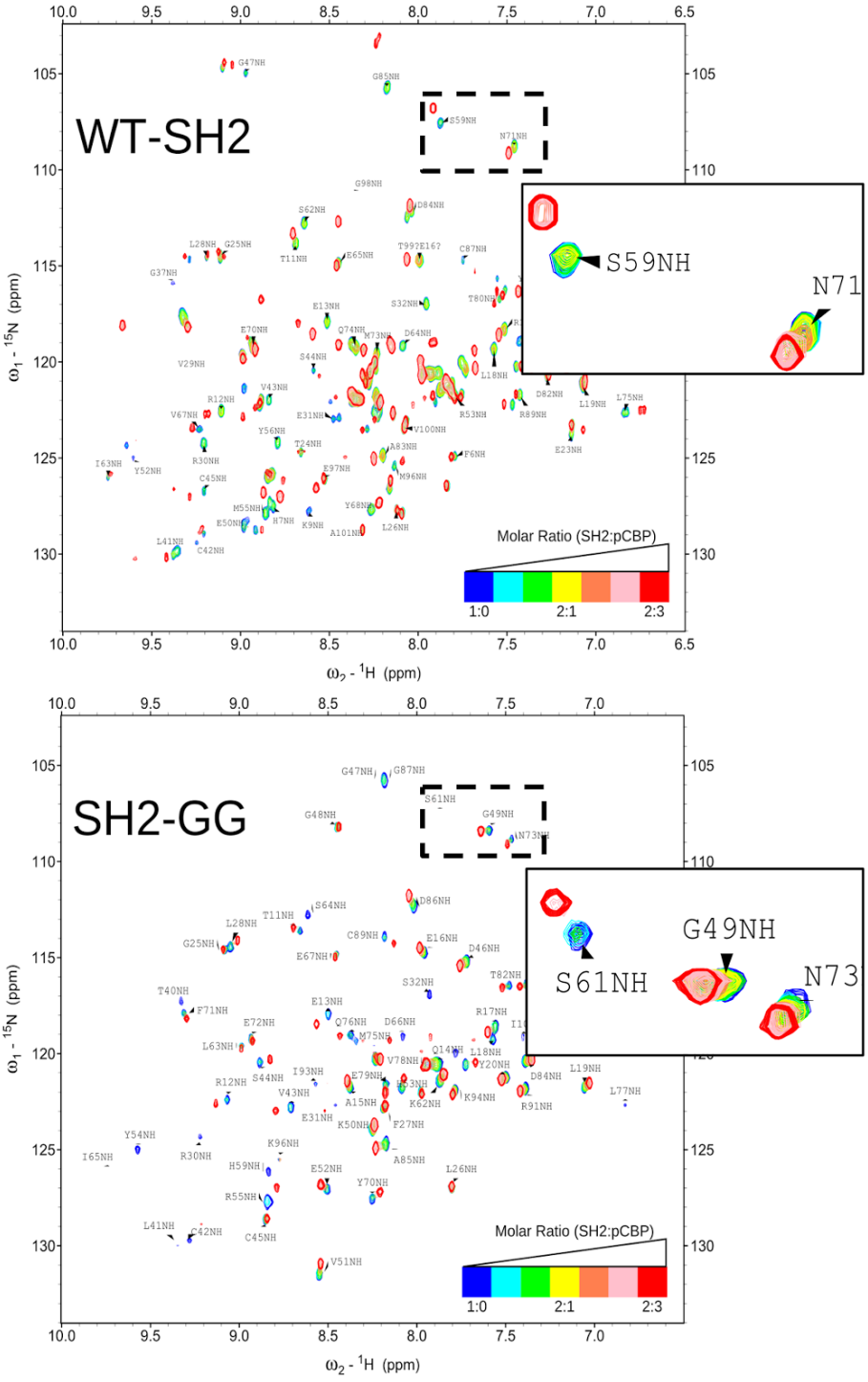

Figure 3-7. NMR-detected SH2 domain binding to phosphorylated CBP peptide

NMR titration experiment for the WT (top) and variant (bottom) Csk SH2 domains as a function of [p-CBP] peptide. Color-coded 2D ^{1}H-^{15}N HSQC spectra are overlaid and shown for each domain along with resonance assignments. Contour levels for the free and bound spectra are intentionally hollow for clarity.

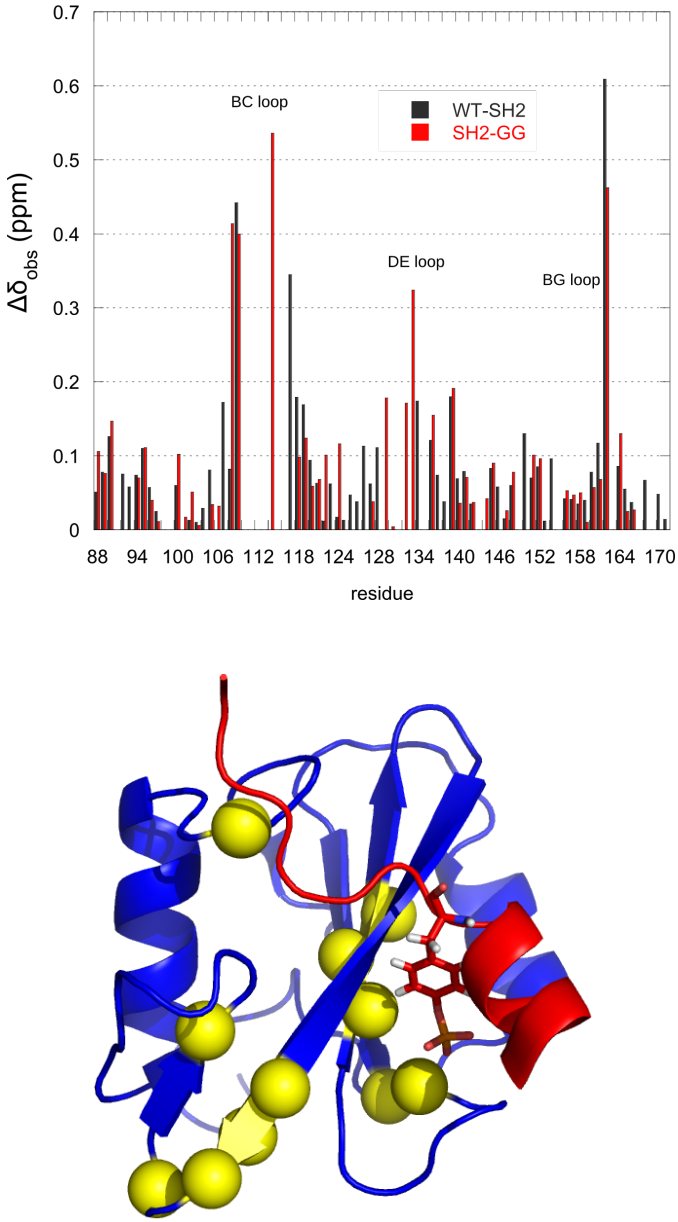

Figure 3-8. p-CBP peptide induced Chemical Shift Perturbations (CSP) for SH2 domains

Top: Changes in backbone amide (combined ^{1}H-^{15}N) chemical shifts are observed for both the WT and variant SH2 domains. The data is extracted from comparison between the CS values of free and bound SH2 domains with p-CBP peptide. Values larger than ~0.12 PPM are deemed significant. *Bottom*: C alpha spheres (yellow) of residues exhibiting significant CSPs are plotted on the SH2 domain structure complexed with CBP peptide (red) (extracted from PDB ID: 2RSY).

Lineshape analysis of amide resonances in 2D NMR titration datasets

A full set of ligand titration data allows for the monitoring of backbone amide NMR observables as a function of ligand concentration to determine free and bound state properties. Careful analysis of lineshapes also provides valuable information on any changes to the intrinsic dissociation rates and affinities especially for sites whose bound state signals are resolved. Such analysis provides information on processes that occur on 10-100 ms time scales [94] and therefore is a good approach for activator binding studies. In the case of our SH2:p-CBP interaction, the titration spectra lack any signals for possible intermediate states like that seen for other SH2 domain variants [95]; therefore we can assume that the interaction can be described by a two state model.

Simple tracking of chemical shift as a function of ligand is the most direct way of probing this interaction. Although a saturation curve can be generated by plotting the chemical shift change (from the free signal) for any specific residue as a function of p-CBP concentration, this method is accurate only if the system is truly in the fast exchange regime. Affinity values extracted by utilizing only peak positions become unreliable as soon as the system deviates from very fast exchange regime because the detected signal would no longer represent the mere average of the free and bound states (i.e the saturation level towards the bound state) [96,97]. Thus, we chose to use lineshape analysis for the p-CBP peptide:SH2 domain binding data as such treatment guarantees that effects leading to line broadening are accounted for along the titration series. Figure 3-9 shows representative ^{1}H-dimension slices for several resonances that exhibit apparent fast-intermediate exchange regimes. As noted before, the raw extracted data (blue traces) show no signs/signals of a detectable intermediate suggesting that the ligand binding process can be described by a 2-state model. The central plots estimate the chemical shifts for the initial (free) and final (bound) states which are used as constants in the actual fitting of lineshape

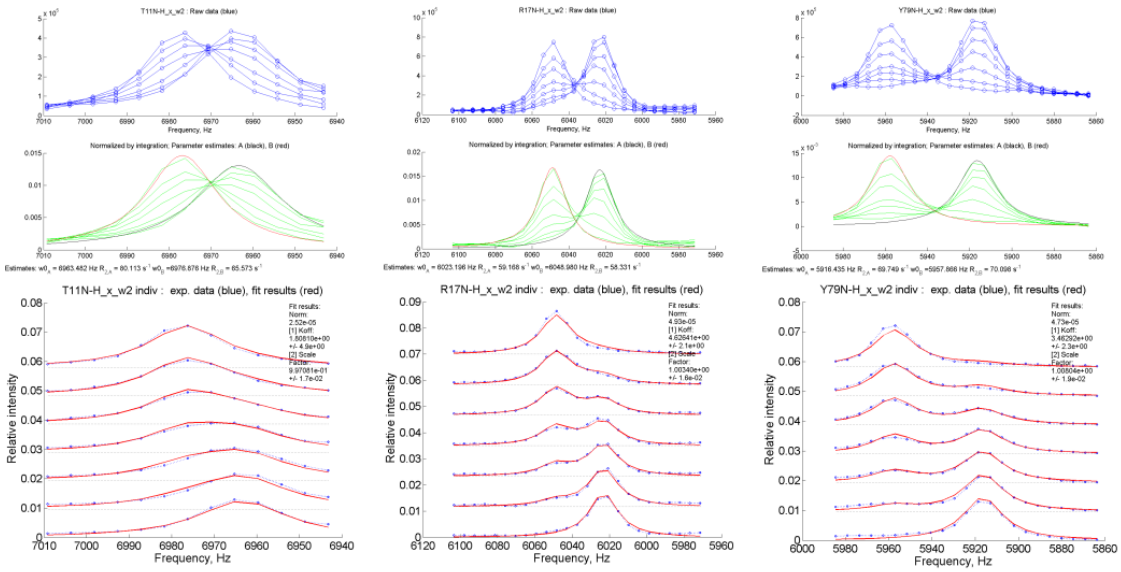

Figure 3-9. NMR lineshape analysis of residue signals from 2D spectra of WT SH2

Plots of residues that undergo CSP and lindewidth changes as a function of ligand titration. *Top*: Raw data for all titration points of an amide resonance extracted from 2D ^{1}H-^{15}N HSQC spectra. *Middle*: plots of the free (black trace) and bound (red trace) frequencies. *Bottom*: fitted traces to a 2-state exchange model to determine dissociation rates at each site.

estimates. The latter are shown at the bottom panels where k_{off} is the only variable after initial estimates of K_d, intensity factors, and initial/final frequencies. Table 3-2 summarizes shows calculated dissociation rates for different sites in the WT SH2 domain and the corresponding ones in the variant domain (note sequence difference for some) as well as the rates when "global" analysis is performed for all reliable binding reporters simultaneously (Figure 3-10).

Table 3-2. Calculated dissociation rates for the p-CBP peptide interaction with WT and variant Csk SH2 domains

Residues used for 2-state model fitting are clustered by regions and assumed to report on a single binding event. The global fit values are results from simultaneous fitting of all the above residues.

Residue cluster	WT $k_{off}(s^{-1})$	GG $k_{off}(s^{-1})$
T11,R17	4.3±1.9	71±15
Y20	N/A	N/A
S44,C45	4±2.2	8.5±10
G47(G49)	2.2±4	75±21
D82/84, A83/85	6.1±2.9	58±13
R89/91	N/A	92.7±48
Global fit	**3.9±1.3**	**60.0±7.8**

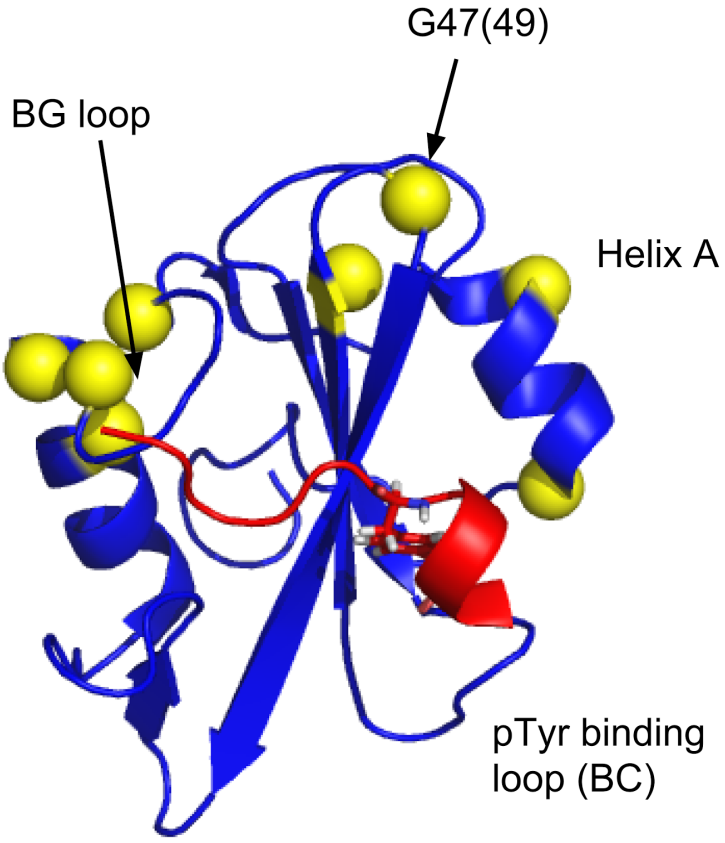

Figure 3-10. Backbone amide reporters used in titration analysis

CBP peptide (red) titration of WT and variant SH2 domains. Yellow spheres represent Alpha carbons for common residues between the two domains that were used to extract data provided in Table 3-2. Structure adapted from PDB ID: 2RSY.

DISCUSSION

Our kinetic, and structural-binding data suggests that a simple view of phosphotyrosine binding of the SH2 domain may not sufficient to explain the full effects that are seen downstream in the signaling pathway. The SH2 domain in Csk is required for kinase activation and localization, where both functions contribute to efficient inactivation of SFKs at the plasma membrane. Specifically, the results show that the CD loop in Csk is positioned to serve as an effective rheostat that controls two coupled functions: 1) the ability to tune basal rates of SFK phosphorylation, 2) control over adaptor tethering rates and therefore cytoplasm/membrane shuttling rates. It is worth noting that although the CD turn in Csk has no canonical function in the WT protein, in the Itk scaffold, the surrounding sequence is optimized for a dual binding role to accommodate two different ligands [61]. The observed difference dissociation rates in the NMR data is perhaps directly linked to the increased inefficiencies of measured kinase activation rates. Indeed, the relative difference in magnitude between p-CBP dissociation rates for the WT and variant domain (Table 3-2) is comparable to the observed reduction in efficiency parameters between the two enzymes (Table 3-1). Csk's internal equilibria notwithstanding, limits to CBP's residence time on Csk's SH2 are sufficient to restrict efficient SFK inactivation. Interestingly, these limitations may not always be undesirable given recent data suggesting an additional physiological function of the C-terminal Src kinase [37]. In such case, a more nuanced tuning of binding dynamics and chemical kinetic efficiency is essential to maintain a healthy control of the canonical Csk-CBP-SFK network as well as eEF2 functional phosphorylation pathway.

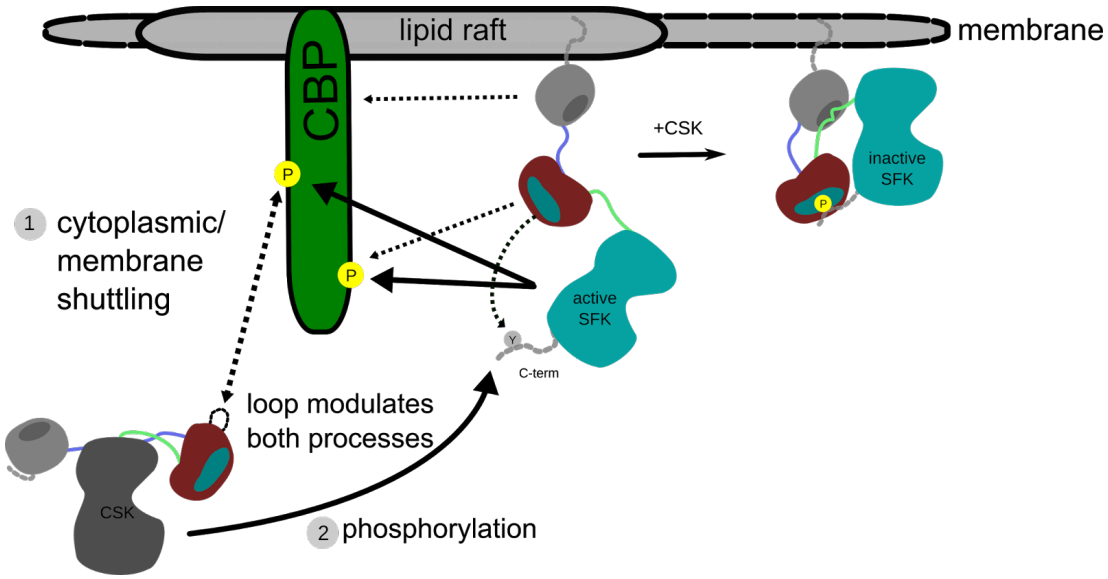

Figure 3-11. CD loop in Csk's SH2 domain can tune intrinsic activity and binding properties and thus SFK downregulation

The SH2-mediated recruitment of Csk to the lipid rafts is affected by CD loop length modifications. Localization of Csk to the membrane is an essential first step towards SFK phosphorylation.

MATERIAL AND METHODS

CBP expression, purification, and phosphorylation

Cbp protein (residues 53-432, extracellular and transmembrane regions deleted) was expressed using a p-GEX-5X1 vector in *Escherichia coli* BL21(DE3) cells (Novagen). The cells were grown to OD_{600} of ~0.6 when expression was induced with 1 mm IPTG (isopropyl 1-thio-β-d-galactopyranoside) and allowed to shake for 4 hours at 37 °C. The cells were harvested by centrifugation at 5,000 × g for 20 min, resuspended in GST binding buffer (150 mM NaCl, 10 mM Na_2HPO_4, 5mM EDTA, pH 7.4), and lysed by sonication. The lysate was cleared by centrifuging at 13,000 × g for 30 min, and the supernatant was removed and run through a 0.45 micron filter. The fusion protein was purified from the cell lysate using a 5 mL Bio-Scale Mini Profinity GST Cartridge (Bio-Rad) on a Bio-Rad Profinia using the standard buffers and purification protocol of the Profinia for GST purification. The eluted GST-Cbp fusion protein was dialyzed into thrombin cleavage buffer (50 mM Tris, 150 mM NaCl, 2.5 mM $CaCl_2$, 0.1% β-mercaptoethanol, pH 8). Cbp was then cleaved from GST with bovine thrombin (Fisher Scientific) at a ratio of 12.5 activity units thrombin per milligram fusion protein. The thrombin cleavage proceeded for 5 hours at room temperature. Following cleavage, the GST was separated from the Cbp using a 5 mL HiTrap Benzamidine FF column (GE Healthcare). The column was equilibrated and washed with wash buffer (50 mM Tris, 200 mM NaCl, pH 7) to remove GST, then Csk was eluted using a high salt buffer (50 mM Tris pH 7, 2 M NaCl). Cbp was dialyzed against a low salt buffer (50 mM Tris, 100 mM NaCl, pH 7) to remove salt and prepare the protein for ion exchange chromatography, a final step to remove any remaining contaminants. A 5 mL HiTrap Q HP column was equilibrated with dialysis buffer, then the protein was loaded onto the column. Cbp was eluted using 40 mL of buffer with the buffer salt concentration increased to 200 mM NaCl. The remaining contaminants were removed from the column using 1 M NaCl buffer. Purified CBP was phosphorylated using recombinant active Src (Invitrogen).

Typically, 0.6 mL reactions contained 100 μM of Cbp and 15 nM Src incubated in 50 mM HEPES (pH 7.5), 150 mM NaCl, 10% glycerol, 5 mM DTT, 0.01% Triton X-100, 10 mM free Mg^{2+}, and 3 mM ATP at 30°C for two hours.

Radiometric Csk activation assay

Initial velocity measurements were performed with 60 or 100 nM Csk in the presence of 100 μM [γ-^{32}P]ATP, 5 μM kdSrc, 10 mM $MgCl_2$, 0-10 μM synthetic p-CBP peptide or 0-2 uM of Src-phosphorylated CBP (cytoplasmic domain). The data were fitted to the following equation to obtain k_{cat} and K_d:

$$v = V_{max}\frac{([E_T]+[A]+K_d) - \sqrt{([E_T]+[A]+K_d)^2 - 4[E_T][A]}}{2[E_T]},$$

where v is initial velocity of the reaction, E_T is the total concentration of Csk, A is the activator (CBP) concentration.

NMR experimental

2D ^{1}H-^{15}N HSQC titration spectra were recorded using an TROSY-enhanced pulse sequence at 23°C. Combined chemical shift perturbation values were calculated using the following equation:

$$CSP\,(\delta PPM) = \sqrt{(1H\ ppm)^2 + \left(\frac{15N\ ppm}{5}\right)^2}$$

NMR line shape data was extracted using SPARKY [83] and subsequent analysis was performed in MATLAB using *LineShapeKin V3.2* [97,98].

Chapter IV

Newton's Cradle and the Effects of the SH3 and SH2 Domains on Csk Activity

ABSTRACT

The Src family of tyrosine kinases (SFKs) regulate numerous aspects of cell growth and differentiation and are under the principal control of the C-terminal Src Kinase (Csk). Although Csk and SFKs share conserved kinase, SH2 and SH3 domains, they differ considerably in three-dimensional structure, regulatory mechanism, and the intrinsic kinase activities. Although the SH2 and SH3 domains are known to up- or down-regulate tyrosine kinase function, little is known about the global motions in the full-length kinase that govern these catalytic variations. Here, we use a combination of accelerated Molecular Dynamics (aMD) simulations and experimental methods to provide a new view of functional motions in the Csk scaffold. These computational studies suggest that high frequency vibrations in the SH2 domain transfer across the N-terminal lobe of the kinase domain and manifest in motions in the SH3 domain. The effects of these reflexive movements on the kinase domain can be viewed using both Deuterium Exchange Mass Spectrometry (DXMS) and steady-state kinetic methods. Removal of several contacts between the SH3 and kinase domains short-circuit these coupled motions leading to reduced catalytic efficiency and stability of the N-lobe of the kinase domain. The data create a new view whereby separate domains productively transfer energy through the kinase domain much like a Newton's Cradle. This transfer may provide the activating force that organizes the active structure of the tyrosine kinase domain of Csk.

INTRODUCTION

The proto-oncogenic SFKs are tightly regulated through molecular and spatio-temporal mechanisms and are only transiently activated upon stimulation [18,26]. All SFKs contain a conserved C-terminal tyrosine kinase domain composed of an N-lobe important for nucleotide binding and a C-lobe important for protein substrate recognition. SFKs also contain two N-terminal Src homology domains (SH2 and SH3) that down-regulate kinase domain activity

through intramolecular contacts [99]. In the case of the prototypical SFK c-Src, crystallographic studies show that the SH2 domain recognizes a phosphotyrosine (pTyr-527) on the C-terminal tail of the kinase domain enforcing close contacts between the SH2 and kinase domains that inhibit catalytic activity. This domain-domain interaction is further stabilized by contacts between the SH3 domain and a polyproline linker connecting the SH2 and kinase domains. Interestingly, dephosphorylation of the C-tail by a protein phosphatase and/or interaction of the SH2 domain with a cellular adapter protein disconnects these inhibitory contacts and activates c-Src.

The C-terminal Src Kinase (Csk) serves as the master regulator and suppressor of all SFKs whose mis-regulation leads canonically to tumorigenesis [34]. Csk phosphorylates the C-tail Tyr-527 of c-Src inducing extensive structural rearrangements that result in enzyme down-regulation [100,101]. While Csk also possesses modular SH domains, notable differences between SFKs and Csk are apparent and most likely linked to regulation. First, whereas the inactive form of c-Src positions the SH3 domain on the N-lobe and the SH2 domain on the C-lobe of the kinase domain, in Csk both regulatory domains are positioned on opposite faces of the same N-lobe. Second, whereas the kinase domain of SFKs require phosphorylation of a tyrosine in a loop segment in the kinase domain (activation loop) for high activity, Csk lacks this tyrosine and does not require an activating phosphorylation step. Third, the architecture of the N-lobe is thought to render the kinase domain of c-Src intrinsically active whereas Csk is intrinsically inactive in the absence of SH domain interactions. Detailed mutagenesis studies have shown that the high catalytic activity of the Src kinase domain compared to Csk may be due to a network of interactions in the N-lobe that has the β4-5 loop as a hub [57]. While this loop activates the N-lobe in Src by interacting with nearby Arg-264 and the C-loop, these critical interactions are broken in Csk in place of new contacts between the β4-5 loop and a helix in the SH2 domain. In accordance with these novel interactions, removal of the SH2 domain significantly reduces Csk catalytic activity whereas the same deletion activates c-Src [54,102,103].

Despite the available data on Csk's SH2 domain, its conformational heterogeneity and its effects on kinase function [68,104,105], motions in other parts of the molecule have been harder to link to functional regulation. The SH2 domain is central to Csk's direct activation via the N-lobe [58,104]. A number of phosphotyrosine ligands including the Csk binding protein (PAG/CBP) [106], pragmin and bacterial peptide effectors possessing the EPIYA sequence [60] can bind to the SH2 domain and enhance catalysis. On the other hand, few studies attempted to address the role of the SH3 domain in the direct activation of Csk. Notably, a previous NMR study on the isolated SH3 domain identified potential interaction segments with the kinase domain by monitoring dynamic parameters upon complexation of a phosphatase peptide-bound SH3 domain with the isolated kinase domain [55]. Nonetheless, a clear view of domain motions, non-canonical interaction sites, and mechanism of activation in the intact kinase remain ambiguous. For example, while prior studies have shown that deletion of the SH2 domain in Csk lowers catalytic activity (i.e.-k_{cat}/K_m for Src) by 30-fold, removal of the SH3 domain lowers activity by 11-fold [107]. These similar changes in activity upon SH2/3 domain removal suggest that the activation mechanism in Csk extends beyond simple SH2-kinase domain contacts and include both regulatory domains. Furthermore, removal of both SH2 and SH3 domains do not significantly lower kinase activity beyond the individual domains [54,107]. Such kinetic findings hint to a cooperative interplay between SH2 and SH3 domains with regard to their ability to activate the C-terminal tyrosine kinase domain in Csk.

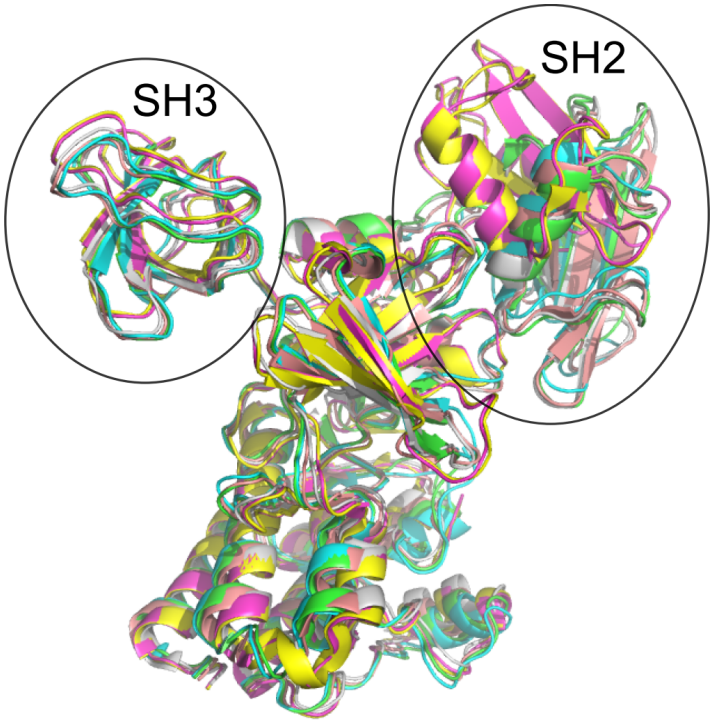

Figure 4-1. Conformational heterogeneity seen for the SH2 domain but not the SH3 domain of Csk

Superimposed units of the crystal structure of Csk (Ogawa et al. 2002) (PDB ID: 1K9A). The dual occupancy of the SH2 domain in the crystal units has long been linked to activation of the kinase. However, the SH3 domain is seen to occupy a single conformation and no motion is implied.

Our starting computational approach here provided new insights into the Csk scaffold and led to the hypothesis that the SH3 domain may be involved in functional motions that are not readily apparent when examining static structures of the full protein. This newly-discovered flexibility is closely linked to established motions by the other regulatory regions like the SH2 domain. Indeed, our combinatorial approach allowed us to identify previously hidden motions in an important part of Csk that assists in directly activating the kinase. We discovered using aMD calculations that the SH3 domain is closely linked to the motion of the SH2 domain on the other end of the molecule; the engagement of one causes the other domain to disengage the kinase domain hinting to a possible cyclical, direct activation by the two regulatory modules. These simulations identify several types of SH3-kinase domain contacts, one of which not apparent in the X-ray structure, that are critical for activating the kinase domain of Csk. The effects of SH2/3 domain motions can be visualized by DXMS methods and linked to changes in the N-lobe of the kinase domain most notably the network hub, β4-5 loop. Moreover, our experimental interrogations of possible contacts between the SH3 and kinase domain show that a structurally intact, conserved SH3 domain is required for such efficient activation. These theoretical and experimental insights paint a new image of Csk in which concerted motions in the SH2 and SH3 domains transfer energy much like a Newton's Cradle through the kinase domain. This transfer may be vital for complete catalytic activation of the central tyrosine kinase domain in Csk.

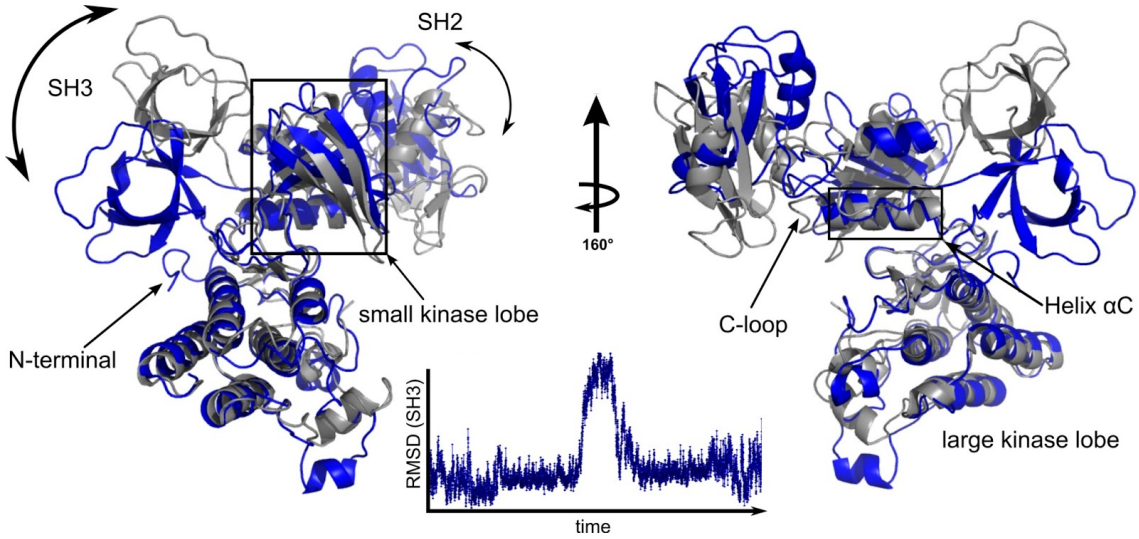

Figure 4-2. Csk's global domain motions observed in aMD

Structural alignment of two representative frames from the aMD trajectory highlighting concerted transitions of the modular domains of full-length apo Csk. The starting conformation (gray) is extracted from the crystal structure (PDB: 1K9A). A plot of root mean square deviation (RMSD) of the SH3 domain (1-70) as a function of aMD simulation time (200 ns).

RESULTS

Accelerated Molecular Dynamics (aMD) Simulations Sample Unique and Concerted Motions between Csk's Regulatory and Kinase Domains

Csk's X-ray structure [68] reveals that the modular SH2 domain can sample two distinct conformations in the absence of significant global changes in the rest of the protein. However, ouro ot SAXS measurements demonstrate that Csk samples an ensemble of conformations in solution that may be relevant for kinase function [71]. To probe possible functional motions, we employed advanced molecular dynamics techniques [108] to access broader samplings of the conformational landscape in Csk. While this method has been applied to relatively small systems, aMD has also been used to examine larger systems such as T.cruzi proline racemase and Get3, a component of the guided entry of TA-protein pathways [109,110].

A striking result from the aMD simulations of Csk was the observation of concerted and seemingly coupled global motions of the two noncatalytic domains (Figure 4-2). The observed trajectory shows an SH2 domain that disengages and moves upwards from the C-loop of the N-lobe, a site of canonical activation via the SH2 module. Concurrently, the SH3 domain populates a new conformation by moving downward and engaging the kinase domain on the other side of the molecule before returning to its baseline coordinates (Figure 4-2 -RMSD plot). Although this reversible transition is the largest observed, a closer inspection of RMSD values for the SH2 and SH3 domains shows coordination of smaller motions about the kinase core, albeit with higher frequency for the SH2 (Figure 4-3).

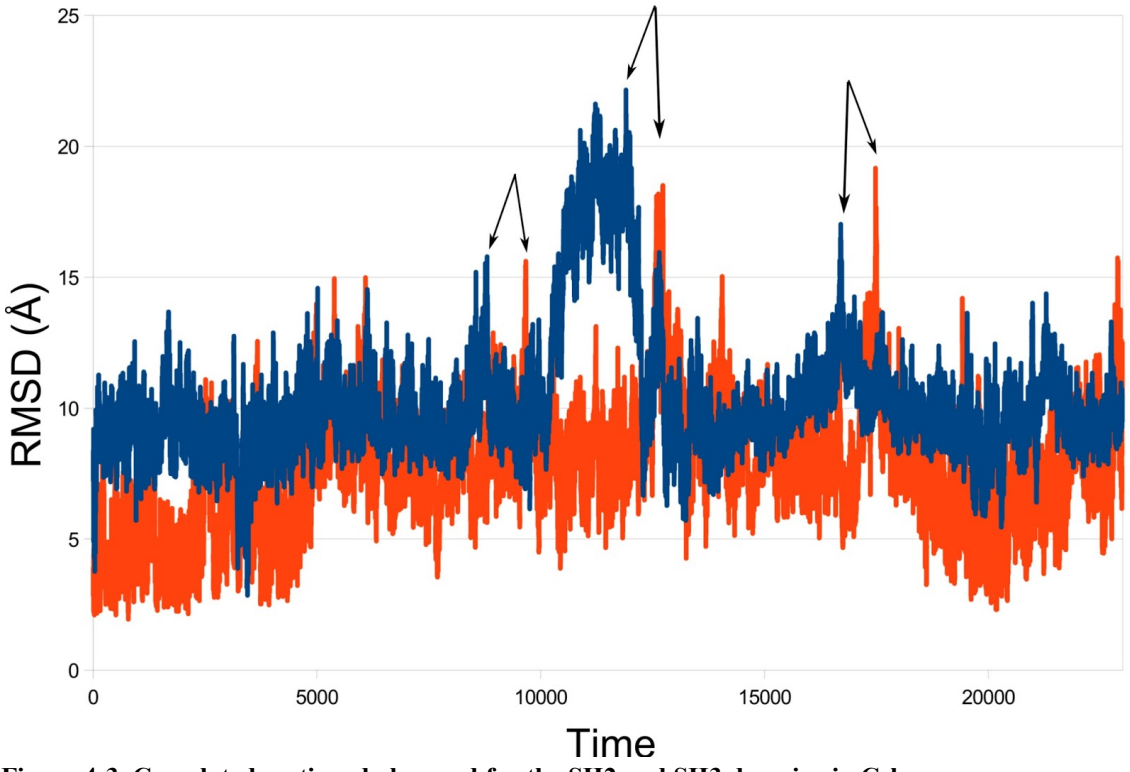

Figure 4-3. Correlated motioned observed for the SH2 and SH3 domains in Csk

The root mean square deviation (RMSD) for the SH3 domain (blue) and SH2 domain (orange) is plotted as a function of aMD simulation time. The calculated values are relative to the kinase domain throughout the simulation time.

Although both domains are mobile, we chose to focus on the SH3 domain owing to the greater shift in position in our aMD simulations. An inspection of the SH3 domain docking surface on the kinase domain reveals significant polar/hydrogen bonding through side-chain interactions between the two domains. Contact Analysis was performed for every residue in the SH3 domain (residues 1-70) and the rest of the protein (residues 71-450) to interrogate functionally relevant interactions by calculating the "percent occupancy" for each inter-domain contact. Occupancy was determined as having a donor acceptor distance of 3.8Å and an angle less than 35°.

A key interaction between the SH3 and kinase domains is mediated by the charge pair E13-R244 is observed in the crystal structure of Csk. This contact is maintained throughout the aMD trajectory and seems to be the most flexible since the R244 side chain undergoes significant rearrangement without severing contacts with E13 (Figure 4-4). Additionally, D34 occupies a conserved acidic position at the end of the RT loop in the SH3 domain. Occupancy analysis shows that D34's acceptor residue on the kinase domain is R215, which is anchored in the β2-β3 loop of the N-lobe. Both E13 and D34 maintain high contact occupancy (~80% of simulation time) throughout the aMD trajectory.

A surprising result from the aMD simulation is that Csk's N-terminal residues participate in electrostatic inter-domain interactions and serve as a third contact region between the SH3 and kinase domains. Unlike E13 and D34, the acceptor sites in this interaction are predominantly two solvent-exposed glutamate side chains (E300/E303) on helix E of the large kinase lobe (Figure 4-4). This interaction could facilitate and/or stabilize the transient coupling interface between the two domains. Interestingly, this "N-tail" interaction was hinted to in a previous study [55] in the form of line broadening of the N-terminal residues in the NMR spectra for the isolated SH3 domain upon complexation with a phosphatase peptide and the isolated kinase domain. However, the kinase contacts were unknown until now.

Interfacial Domain Contact Disruptions Have Differential Effects on Catalytic Function

To test our aMD results, we initially generated a Csk construct that deletes the entire SH3 domain (ΔSH3; residues 66-450). For ΔSH3, we chose to retain the long, unstructured SH3-SH2 linker as previous studies deemed these residues to be essential for Csk's activation and packing [55,104]. We found that ΔSH3 exhibited a ~ 33-fold reduction in catalytic activity towards the protein substrate kdSrc (Figure 4-5) in agreement with results from the Sun lab [107]. Next, we used alanine substitution to remove several charged contacts that were identified in the aMD calculations. The two acidic residues E13 and D34 maintain extensive occupancy with R244 and R215 of the small lobe, respectively, throughout the simulation (~80%) and, thus, are thought to be important for regulating SH3 domain motion in Csk. The E13A and D34A Csk variants exhibited 60-80% reductions in Csk's kinase activity towards kdSrc compared to the wild type enzyme (Figure 4-5). These findings highlight the significance of these charged residues with regard to kinase domain function.

To determine the functional importance of the N-terminal interactions with the large lobe of the kinase domain that were observed *in silico*, we generated two constructs that delete the first 4 (ΔN4) or 8 residues (ΔN8). The two truncated enzymes exhibited 60-70% reductions in catalytic activity compared to the wild-type enzyme indicating that the unstructured N-terminal residues are, indeed, involved in an SH3-dependent activation of Csk. An additional construct was generated (D34A/ΔN13) that included a 13-residue N-terminal deletion and the individual D34A substitution. This construct eliminates the three charged contacts at the interface discussed so far and indeed D34A/ΔN13 exhibited a 6-fold reduction in kinase activity -the lowest second to ΔSH3 (Figure 4-5). Overall, these findings suggest that the *in silico* contacts between the N-terminus and kinase domain are equally important as those identified in the X-ray structure in supporting kinase function. Also, it appears that both sets of interactions act in an additive manner to support Src phosphorylation.

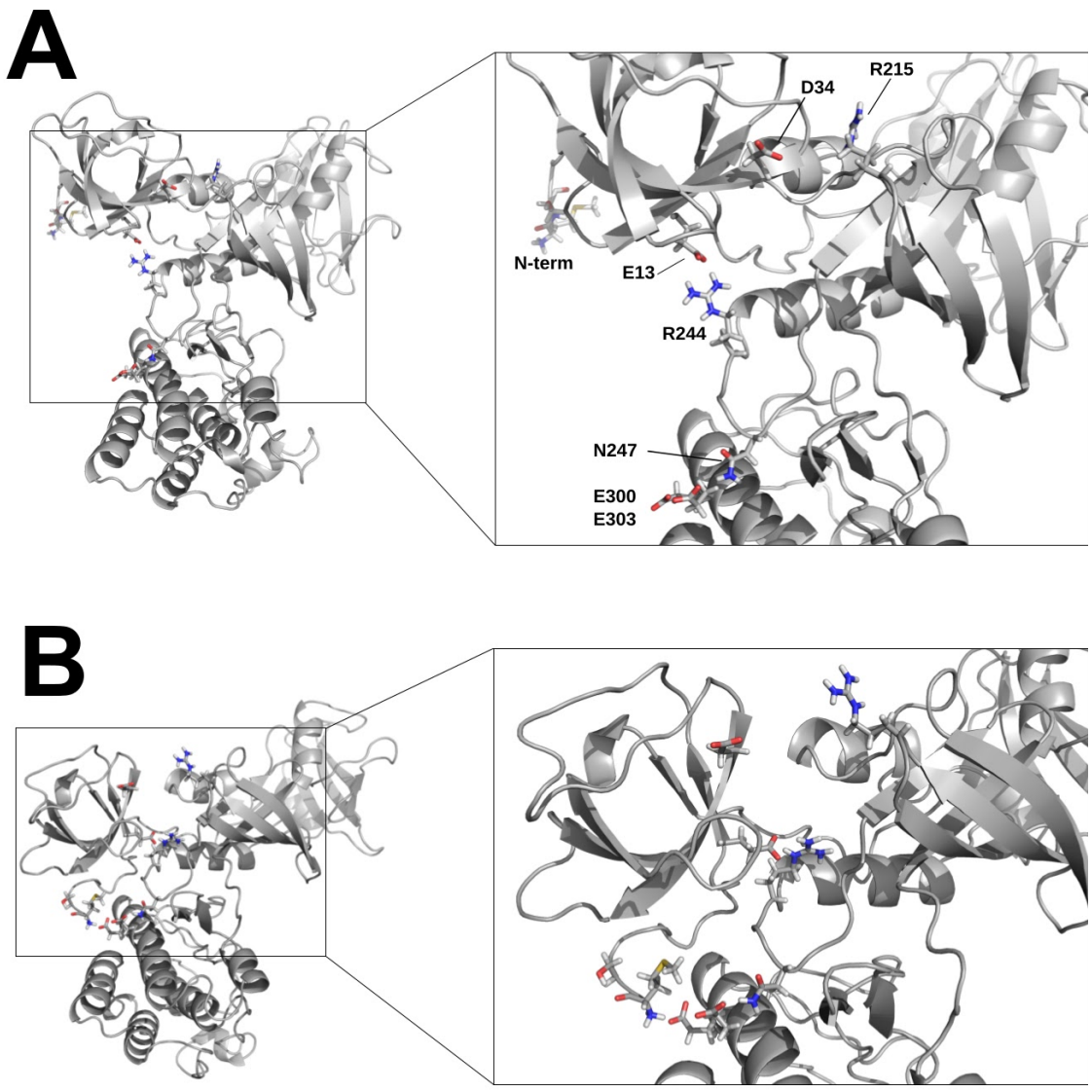

Figure 4-4. Functional interdomain contacts suggest SH3-mediated activation

High occupancy polar contacts at the SH3-kinase core interface in Csk show flexible hydrogen bonding network in the starting, "SH3 up" state, A. The same network of residues is shown from a simulation frame of the "SH3 down" conformation, B.

Since Csk's kinase activity is a function of substrate binding and turnover rate, we measured the steady-state kinetic parameters of the variants (Table 4-1). The data indicate that deleting the entire SH3 domain led to a large ~6-fold reduction in k_{cat} and a ~4-fold increase in the K_m for kdSrc. These results imply that the reduction in observed catalytic activity for ΔSH3 is the result of changes in both protein substrate binding and maximum turnover. In contrast, the D34A variant which eliminates the charged side chain at the predicted interface exclusively reduces k_{cat} by ~6-fold without affecting substrate binding. Removal of the N-terminal residues has a much smaller effect on k_{cat} but increases the substrate K_m by 3-fold. These findings suggest that the N-terminus plays an important role in substrate binding. It is also interesting to note that K_m (ATP) was largely unaffected (Table 4-1) in all tested variants which suggests that the functional integrity of the small kinase lobe motifs were not compromised. Overall, the steady-state kinetic data indicate that the contact regions serve different functions with regard to Src binding and turnover. Whereas the contacts identified in the X-ray structure (e.g., D34-R215) enhance maximum substrate turnover, the contacts identified *in silico* (N-terminus) are important for apparent substrate binding.

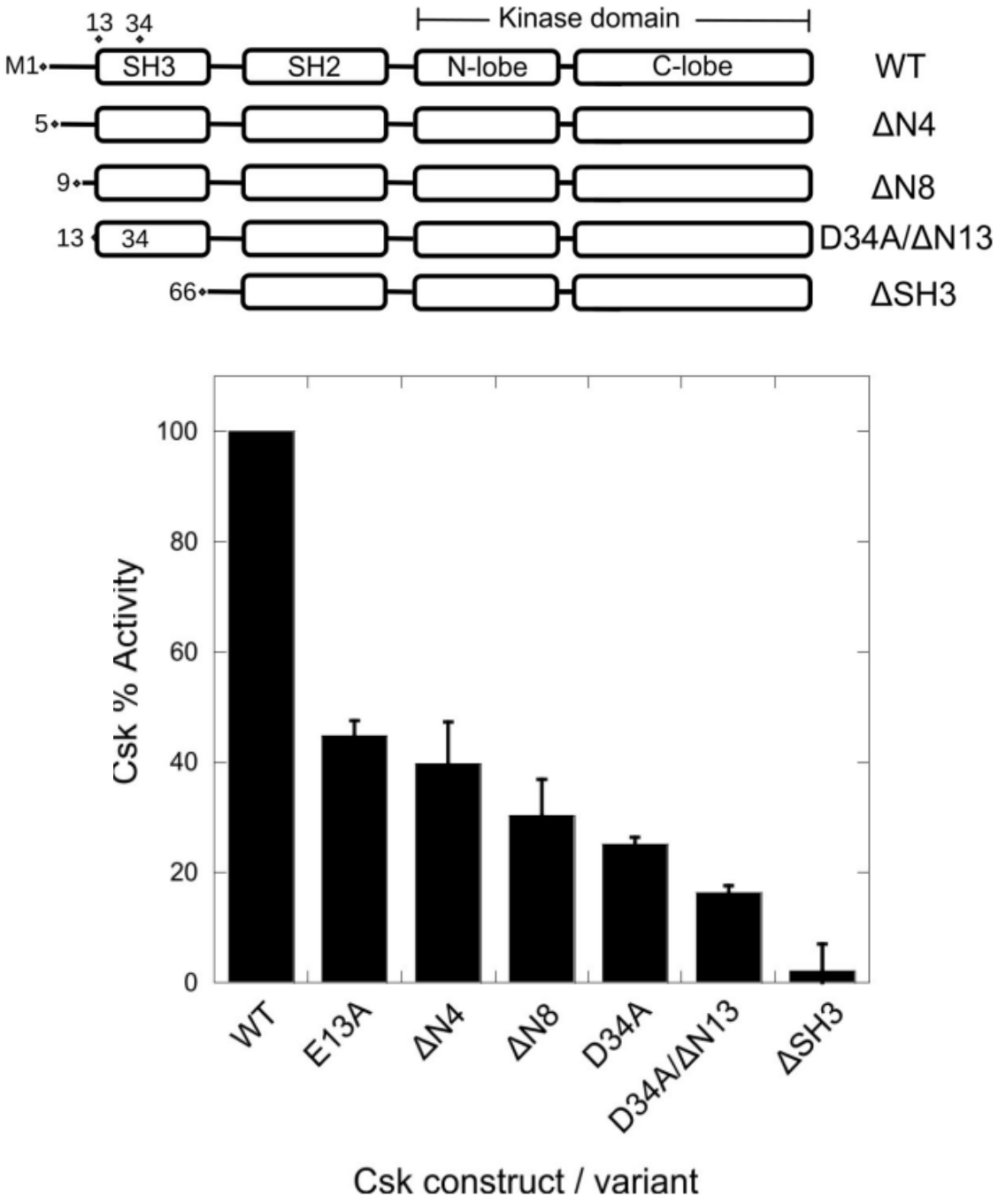

Figure 4-5. Perturbations to SH3 domain contacts inhibit kinase activation

Top: schematic representations of some Csk constructs used in this study. Bottom: Csk kinase activity assay is used to determine the extent of SH3-mediated kinase activation. Kinase activity was monitored in a [γ-^{32}P]ATP coupled radioactive assay in which a kinase dead substrate (kdSrc) is phosphorylated as a function of time. The reactions typically included 100 nM Csk, 5 μM kdSrc, 10 mM $MgCl_2$, 1 mM $MnCl_2$ and were initiated with 100 μM ATP at 23°C.

Table 4-1. Relative Steady State kinetic parameters for select SH3 domain variants

	Km (ATP), µM	**kcat (kdSrc), min^{-1}**	**Km (kdSrc), µM**	**kcat/km (kdSrc)**	**relative k_{cat}/km**
WT CSK	44.2±5.6	33.1±1.8	5.6±0.8	5.91	1
ΔN8	37.3±7.2	26.9±3.3	14.7±3.6	1.83	0.31
D34A	63.9±10	5.1±1.4	3.6±2.5	1.42	0.24
ΔSH3	39.1±9.0	5.1±0.5	22.8±4.1	0.22	0.04
E13A		3.0±0.28	6.8±1.6	0.44	0.07
D34A/ΔN13		37.7±4.3	23.4±4.5	1.61	0.27

DXMS Studies Highlight Structural Conduits of Interdomain Communication

Structural and dynamic studies of Csk revealed the importance of maintaining optimal dynamics for efficient catalysis [65,70,111]. Perturbations to large global domain motions are likely to shift the exchange between solution state ensembles that can be detected via established solution methods. We sought to understand how the N-terminal (ΔN8) and SH3 domain truncations (ΔSH3) may influence the structural flexibility of the overall protein in solution. To address this, we evaluated the native dynamics of Csk using Deuterium Exchange Mass Spectrometry (DXMS).

Select DXMS deuteration profiles are plotted for the two truncation variants in (Figure 4-6). Compared to wild-type Csk, both variants show higher uptake of solvent deuterons as a function of incubation time in a D_2O buffer. This suggests that both the short and longer truncations perturb the same interaction mode, namely the SH3-dependent activation of the kinase domain. This deprotection effect is mostly localized to the core of the N-lobe of the kinase domain yet spans motifs that spatially bridge multiple functional ends of the molecule. A significant increase in solvent deuterium incorporation is detected for overlapping peptide probes that make up core motifs within the N-lobe such as the αC-β4 loop, β4-β5 loop, and the kinase hinge region (Figure 4-7). The latter region extends to the start of αD which harbors many of the substrate binding residues (Arg/Ser) [35,36]. Also, the β4-5 loop has been identified previously by Sun and coworkers as a critical network hub for interactions that stabilize and facilitate the active state of the N-lobe of the kinase domain in Csk .

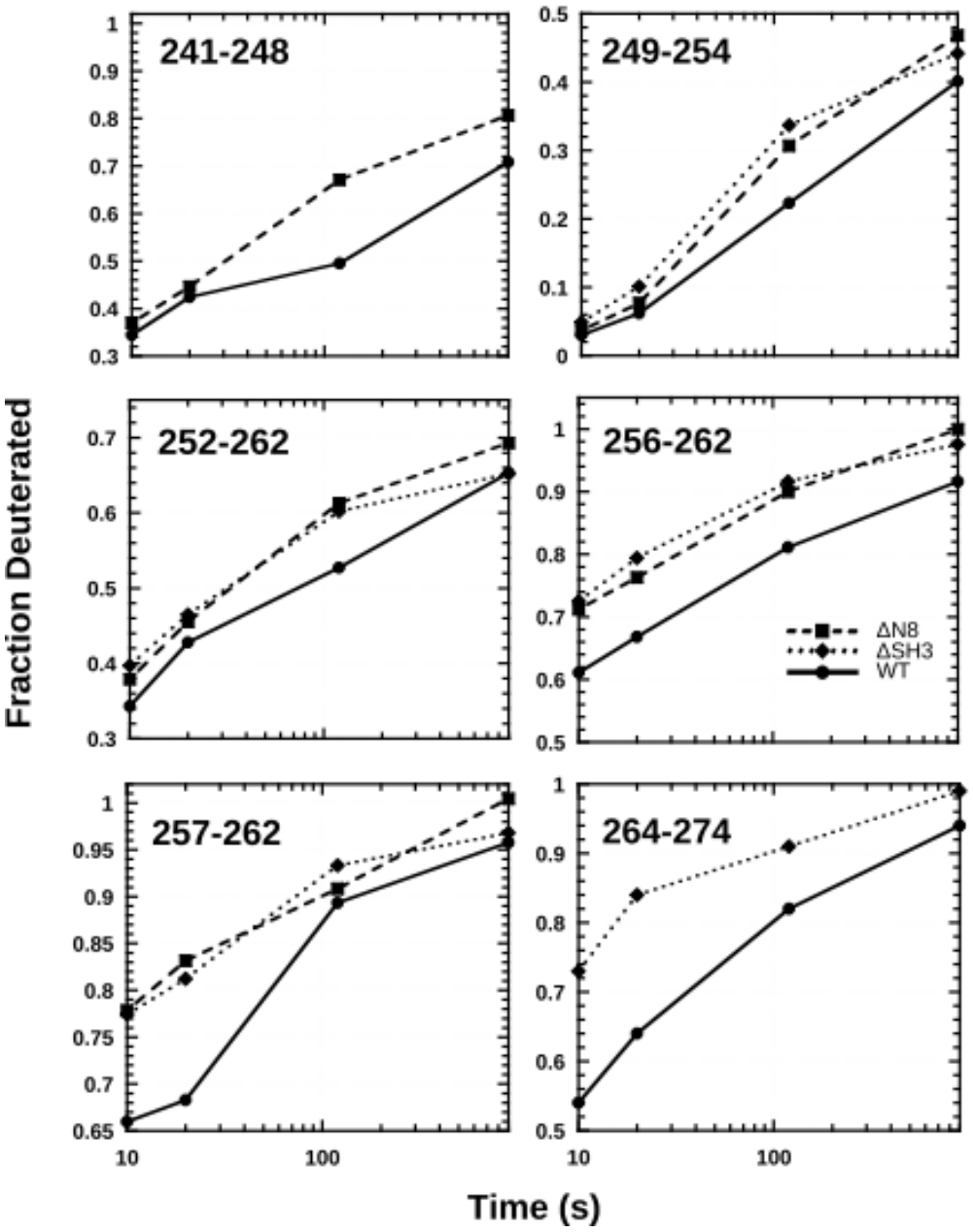

Figure 4-6. Effects of SH3 domain truncations on time-dependent solvent deuterium incorporation into Csk peptide probes

Deuterium incorporation into several probes in wild type, ΔN8, and ΔSH3 Csk is plotted as a function of time. Data were obtained over time courses of 1000 s at room temperature in deuterated buffer.

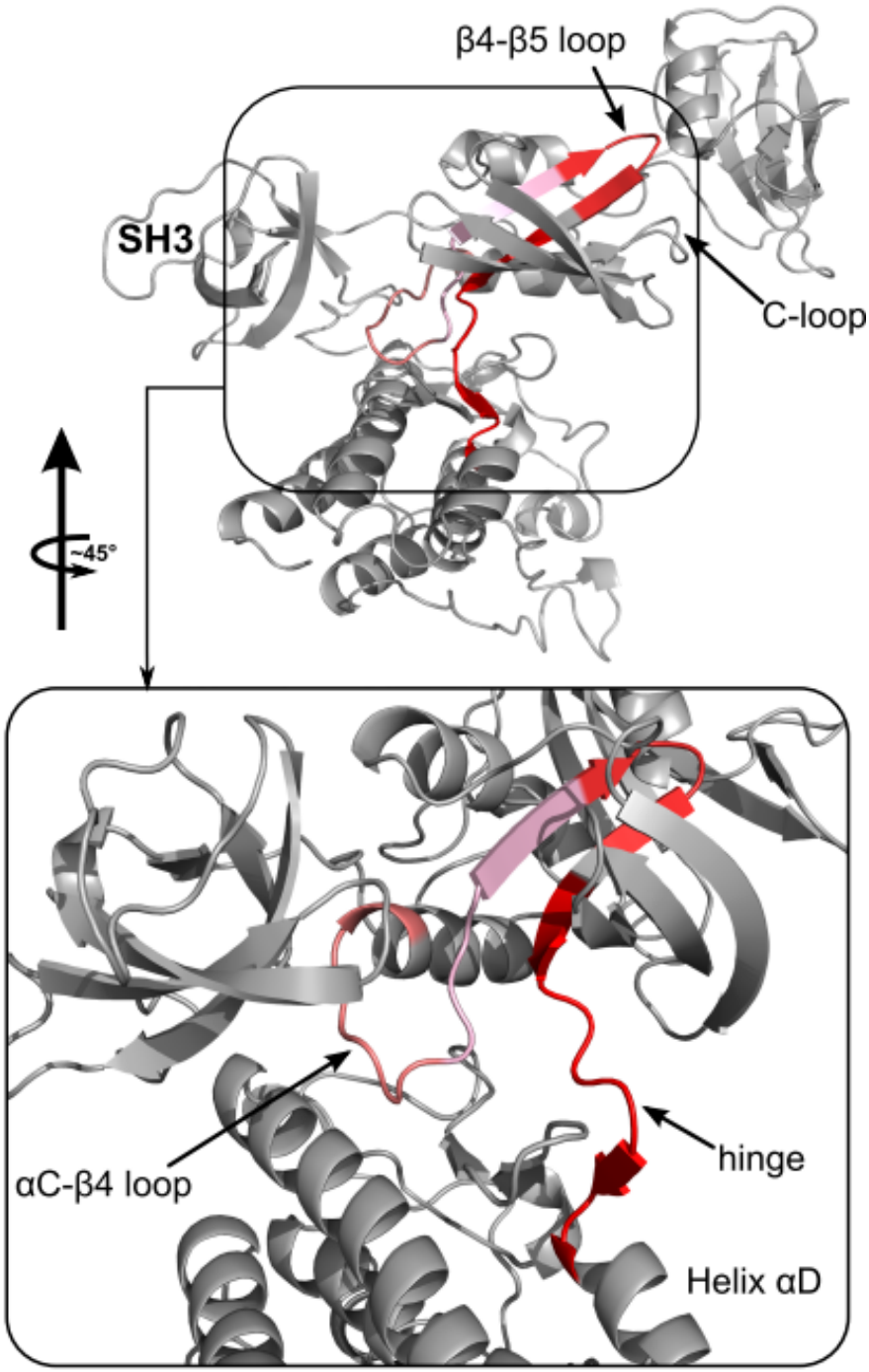

Figure 4-7. Effects of SH3 domain truncations on time-dependent solvent deuterium incorporation into Csk peptide probes

Peptides with significant DXMS changes are plotted on the crystal structure of Csk. Red color gradient indicates level of HDX deprotection for each probe in the truncated constructs (ΔN8, ΔSH3) with respect to wild type.

DISCUSSION

Many studies have established the presence of built-in mechanisms of kinase activation and inhibition that rely on peripheral motifs and modules. For SFKs, the tyrosine kinase domain possesses high, intrinsic catalytic activity that is down-regulated by interactions between the SH2 domain and a phosphorylated C-tail. This inhibitory conformation can be relieved by a protein phosphatase that removes the C-tail phosphate or by an adapter protein such as Cbp/PAG that disrupts the inhibitory SH2-kinase interaction [26]. The importance of this inhibitory mode is evident in several oncogenic forms of c-Src that through mutation dislodge the inhibitory SH2 domain and present a constitutively active kinase domain that hyper-phosphorylates substrates important for cell division [112,113]. For Csk, the SH2 domain is not involved in such catalytic repression but instead takes on an activating role. These large differences in regulatory mechanism are manifest in very different three-dimensional structures for the two kinases. Whereas the SH2 and SH3 domains interact with the both the N- and C-lobes of the kinase domain in SFKs, they interact with only the N-lobe of the kinase domain of Csk. These structural comparisons have led to an interesting hypothesis regarding how the weakly catalytic kinase domain of Csk is activated. For the kinase domain of c-Src, internal contacts within the N-lobe (Arg-264 & C-loop) stabilize a hub centered on the β4-5 loop. However, Csk appears to lack these internal contacts and instead relies on direct inter-domain contacts between a helix in the neighboring SH2 domain and the β4-5 loop. Although these contacts provide a rudimentary explanation for understanding how the SH2 domain activates the Csk kinase domain, they do not adequately provide a framework for understanding the role of the SH3 domain in enhancing kinase domain function.

In recent years it has become apparent that a complete picture of Csk regulation through domain contacts will not be fully realized through only a consideration of the X-ray structure of this kinase. Although the present structure offers several novel inter-domain contacts, other

studies now reveal that the kinase adopts numerous forms in solution, some of which depart boldly from the conformation of the crystal structure. For example, recent SAXS studies from our lab demonstrate that Csk accesses an ensemble of structures in solution with many forms highly extended relative to the more compact X-ray structure [71]. These and other solution studies point to a highly dynamic structure where domains are likely to interact in unanticipated manners. In our aMD studies we show that the SH2 and SH3 domains in Csk can move in a synchronous fashion along the N-lobe of the kinase domain. We found that a high frequency motion in the SH2 induces a large, transitory movement of the SH3 domain. We have characterized the nature of these movements and identified several contacts that appear to be important with regard to the SH3 domain movement. These contacts consist of two electrostatic pairs also visible in the X-ray structure along with several new contacts between the N-terminus of the SH3 domain and the C-lobe of the kinase domain. We demonstrated that these contacts detected both in the X-ray structure and *in silico* have significant effects on Src phosphorylation upon mutation.

The computational methods presented herein point to a new way to view the activation mechanism of Csk. Rather than relying solely on the static contacts visible in the X-ray structure, the aMD analyses expand upon these, define novel contacts and demonstrate that SH2 and SH3 domains move in opposing, yet coupled directions. These motions bear similarity to a Newton's Cradle where movement in one domain (SH2) causes the opposite movement in another (SH3). In this model, the N-lobe of the kinase domain serves as a somewhat elastic surface for these counter movements. Interestingly, we showed using DXMS that the hub identified in the N-lobe (β4-5 loop) is affected by these motions suggesting that the back and forth rocking of the SH2 and SH3 domains help to organize this critical region. This model is supported by the kinetic analyses which demonstrate that the disruption of contacts between the SH3 and kinase domain also lower Src phosphorylation rates. In prior studies we showed Src phosphorylation is limited by conformational changes in Csk [70].

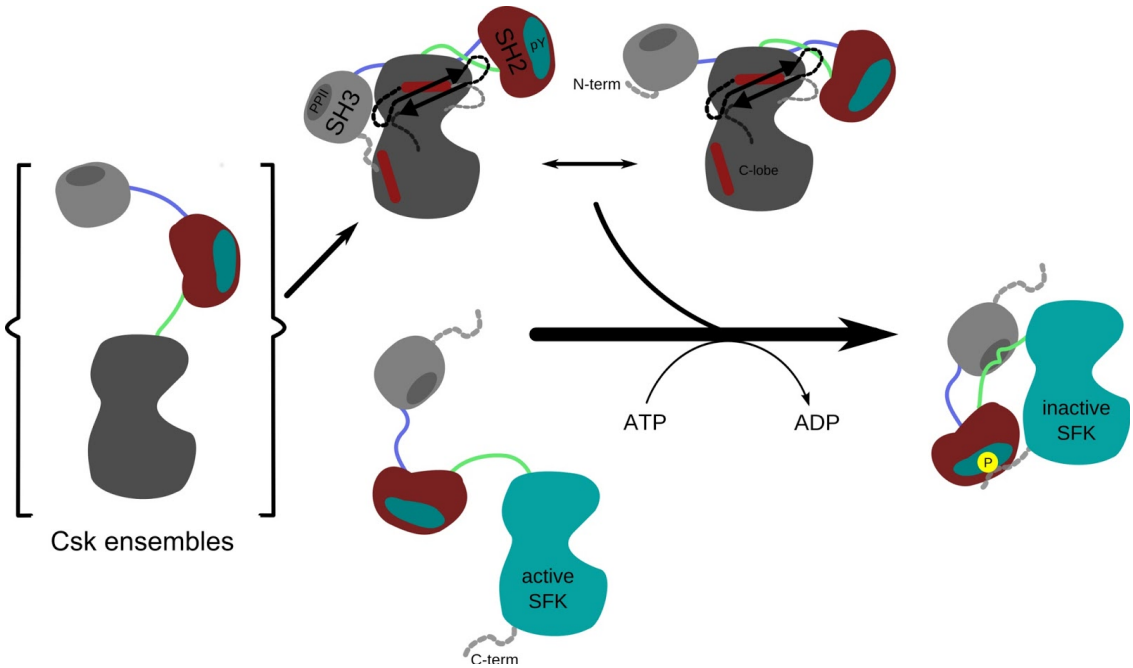

Figure 4-8. Dynamic interdomain activation in Csk

In the compact activated form, the functional motions of Csk's modular domains are correlated for efficient activation of the kinase core to phosphorylate and downregulate SFKs.

CONCLUSIONS

Our new model (Figure 4-8) suggests that synchronous domain-domain motions of the type revealed in the aMD studies may underlie the rate-limiting conformational changes that limit Src phosphorylation and downregulation by Csk. Overall, the variances among kinases can be subtle as most share canonical folds and modules but dynamic modes of regulation are now being elucidated in many signaling systems [53,71,114]. By studying a critical signaling kinase that regulates all SFKs, our results demonstrate that recent advancements in computational tools can be a great asset in uncovering functional motions in modular proteins that may be harder to assign when studied by classical biophysical techniques.

MATERIAL AND METHODS

Protein Expression and Purification

$(His)_6$ tagged Csk and kdSrc were expressed and purified as previously described [111]. Site-Directed mutagenesis was performed according to standard protocols. Truncated constructs were generated using the Phusion Site-Directed Mutagenesis Kit (Thermo Scientific). Enzymes were purified to new homogeneity as judged by SDS-PAGE analysis. A final purification step was performed on HiTrap Q HP anion exchange column (GE Healthcare) when deemed necessary.

Kinase Activity Measurements

Time-dependent phosphorylation of kinase dead Src (kdSrc) by wild type or variant Csk enzymes was typically carried out in assay buffer: 100 mM MOPS (pH 7.0), 100 mM NaCl, 10 mM $MgCl_2$, 1mM $MnCl_2$, 100 μM [γ-^{32}P]ATP (4000-6000 cpm $pmol^{-1}$) and 10 mM DTT at lab temperature (23°C). Reactions were initiated by adding ATP to the master mix containing all enzymes and reagents. a fraction of the reaction was quenched at several time points and analyzed by SDS-PAGE. Bands corresponding to the phosphorylated kdSrc substrate were excised and

quantified on the ^{32}P channel in liquid scintillator. The specific activity of [γ-^{32}P]ATP was determined by measuring the total counts of the reaction mixture. The time-dependent concentration of ^{32}P-kdSrc was then determined by considering the total counts per minute (CPM), the specific activity of the reaction mixture, and the background phosphorylation. Non-linear regression analysis were performed to quantify the activity of each construct from phosphorylation time course of a fixed amount of kdSrc. The data were fitted to the following equation to obtain rates (half-life): $P=A(1-e^{kt})$ where P is the phospho-product, A is the total substrate concentration, k is the rate constant, and t is time. Initial velocity reactions were typically initiated with variable amounts of substrates (kdSrc or ATP) and data were fitted to a Michaelis–Menten model to obtain steady state parameters.

Deuterium Exchange-Mass Spectrometry (DXMS)

Proteolysis conditions and operation

Optimal proteolysis conditions for Csk were previously established [111]. The instrument setup and operation was previously described [115]. All frozen samples were thawed and run using the conditions determined during fragmentation optimization.

Deuterium On-exchange Experiments

The exchange time course experiments for wild type and variant Csk samples were all performed simultaneously at lab temperature (23°C) as follows:: Deuteration was initiated by adding 24 µL of ~20 µM protein stock solution (50 mM Tris, 150 mM NaCl, 10% glycerol, 2 mM DTT, pH 7.0) to 120 µL of the equivalent deuterated exchange buffer for a final D_2O of 83%. The deuterated exchange buffer (50 mM d-Tris, 150 mM NaCl, 10% glycerol, 2 mM d-DTT) was prepared using 99.9 % D_2O and adjusted to pD 7.0 with DCl. 24 µL of the exchange reaction was quenched at specified time points (10, 20, 120, 900 s) into pre-chilled high recovery autosampler vials containing 6 µL of quench buffer (2.5M Gdn-HCl, 225mM TCEP, 2.5% Formic acid, 25% Glycerol). The vials were sealed and frozen over dry ice, then stored at -80°C until analysis. The

in-exchange control consisted of the protein added directly to the pre-chilled deuterated and quench buffers, then immediately followed by the normal sample preparation procedure. The back exchange control was performed by incubating samples in 0.5% formic acid in D_2O buffer overnight.

Sequence Identification of Peptide Fragments

The most likely identity of the parent peptide ions was determined using the Proteome Discoverer software program (ThermoFisher) and data dependent MS/MS data. The quality of each peptide was monitored by individually examining each measured isotopic envelope spectrum for the entire time course exchange. The deuterium content was calculated for each time point by using specialized software as previously described [85].

Computational Methods

The PDB structure 1K9A was prepared using Schrodinger's protein preparation wizard, modeling in the missing residues of the N-terminus and the activation loop. The structure was minimized and solvated in an octahedral TIP3P water box. The system was then equilibrated and a 50ns conventional molecular dynamics NVT simulations was run using the AMBER ff99SB-ILDN force field [116]. The standard aMD protocol was used [117]; average dihedral and total potential energies were calculated from the 50ns cMD simulation and used to select the acceleration parameters used in the 500ns accelerated molecular dynamics simulation (aMD).

Chapter V

Conclusions and Further Directions

GENERAL CONCLUSIONS

The studies presented in the preceding chapters aimed to explore Csk's central role as a major cell-roving signaling hub. First, the importance of the SH2 domain structural divergence from homologous modules was characterized using extended biophysical, activity techniques and conventional molecular dynamics simulations (Chapter 2). This analysis revealed that Csk's native ensemble dynamics and kinase activity are sensitive to changes to its framework at a peripheral site (CD loop) and that distal perturbation at that site leads to dampening of native flexibility in the kinase core despite the increase in local motions. Since the distal motif is within an adaptor domain (SH2), we then characterized the changes in Csk's interaction with its physiological, membrane-recruiting activator, Cbp (Chapter 3). Our enzymatic activation assays and NMR binding analysis indicate that while the magnitude of maximal CBP-activation of the kinase is minimally affected, overall catalytic efficiency of the kinase is hampered by a non-contacting loop thereby allowing for simultaneous and tunable control of localization and intrinsic activity. Finally, we utilized advanced calculations for full-length Csk to predict large-scale coupled transitions like those routinely captured in related modular proteins. The theoretical results were corroborated experimentally using our established kinetic, mutational, and structural-dynamic techniques and revealed that global and guided motions about the kinase core are inherently linked to Csk's enzymatic tasks: binding its substrates and the catalytic steps (Chapter 4).

```
CSK_HUMAN  1   WFHGKITREQAERLLYPPE--TGLFLVRESTNYPGDYTLCVSC-------DGKVEHYRI-   50
MATK_HUMAN 1   WFHGKISGQEAVQQLQPPE--DGLFLVRESARHPGDYVLCVSF-------GRDVIHYRV-   50
ABL1_HUMAN 1   WYHGPVSRNAAEYLLSSGI--NGSFLVRESESSPGQRSISLRY-------EGRVYHYRI-   50
SRC_HUMAN  1   WYFGKITRRESERLLLNAENPRGTFLVRESETTKGAYCLSVSDFD--NAKGLNVKHYKI-   57
TEC_HUMAN  1   WYCRNMNRSKAEQLLRSED-KEGGFMVRDSS-QPGLYTVSLYTKF-GGEGSSGFRHYHIK   57
ITK_HUMAN  1   WYNKSISRDKAEKLLLDTG-KEGAFMVRDSR-TAGTYTVSVFTKAVVSENNPCIKHYHIK   58
               *:   :.   :   *       * *:**:*    *   :.:            . **::

CSK_HUMAN  51  -MY-HASKLSIDEEVYFENLMQLVEHYTSDADGLCTRLIKPK   90
MATK_HUMAN 51  -LH-RDGHLTIDEAVFFCNLMDMVEHYSKDKGAICTKLVRPK   90
ABL1_HUMAN 51  -NTASDGKLYVSSESRFNTLAELVHHHSTVADGLITTLHYPA   91
SRC_HUMAN  58  -RKLDSGGFYITSRTQFNSLQQLVAYYSKHADGLCHRLTTVC   98
TEC_HUMAN  58  ETTTSPKKYYLAEKHAFGSIPEIIEYHKHNAAGLVTRLRYPV   99
ITK_HUMAN  59  ETNDNPKRYYVAEKYVFDSIPLLINYHQHNGGGLVTRLRYPV  100
                        : .   * .:  :: ::     .:   *
```

Figure 5-1. Sequence Alignment of SH2 domains

Src-subgroup families of tyrosine kinases (TK) exhibit diverse length of surface-exposed CD loops (centered at residue #40). ClustalW alignment of human protein sequences performed using the UniProt database.

DISCUSSION AND FUTURE DIRECTIONS

The extensive kinetic-enzymological analysis of Csk over the past 15 years [35,56,59,67,70,118–120] provided a solid foundation for the subsequent structural-dynamic characterization of this protein [36,58,71,78,107,111]. We began this work by examining structural divergence at seemingly benign sites with little or no sequence conservation within the framework of Csk and its homologous scaffolds. The unique presence of a tight turn in the SH2 domain when compared to other loops (Figure 5-1) prompted our questioning about possible selection at that surface site that is tailored to Csk's family and closely related kinases like CHK/MATK and ABL1. Our complimentary use of structural-functional experimental methods and statistical computational tools helped reveal routes of intramolecular and long-range communications within Csk's framework.

While interesting by themselves, these insights may provide a general framework for identifying potential sites for specific targeting by design that aid in kinase activity modulation; a therapeutic strategy of great interest. It would be of extreme use to validate the response of other kinases with short CD loops (CHK, ABL) to similar modifications; Similarly, conservative truncations of longer loops (as in SFKs) might be worth pursuing to build folding and functional "tolerance" datasets with a range of tunable settings. In the case of SFKs, the intramolecular binding of the tail to a potentially loop-modified SH2 domain provides a curious scenario for predicting the output from such a circuit as the competing action between the C-terminal tail:SH2 inhibitory mode is contrasted to CBP's activating capacity towards Csk. Moreover, introduction of newly discovered phosphatases and peripheral actors like Crk- which was found recently to bind Csk's SH2 domain through a previously unknown site [121]- to the study of an expanding circuit might be of use for fully understanding Csk's canonical and non-canonical signaling. A systematic and high-throughput (e.g. phospho-proteomics in relevant tissues) might be a desirable approach to resolve transient and localized events that could be key to capturing "pathway

switching" events involving Csk. A recent study utilizing a modified form of Csk that is amenable to rapid inactivation revealed important circuit dynamics of basal TCR signaling machinery where fast signaling responses are rooted in the dynamic control of SFK member Lck by Csk and CD45 phosphatase [122].

Despite the major advances in crystallographic techniques and instrumentation, one of the remaining hurdles in the field is that highly dynamic molecules with large functional motions of important substructures are often hard to trace in the crystal view or may even be artificially influenced by the artificial conditions. Csk's SH3 domain motion delineates this problem in that its inclusion with the other domain scaffolds hindered the formation of a stable complex suitable for crystallization [36]. Indeed the authors of that extensive study note that only when the SH3 domain was deleted from their constructs they were able to co-crystallize Csk's kinase domain/SH2 with its substrate Src. Although recently developed SAXS methods have shed light on solution dynamics of highly mobile regions of these proteins [71,80,123], the resolution needed to resolve specific contacts and motif motions within the molecule remains missing. We therefore set out to utilize the ability of advanced molecular dynamics methods in generating hypotheses about functional motions with sub-domain resolution and validated the observations experimentally with site-directed perturbations. The power of this approach is that computational power and theory continue to grow and such advantage directly contributes to the sampling efficiency for ever-larger systems and adds resolution to models extracted from experiments alone. For instance, the importance of the inherent dichotomy in tertiary arrangements of the SH modules between Csk and Src was only fully realized when MD simulations examined the nuanced intramolecular total correlations across domains in c-Src [31]. Despite intensive efforts, Csk's exact mode of action remained elusive until reliable, systematic [57] and intriguing [59,70,124] experimental data hinted to internal transitions and coupled motions allowed for the initiation of such efforts that we partly presented in chapters 2 and 4 of this work.

Furthermore, the added layer of complexity in these molecular networks stems from the spatiotemporal necessity for localization of signal and specificity of activation. CBP's classic role as an extended platform around which signalosomes assemble is well documented [41]. However, it is also becoming clear that such scaffolding sites may have tissue-specific roles. For example, several studies have shown that CBP can indeed be expendable with no apparent phenotype for the organism (knock-out mice) as a whole [125,126] in contrast to the overexpression studies in specific cell types. It is conceivable that the current thinking about CBP as a unique molecule as opposed to a semi-generic platform possessing other redundant copies or clones in many cell types that can perform -at least partially- some of CBP's functions. This possibility would explain why other adaptor proteins like LIME can also bind SFKs and Csk but cannot prevent SFK-induced tumorigenesis [127]; hinting to a Csk-independent role for CBP in suppressing Src oncogenic potential.

The overall picture seems to be uncertain with regards to the function of lipid-raft associated CBP. After all, the literature contains contradictory evidence on this adaptor as a positive and/or negative regulator of SFK potential oncogenesis. What is known for sure is that the third player in this circuit, Csk, interacts specifically with CBP as a binding partner and SFKs as a canonical suppressor. As the results from chapter 3 suggest, the apparent binding affinity between Csk's SH2 domain and CBP is enhanced when we utilize the full-length cytoplasmic domain as opposed to the shorter phosphorylated peptide containing the pY moiety. A recent solution structure [78] shed some light on a possible explanation with the identification of an extra binding motif upstream of the canonical phosphotyrosine; however, reliable binding data that corroborates that model is still sparse. Utilizing a reductionist approach, we attempted to address the question of whether the perturbed domain topology induced by the Gly-Gly extension of a surface loop had any potential influence on the apparent membrane tethering rate as determined from NMR observables of [P]-[L] interactions. In both specific and global treatment

of the data, the dissociation rate of the effector peptide bound to the SH2 domain was higher for the variant domain than the wild type. The biological implication for such effects might exhibit pathway shuttling of an important upstream node (Csk), i.e. switching from SFK downregulation to eEF2 controls or vice versa; a necessarily delicate process due to the oncogenic risk in both directions. As an intrinsically disordered protein, CBP's differential molecular actions might be grounded in thermodynamic couplings and compensatory effects between binding and function [128]. Additionally, the well-established kinase-phosphatase interaction between Csk and LYP and the "actin barrier" in SFK signaling [129,130] needs to be accounted for in relevant tissues to completely resolve an intrinsically complex model.

Ideally, results and potential biological effects mentioned above need to be carefully examined further using a range of tools spanning all relevant time and cellular scales. Theoretically, "systems biology" approaches can provide robust treatments of circuit modeling and predictions of pathway perturbation outcomes; while on the molecular level, cMD and aMD can bridge the gap between ensemble measurements and specific correlations of inter- and intramolecular motions of multiple circuit members (Csk, SFK, CBP, eEF2, Crk or a combination thereof). Experimental tools are now available to probe global responses in bigger systems. For example, to address how Csk:p-CBP binding leads to SFK substrate recognition enhancement, solution methods like NMR can accommodate multiple distinct proteins yet report on selective changes in a subset of the molecules. By selectively labelling surface reporters (e.g. methyl groups in hydrophobic sidechains) one can potentially monitor not only dynamic changes to the activator binding surface but also to substrate binding surfaces tens of angstroms away; such strategies are being employed for large macromolecular assemblies [131,132]. Also worth exploring are new chemical tools that take advantage of conserved structural motifs in protein kinases and report on their activation state [133]. It has long been realized that the modular design

of signaling molecules isn't for simple coupling mechanisms [4], we can now use an arsenal of powerful tools to reveal their true dynamic nature.

References

1. O'Connor CM, Adams JU (2010) Introduction to Essentials of Cell Biology | Learn Science at Scitable. Available: http://www.nature.com/scitable/scitable/ebooks/essentials-of-cell-biology-14749010. Accessed 17 November 2014.

2. Lim W, Mayer B, Pawson T (2014) Cell Signaling: principles and mechanisms. Taylor & Francis Group.

3. Bhattacharyya RP, Reményi A, Yeh BJ, Lim WA (2006) Domains, motifs, and scaffolds: the role of modular interactions in the evolution and wiring of cell signaling circuits. Annu Rev Biochem 75: 655–680.

4. Pawson T (2007) Dynamic control of signaling by modular adaptor proteins. Curr Opin Cell Biol 19: 112–116.

5. Aggarwal BB, Sethi G, Baladandayuthapani V, Krishnan S, Shishodia S (2007) Targeting cell signaling pathways for drug discovery: an old lock needs a new key. J Cell Biochem 102: 580–592.

6. Zhu J, Adli M, Zou JY, Verstappen G, Coyne M, et al. (2013) Genome-wide chromatin state transitions associated with developmental and environmental cues. Cell 152: 642–654.

7. Prabakaran S, Lippens G, Steen H (2012) Post-translational modification: nature's escape from genetic imprisonment and the basis for dynamic information encoding. : Systems Biology and …. Available: http://onlinelibrary.wiley.com/doi/10.1002/wsbm.1185/full.

8. Levene PA, Alsberg CL (1906) THE CLEAVAGE PRODUCTS OF VITELLIN. J Biol Chem 2: 127–133.

9. Burnett G, Kennedy EP (1954) The enzymatic phosphorylation of proteins. J Biol Chem 211: 969–980.

10. Kemp BE (1990) Peptides and Protein Phosphorylation. Taylor & Francis.

11. Introduction to Kinases - WikiKinome (n.d.). Available: http://kinase.com/wiki/index.php/Introduction_to_Kinases. Accessed 11 November 2014.

12. Manning G, Whyte DB, Martinez R, Hunter T, Sudarsanam S (2002) The protein kinase complement of the human genome. Science 298: 1912–1934.

13. Peyton Rous: father of the tumor virus (2005). J Exp Med 201: 320.

14. Rous P (1910) A TRANSMISSIBLE AVIAN NEOPLASM. (SARCOMA OF THE COMMON FOWL.). J Exp Med 12: 696–705.

15. Weiss RA, Vogt PK (2011) 100 years of Rous sarcoma virus. J Exp Med 208: 2351–2355.

16. Brugge JS, Erikson RL (1977) Identification of a transformation-specific antigen induced by an avian sarcoma virus. Nature 269: 346–348.

17. Brown MT, Cooper JA (1996) Regulation, substrates and functions of src. Biochim Biophys Acta 1287: 121–149.

18. Thomas SM, Brugge JS (1997) Cellular functions regulated by Src family kinases. Annu Rev Cell Dev Biol 13: 513–609.

19. Parsons SJ, Parsons JT (2004) Src family kinases, key regulators of signal transduction. Oncogene 23: 7906–7909.

20. Playford MP, Schaller MD (2004) The interplay between Src and integrins in normal and tumor biology. Oncogene 23: 7928–7946.

21. Di Florio A, Capurso G, Milione M, Panzuto F, Geremia R, et al. (2007) Src family kinase activity regulates adhesion, spreading and migration of pancreatic endocrine tumour cells. Endocr Relat Cancer 14: 111–124.

22. Frame MC (2002) Src in cancer: deregulation and consequences for cell behaviour. Biochim Biophys Acta 1602: 114–130.

23. Sen B, Johnson FM (2011) Regulation of SRC family kinases in human cancers. J Signal Transduct 2011: 865819.

24. Bromann PA, Korkaya H, Courtneidge SA (2004) The interplay between Src family kinases and receptor tyrosine kinases. Oncogene 23: 7957–7968.

25. Groveman BR, Feng S, Fang X-Q, Pflueger M, Lin S-X, et al. (2012) The regulation of N-methyl-D-aspartate receptors by Src kinase. FEBS J 279: 20–28.

26. Ingley E (2008) Src family kinases: regulation of their activities, levels and identification of new pathways. Biochim Biophys Acta 1784: 56–65.

27. Cloutier JF, Chow LM, Veillette A (1995) Requirement of the SH3 and SH2 domains for the inhibitory function of tyrosine protein kinase p50csk in T lymphocytes. Mol Cell Biol 15: 5937–44.

28. Courtneidge SA (1985) Activation of the pp60c-src kinase by middle T antigen binding or by dephosphorylation. EMBO J 4: 1471–1477.

29. Cooper JA, Gould KL, Cartwright CA, Hunter T (1986) Tyr527 is phosphorylated in pp60c-src: implications for regulation. Science 231: 1431–1434.

30. Xu W, Harrison SC, Eck MJ (1997) Three-dimensional structure of the tyrosine kinase c-Src. Nature 385: 595–602.

31. Young MA, Gonfloni S, Superti-Furga G, Roux B, Kuriyan J (2001) Dynamic coupling between the SH2 and SH3 domains of c-Src and Hck underlies their inactivation by C-terminal tyrosine phosphorylation. Cell 105: 115–26.

32. Cowan-Jacob SW, Fendrich G, Manley PW, Jahnke W, Fabbro D, et al. (2005) The crystal structure of a c-Src complex in an active conformation suggests possible steps in c-Src activation. Structure 13: 861–871.

33. Okada M, Nada S, Yamanashi Y, Yamamoto T, Nakagawa H (1991) CSK: a protein-tyrosine kinase involved in regulation of src family kinases. J Biol Chem 266: 24249–24252.

34. Okada M (2012) Regulation of the SRC family kinases by Csk. Int J Biol Sci 8: 1385–1397.

35. Lee S, Lin X, Nam NH, Parang K, Sun G (2003) Determination of the substrate-docking site of protein tyrosine kinase C-terminal Src kinase. Proc Natl Acad Sci U S A 100: 14707–14712.

36. Levinson NM, Seeliger MA, Cole PA, Kuriyan J (2008) Structural basis for the recognition of c-Src by its inactivator Csk. Cell 134: 124–134.

37. Yao Q, Liu B-Q, Li H, McGarrigle D, Xing B-W, et al. (2014) C-terminal Src kinase (Csk)-mediated phosphorylation of eukaryotic elongation factor 2 (eEF2) promotes proteolytic cleavage and nuclear translocation of eEF2. J Biol Chem 289: 12666–12678.

38. Kawabuchi M, Satomi Y, Takao T, Shimonishi Y, Nada S, et al. (2000) Transmembrane phosphoprotein Cbp regulates the activities of Src-family tyrosine kinases. Nature 404: 999–1003.

39. Brdicka T, Pavlistova D, Leo A, Bruyns E, Korinek, V, et al. (2000) Phosphoprotein associated with glycosphingolipid-enriched microdomains (PAG), a novel ubiquitously expressed transmembrane adaptor protein, binds the protein tyrosine kinase csk and is involved in regulation of T cell activation. J Exp Med 191: 1591–604.

40. Oneyama C, Hikita T, Enya K, Dobenecker M-W, Saito K, et al. (2008) The lipid raft-anchored adaptor protein Cbp controls the oncogenic potential of c-Src. Mol Cell 30: 426–436.

41. Hrdinka M, Horejsi V (2014) PAG - a multipurpose transmembrane adaptor protein. Oncogene 33: 4881–4892.

42. Knighton DR, Zheng JH, Ten Eyck LF, Ashford VA, Xuong NH, et al. (1991) Crystal structure of the catalytic subunit of cyclic adenosine monophosphate-dependent protein kinase. Science 253: 407–414.

43. Englander SW, Sosnick TR, Englander JJ, Mayne L (1996) Mechanisms and uses of hydrogen exchange. Curr Opin Struct Biol 6: 18–23.

44. Woods VL Jr, Hamuro Y (2001) High resolution, high-throughput amide deuterium exchange-mass spectrometry (DXMS) determination of protein binding site structure and dynamics: utility in pharmaceutical design. J Cell Biochem Suppl Suppl 37: 89–98.

45. Cavanagh J, Fairbrother WJ, Palmer AG Iii, Rance M (n.d.) PROTEIN NMR SPECTROSCOPY.

46. Wong L, Jennings PA, Adams JA (2004) Communication pathways between the nucleotide pocket and distal regulatory sites in protein kinases. Acc Chem Res 37: 304–311.

47. Mills JE, Whitford PC, Shaffer J, Onuchic JN, Adams JA, et al. (2007) A novel disulfide bond in the SH2 Domain of the C-terminal Src kinase controls catalytic activity. J Mol Biol 365: 1460–1468.

48. Cole PA, Shen K, Qiao Y, Wang D (2003) Protein tyrosine kinases Src and Csk: a tail's tale. Curr Opin Chem Biol 7: 580–585.

49. Ia KK, Mills RD, Hossain MI, Chan KC, Jarasrassamee B, et al. (2010) Structural elements and allosteric mechanisms governing regulation and catalysis of CSK-family kinases and their inhibition of Src-family kinases. Growth Factors 28: 329–350.

50. Tollinger M, Skrynnikov NR, Mulder FA, Forman-Kay JD, Kay LE (2001) Slow dynamics in folded and unfolded states of an SH3 domain. J Am Chem Soc 123: 11341–11352.

51. Filippakopoulos P, Muller S, Knapp S (2009) SH2 domains: modulators of nonreceptor tyrosine kinase activity. Curr Opin Struct Biol 19: 643–649.

52. Saksela K, Permi P (2012) SH3 domain ligand binding: What's the consensus and where's the specificity? FEBS Lett 586: 2609–2614.

53. Jankowski W, Saleh T, Pai MT, Sriram G, Birge RB, et al. (2012) Domain organization differences explain Bcr-Abl's preference for CrkL over CrkII. Nat Chem Biol 8: 590–596.

54. Sondhi D, Cole PA (1999) Domain interactions in protein tyrosine kinase Csk. Biochemistry 38: 11147–11155.

55. Shekhtman A, Ghose R, Wang D, Cole PA, Cowburn D (2001) Novel mechanism of regulation of the non-receptor protein tyrosine kinase Csk: insights from NMR mapping studies and site-directed mutagenesis. J Mol Biol 314: 129–138.

56. Lin X, Wang Y, Ahmadibeni Y, Parang K, Sun G (2006) Structural Basis for Domain–Domain Communication in a Protein Tyrosine Kinase, the C-terminal Src Kinase. J Mol Biol 357: 1263–1273.

57. Huang K, Wang Y-H, Brown A, Sun G (2009) Identification of N-terminal lobe motifs that determine the kinase activity of the catalytic domains and regulatory strategies of Src and Csk protein tyrosine kinases. J Mol Biol 386: 1066–1077.

58. Mikkola ET, Gahmberg CG (2010) Hydrophobic interaction between the SH2 domain and the kinase domain is required for the activation of Csk. J Mol Biol 399: 618–627.

59. Wong L, Lieser SA, Miyashita O, Miller M, Tasken K, et al. (2005) Coupled motions in the SH2 and kinase domains of Csk control Src phosphorylation. J Mol Biol 351: 131–143.

60. Safari F, Murata-Kamiya N, Saito Y, Hatakeyama M (2011) Mammalian Pragmin regulates Src family kinases via the Glu-Pro-Ile-Tyr-Ala (EPIYA) motif that is exploited by bacterial effectors. Proc Natl Acad Sci U S A 108: 14938–14943.

61. Mallis RJ, Brazin KN, Fulton DB, Andreotti AH (2002) Structural characterization of a proline-driven conformational switch within the Itk SH2 domain. Nat Struct Biol 9: 900–905.

62. Andrews BT, University of California SDC (2008) On the Rough Folding Landscape of Green Fluorescent Protein. University of California, San Diego.

63. Sharma D, Rajarathnam K (2000) 13C NMR chemical shifts can predict disulfide bond formation. J Biomol NMR 18: 165–171.

64. Neal S, Berjanskii M, Zhang H, Wishart DS (2006) Accurate prediction of protein torsion angles using chemical shifts and sequence homology. Magn Reson Chem 44 Spec No: S158–67.

65. Wong L, Lieser S, Chie-Leon B, Miyashita O, Aubol B, et al. (2004) Dynamic coupling between the SH2 domain and active site of the COOH terminal Src kinase, Csk. J Mol Biol 341: 93–106.

66. Hubbard SR, Till JH (2000) Protein tyrosine kinase structure and function. Annu Rev Biochem 69: 373–398.

67. Lin X, Lee S, Sun G (2003) Functions of the activation loop in Csk protein-tyrosine kinase. J Biol Chem 278: 24072–24077.

68. Ogawa A, Takayama Y, Sakai H, Chong KT, Takeuchi S, et al. (2002) Structure of the carboxyl-terminal Src kinase, Csk. J Biol Chem 277: 14351–14354.

69. Wang D, Huang XY, Cole PA (2001) Molecular determinants for Csk-catalyzed tyrosine phosphorylation of the Src tail. Biochemistry 40: 2004–2010.

70. Lieser SA, Shaffer J, Adams JA (2006) SRC tail phosphorylation is limited by structural changes in the regulatory tyrosine kinase Csk. J Biol Chem 281: 38004–38012.

71. Jamros MA, Oliveira LC, Whitford PC, Onuchic JN, Adams JA, et al. (2010) Proteins at work: a combined small angle X-RAY scattering and theoretical determination of the multiple structures involved on the protein kinase functional landscape. J Biol Chem 285: 36121–36128.

72. Bale S, Liu T, Li S, Wang Y, Abelson D, et al. (2011) Ebola virus glycoprotein needs an additional trigger, beyond proteolytic priming for membrane fusion. PLoS Negl Trop Dis 5: e1395.

73. McClendon CL, Hua L, Barreiro A, Jacobson MP (2012) Comparing Conformational Ensembles Using the Kullback-Leibler Divergence Expansion. J Chem Theory Comput 8: 2115–2126.

74. Case DA, Cheatham TE 3rd, Darden T, Gohlke H, Luo R, et al. (2005) The Amber biomolecular simulation programs. J Comput Chem 26: 1668–1688.

75. Salomon-Ferrer R, Case DA, Walker RC (2013) An overview of the Amber biomolecular simulation package. Wiley Interdiscip Rev Comput Mol Sci 3: 198–210.

76. Gotz AW, Williamson MJ, Xu D, Poole D, Le Grand S, et al. (2012) Routine Microsecond Molecular Dynamics Simulations with AMBER on GPUs. 1. Generalized Born. J Chem Theory Comput 8: 1542–1555.

77. Jacobson MP, Pincus DL, Rapp CS, Day TJ, Honig B, et al. (2004) A hierarchical approach to all-atom protein loop prediction. Proteins 55: 351–367.

78. Tanaka H, Akagi K-I, Oneyama C, Tanaka M, Sasaki Y, et al. (2013) Identification of a new interaction mode between the Src homology 2 domain of C-terminal Src kinase (Csk) and Csk-binding protein/phosphoprotein associated with glycosphingolipid microdomains. J Biol Chem 288: 15240–15254.

79. Hammes-Schiffer S, Benkovic SJ (2006) Relating protein motion to catalysis. Annu Rev Biochem 75: 519–541.

80. Yang S, Blachowicz L, Makowski L, Roux B (n.d.) Multidomain assembled states of Hck tyrosine kinase in solution. Proc Natl Acad Sci U S A 107: 15757–15762.

81. Good MC, Zalatan JG, Lim WA (2011) Scaffold proteins: hubs for controlling the flow of cellular information. Science 332: 680–686.

82. Delaglio F, Grzesiek S, Vuister GW, Zhu G, Pfeifer J, et al. (1995) NMRPipe: a multidimensional spectral processing system based on UNIX pipes. J Biomol NMR 6: 277–293.

83. Goddard TD, Kneller DG (2007) SPARKY. University of California, San Francisco.

84. Keller RLJ (2005) Optimizing the process of nuclear magnetic resonance spectrum analysis and computer aided resonance assignment [PhD diss.]. ETH.

85. Hamuro Y, Anand GS, Kim JS, Juliano C, Stranz DD, et al. (2004) Mapping intersubunit interactions of the regulatory subunit (RIalpha) in the type I holoenzyme of protein kinase A by amide hydrogen/deuterium exchange mass spectrometry (DXMS). J Mol Biol 340: 1185–1196.

86. Horn HW, Swope WC, Pitera JW, Madura JD, Dick TJ, et al. (2004) Development of an improved four-site water model for biomolecular simulations: TIP4P-Ew. J Chem Phys 120: 9665–9678.

87. Wong, V, Case DA (2008) Evaluating rotational diffusion from protein MD simulations. J Phys Chem B 112: 6013–6024.

88. Jorgensen WL, Chandrasekhar J, Madura JD, Impey RW, Klein ML (1983) Comparison of simple potential functions for simulating liquid water. J Chem Phys 79: 926–935.

89. Lippert RA, Bowers KJ, Dror RO, Eastwood MP, Gregersen BA, et al. (2007) A common, avoidable source of error in molecular dynamics integrators. J Chem Phys 126: 46101.

90. Berendsen HJC, Postma JPM, van Gunsteren WF, DiNola A, Haak JR (1984) Molecular dynamics with coupling to an external bath. J Chem Phys 81: 3684–3690.

91. Darden T, York D, Pedersen L (1993) Particle mesh Ewald: An N·log (N) method for Ewald sums in large systems. J Chem Phys. Available: http://scitation.aip.org/content/aip/journal/jcp/98/12/10.1063/1.464397.

92. Le Grand S, Götz AW, Walker RC (2013) SPFP: Speed without compromise—A mixed precision model for GPU accelerated molecular dynamics simulations. Comput Phys Commun 184: 374–380.

93. Tauzin S, Ding H, Khatib K, Ahmad I, Burdevet D, et al. (2008) Oncogenic association of the Cbp/PAG adaptor protein with the Lyn tyrosine kinase in human B-NHL rafts. Blood 111: 2310–2320.

94. Kleckner IR, Foster MP (2011) An introduction to NMR-based approaches for measuring protein dynamics. Biochim Biophys Acta 1814: 942–968.

95. Mittag T, Schaffhausen B, Günther UL (2004) Tracing kinetic intermediates during ligand binding. J Am Chem Soc 126: 9017–9023.

96. Markley JL, Kato I (1975) Assignment of the histidine proton magnetic resonance peaks of soybean trypsin inhibitor (Kunitz) by a differential exchange technique. Biochemistry 14: 3234–3237.

97. Kovrigin EL (2012) NMR line shapes and multi-state binding equilibria. J Biomol NMR 53: 257–270.

98. Kovrigin EL, Loria JP (2006) Enzyme dynamics along the reaction coordinate: critical role of a conserved residue. Biochemistry 45: 2636–2647.

99. Seidel-Dugan C, Meyer BE, Thomas SM, Brugge JS (1992) Effects of SH2 and SH3 deletions on the functional activities of wild-type and transforming variants of c-Src. Mol Cell Biol 12: 1835–1845.

100. Sicheri F, Moarefi I, Kuriyan J (1997) Crystal structure of the Src family tyrosine kinase Hck. Nature 385: 602–609.

101. Xu W, Doshi A, Lei M, Eck MJ, Harrison SC (1999) Crystal structures of c-Src reveal features of its autoinhibitory mechanism. Mol Cell 3: 629–638.

102. Sun G, Budde RJ (1999) Mutations in the N-terminal regulatory region reduce the catalytic activity of Csk, but do not affect its recognition of Src. Arch Biochem Biophys 367: 167–172.

103. Xu B, Miller WT (1996) Src homology domains of v-Src stabilize an active conformation of the tyrosine kinase catalytic domain. Mol Cell Biochem 158: 57–63.

104. Lin X, Wang Y, Ahmadibeni Y, Parang K, Sun G (2006) Structural basis for domain-domain communication in a protein tyrosine kinase, the C-terminal Src kinase. J Mol Biol 357: 1263–1273.

105. Ayrapetov MK, Nam NH, Ye G, Kumar A, Parang K, et al. (2005) Functional diversity of Csk, Chk, and Src SH2 domains due to a single residue variation. J Biol Chem 280: 25780–25787.

106. Tanaka H, Akagi K-I, Oneyama C, Tanaka M, Sasaki Y, et al. (2013) Identification of a new interaction mode between the Src homology 2 domain of C-terminal Src kinase (Csk) and Csk-binding protein/phosphoprotein associated with glycosphingolipid microdomains. J Biol Chem 288: 15240–15254.

107. Lin X, Ayrapetov MK, Lee S, Parang K, Sun G (2005) Probing the communication between the regulatory and catalytic domains of a protein tyrosine kinase, Csk. Biochemistry 44: 1561–1567.

108. Hamelberg D, Mongan J, McCammon JA (2004) Accelerated molecular dynamics: a promising and efficient simulation method for biomolecules. J Chem Phys 120: 11919–11929.

109. De Oliveira CAF, Grant BJ, Zhou M, McCammon JA (2011) Large-scale conformational changes of Trypanosoma cruzi proline racemase predicted by accelerated molecular dynamics simulation. PLoS Comput Biol 7: e1002178.

110. Wereszczynski J, McCammon JA (2012) Nucleotide-dependent mechanism of Get3 as elucidated from free energy calculations. Proc Natl Acad Sci U S A 109: 7759–7764.

111. Barkho S, Pierce LCT, McGlone ML, Li S, Woods VL Jr, et al. (2013) Distal loop flexibility of a regulatory domain modulates dynamics and activity of C-terminal SRC kinase (csk). PLoS Comput Biol 9: e1003188.

112. Blume-Jensen P, Hunter T (2001) Oncogenic kinase signalling. Nature 411: 355–365.

113. Bjorge JD, Jakymiw A, Fujita DJ (2000) Selected glimpses into the activation and function of Src kinase. Oncogene 19: 5620–5635.

114. Shan Y, Arkhipov A, Kim ET, Pan AC, Shaw DE (2013) Transitions to catalytically inactive conformations in EGFR kinase. Proc Natl Acad Sci U S A 110: 7270–7275.

115. Marsh JJ, Guan HS, Li S, Chiles PG, Tran D, et al. (2013) Structural insights into fibrinogen dynamics using amide hydrogen/deuterium exchange mass spectrometry. Biochemistry 52: 5491–5502.

116. Lindorff-Larsen K, Piana S, Palmo K, Maragakis P, Klepeis JL, et al. (2010) Improved side-chain torsion potentials for the Amber ff99SB protein force field. Proteins 78: 1950–1958.

117. Pierce LC, Salomon-Ferrer R, Augusto F de OC, McCammon JA, Walker RC (2012) Routine Access to Millisecond Time Scale Events with Accelerated Molecular Dynamics. J Chem Theory Comput 8: 2997–3002.

118. Sun G, Budde RJ (1999) Substitution studies of the second divalent metal cation requirement of protein tyrosine kinase CSK. Biochemistry 38: 5659–5665.

119. Kim K, Parang K, Lau OD, Cole PA (2000) Tyrosine analogues as alternative substrates for protein tyrosine kinase Csk: insights into substrate selectivity and catalytic mechanism [In Process Citation]. Bioorg Med Chem 8: 1263–1268.

120. Lieser SA, Shindler C, Aubol BE, Lee S, Sun G, et al. (2005) Phosphoryl transfer step in the C-terminal Src kinase controls Src recognition. J Biol Chem 280: 7769–7776.

121. Sriram G, Jankowski W, Kasikara C, Reichman C, Saleh T, et al. (2014) Iterative tyrosine phosphorylation controls non-canonical domain utilization in Crk. Oncogene. Available: http://dx.doi.org/10.1038/onc.2014.361.

122. Schoenborn JR, Tan YX, Zhang C, Shokat KM, Weiss A (2011) Feedback circuits monitor and adjust basal Lck-dependent events in T cell receptor signaling. Sci Signal 4: ra59.

123. Bernadó P, Blackledge M (2010) Structural biology: Proteins in dynamic equilibrium. Nature 468: 1046–1048.

124. Lieser SA, Aubol BE, Wong L, Jennings PA, Adams JA (2005) Coupling phosphoryl transfer and substrate interactions in protein kinases. Biochim Biophys Acta 1754: 191–199.

125. Xu S, Huo J, Tan JE-L, Lam K-P (2005) Cbp deficiency alters Csk localization in lipid rafts but does not affect T-cell development. Mol Cell Biol 25: 8486–8495.

126. Dobenecker M-W, Schmedt C, Okada M, Tarakhovsky A (2005) The ubiquitously expressed Csk adaptor protein Cbp is dispensable for embryogenesis and T-cell development and function. Mol Cell Biol 25: 10533–10542.

127. Oneyama C, Iino T, Saito K, Suzuki K, Ogawa A, et al. (2009) Transforming potential of Src family kinases is limited by the cholesterol-enriched membrane microdomain. Mol Cell Biol 29: 6462–6472.

128. Flock T, Weatheritt RJ, Latysheva NS, Babu MM (2014) Controlling entropy to tune the functions of intrinsically disordered regions. Curr Opin Struct Biol 26C: 62–72.

129. Vang T, Liu WH, Delacroix L, Wu S, Vasile S, et al. (2012) LYP inhibits T-cell activation when dissociated from CSK. Nat Chem Biol 8: 437–446.

130. Dustin ML, Davis SJ (2014) TCR signaling: the barrier within. Nat Immunol 15: 136–137.

131. Sprangers R, Kay LE (2007) Quantitative dynamics and binding studies of the 20S proteasome by NMR. Nature 445: 618–622.

132. Saio T, Guan X, Rossi P, Economou A, Kalodimos CG (2014) Structural basis for protein antiaggregation activity of the trigger factor chaperone. Science 344: 1250494.

133. Xie Q, Fulton DB, Andreotti AH (2014) A Selective NMR Probe to Monitor the Conformational Transition from Inactive to Active Kinase. ACS Chem Biol. Available: http://dx.doi.org/10.1021/cb5004702.